ABSTRACT

Solving Degenerate Stochastic Kawarada Partial Differential Equations via Adaptive Splitting Methods

Joshua Lee Padgett, Ph.D.

Advisor: Qin Sheng, Ph.D.

In this dissertation, we explore and analyze highly effective and efficient computational procedures for solving a class of nonlinear and stochastic partial differential equations. We are particularly interested in degenerate Kawarada equations arising from numerous multiphysics applications including solid fuel combustion and oil pipeline decay. These differential equations are characterized by their strong degeneracies on the boundary, quenching blow-up singularities in the spatial domain, and vibrant stochastic influences in the evolution processes. In addition, physically relevant numerical solutions to Kawarada-type equations must preserve their positivity and monotonicity in time throughout computations, for all valid initial datum. In light of these concerns and challenges, the numerical methods and analysis developed in this dissertation incorporate nonuniform finite difference approximations of the underlying singular differential equation on arbitrary spatial grids. These approximations are then advanced in time via proper adaptive mechanisms and splitting procedures, when multiple dimensions are involved.

Degenerate stochastic Kawarada equations in one-, two-, and three-dimensions are explored. The numerical procedures developed in each case are rigorously shown to not only be unconditionally stable, but also preserve the anticipated solution positivity and monotonicity throughout computations. While the numerical stability

is proven in the local linearized sense, the stability analysis has been successfully extended to a novel setting that significantly considers all nonlinear influences. Nonlinear convergence of the quenching numerical solutions, as well as their temporal derivatives, are discussed and assessed through generalized Milne devices for the two-dimensional problem. These explorations offer new insights into the computations of similar singular and stochastic differential equation problems. Intensive simulation experiments and validations are provided.

Solving Degenerate Stochastic Kawarada Partial Differential Equations via Adaptive Splitting Methods

by

Joshua Lee Padgett, B.S.

A Dissertation

Approved by the Department of Mathematics

_____

Lance L. Littlejohn, Ph.D., Chairperson

Submitted to the Graduate Faculty of
Baylor University in Partial Fulfillment of the
Requirements for the Degree
of
Doctor of Philosophy

Approved by the Dissertation Committee

_____

Qin Sheng, Ph.D., Chairperson

_____

Gerald B. Cleaver, Ph.D.

_____

Johnny Henderson, Ph.D.

_____

Frank Mathis, Ph.D.

_____

Ronald Morgan, Ph.D.

Accepted by the Graduate School
August 2017

_____

J. Larry Lyon, Ph.D., Dean

Page bearing signatures is kept on file in the Graduate School.

Copyright © 2017 by Joshua Lee Padgett
All rights reserved

TABLE OF CONTENTS

LIST OF FIGURES vii

LIST OF TABLES ix

ACKNOWLEDGMENTS x

DEDICATION xi

1 Introduction 1

2 Mathematical Preliminaries 7

2.1 Finite Difference Methods on Arbitrary Grids 7

2.2 The Matrix Exponential 9

2.2.1 Approximating the Matrix Exponential 9

2.2.2 The Logarithmic Norm 11

2.2.3 Exponential Splitting 12

3 The One-Dimensional Degenerate Stochastic Kawarada Equation 18

3.1 Introduction 18

3.2 Semi-adaptive Crank-Nicolson Scheme and its Positivity 21

3.3 Monotonicity 26

3.4 Stability 31

3.5 Numerical Experiments 37

4 The Two-Dimensional Degenerate Stochastic Kawarada Equation 56

4.1 Introduction 56

4.2 Derivation of Scheme 58

4.3 Positivity 63
4.4 Monotonicity 69
4.5 Stability 71
4.6 Numerical Experiments 77

5 The Three-Dimensional Degenerate Stochastic Kawarada Equation 90
5.1 Introduction 90
5.2 Semi-Adaptive LOD Scheme 91
5.3 Positivity 95
5.4 Monotonicity 97
5.5 Stability 104

6 Summary 110
6.1 Thesis Contributions 110
6.2 Future Research 112
6.2.1 Fractional Quenching-Combustion Problems 112
6.2.2 Nonlinear Biological Models 116

BIBLIOGRAPHY 119

LIST OF FIGURES

3.1 Evaluation of one-dimensional critical domain. 19
3.2 One-dimensional initial function and its derivative. 41
3.3 Thermal flow of non-quenching solution and derivative. 41
3.4 Curvatures of one-dimensional non-quenching solution and derivative. 42
3.5 One-dimensional non-quenching solution and derivative profiles. . . . 42
3.6 Curvatures of one-dimensional quenching solution and derivative. . . 43
3.7 One-dimensional quenching solution and derivative profiles. 43
3.8 Quenching time and domain size dynamic relationship. 44
3.9 Thermal flow of degenerate solution and derivative. 45
3.10 Curvatures of one-dimensional degenerate solution and derivative. . . 46
3.11 One-dimensional degenerate solution and derivative profiles. 47
3.12 Relationship between quenching position and degeneracy. 47
3.13 Stochastic influence plots. 50
3.14 Curvatures of first one-dimensional stochastic solution and derivative. 50
3.15 First one-dimensional stochastic solution and derivative profiles. . . . 51
3.16 Curvatures of second one-dimensional degenerate solution and derivative. 52
3.17 Second one-dimensional stochastic solution and derivative profiles. . . 52
3.18 Stochastic solution and derivative near quenching. 53
3.19 Two-dimensional stochastic solution and derivative comparison. . . . 55
3.20 Two-dimensional stochastic solution and derivative projections. . . . 55

4.1 Two-dimensional quenching solution and derivative. 78
4.2 Sample two-dimensional nonuniform meshes. 79
4.3 Convergence rates for standard two-dimensional quenching problem. . 82

4.4 Three-dimensional solution and convergence profiles. 83
4.5 Three-dimensional convergence profiles of u_t. 84
4.6 Two-dimensional stochastic degenerate quenching solution and derivative. 86
4.7 Convergence rates for two-dimensional stochastic degenerate quenching case. 87
4.8 Three-dimensional stochastic degenerate solution and convergence profiles. 88
4.9 Three-dimensional convergence profiles of u_t with stochastic and degenerate influences. 89

5.1 Sample three-dimensional nonuniform meshes. 94

6.1 One-dimensional fractional quenching solution. 116

LIST OF TABLES

3.1 Stochastic quenching locations. 54

4.1 Convergence rates for standard two-dimensional quenching problem . 83

4.2 Convergence rates for two-dimensional stochastic degenerate quenching case 86

ACKNOWLEDGMENTS

I would first like to thank my advisor, Qin Sheng, for his invaluable insight and guidance throughout my graduate studies and this dissertation process. I will always appreciate the kindness and support that he has always offered, but most importantly, I appreciate the fact that he taught me how to research, rather than simply helping me get a degree. I am grateful to Constanze Liaw for her constant encouragement, advice, and excellent instruction she provided me during my time at Baylor University as well as the unique research opportunities that we pursued together. I would like to thank Johnny Henderson for always taking the time to share his wealth of knowledge with me and for the many conversations that we shared. I would also like to express my gratitude to the members of my committee for their time and effort and all of the Baylor University professors from whom I learned so much. In addition, the interactions with my fellow graduate students have not only been valuable resources to my studies, but also my sanity.

I am eternally grateful to my family and loved ones for their unwavering love, support, and encouragement. While every loved one has supported me in their own unique ways these past five years, I am particularly grateful to my mother, Michelle, and stepfather, Danny. Their love and humor no doubt made this process easier. Finally, I would like to express my gratitude to my late father, Jeff. His love of life and kindness are missed, and his love of learning inspired my passion for mathematics and motivated my many pursuits.

To my parents,

Michelle, Jeff, and Danny

CHAPTER ONE

Introduction

Kawarada reaction-diffusion partial differential equations are fundamentally important to the study of numerous natural phenomena or processes. In particular, these equations model solid-fuel combustion processes, electric current transients in polarized ionic chambers, or enzyme kinematics for which singularities develop as the solution evolves in time. These aforementioned singularities often result from the energy of the system concentrating and approaching its activation energy [99]. This phenomenon is modeled by the temporal derivative of the solution growing at an explosive rate, while the solution remains bounded [36, 69].

In a typical solid-fuel ignition model, if a combustion chamber with fuel and air is being appropriately mixed, the temperature in the chamber increases monotonically until a certain critical value is reached. Once this value is reached, ignition occurs, and an explosion takes place within the chamber. Increasing pressure in the chamber causes the temperature to increase throughout the media, in a possibly nonuniform manner, and this nonuniform distribution of heat may result in high temperatures being extremely localized within the combustion chamber [22,99]. Ignition occurs once the peak temperature reaches the critical value, which is accompanied by the rate of change of the temperature becoming unbounded while the temperature remains bounded. The localized region of explosive temperature increase is the ignition location and is of great importance. This strong nonlinear singularity, which is referred to as a *quenching singularity*, is a fundamental part of the mathematical model.

Solid fuel combustion models can be quite sophisticated, however, the models can be simplified if one considers the problem asymptotically close to the ignition

time. In this case, the equation for temperature can be decoupled from the chemistry and mass fraction [22,99]. This decoupling results in a highly nonlinear singular reaction-diffusion equation. One such model is the following initial-boundary value problem, which is a generalized version of the problem originally studied by Hideo Kawarada in 1975 [69]. Let $u(\boldsymbol{x}, t)$ be the temperature distribution within the combustion chamber and consider

$$\begin{aligned} \sigma(\boldsymbol{x})u_t - \nabla \cdot (d(\boldsymbol{x})\nabla u) &= f(\varepsilon(\boldsymbol{x}), u), \quad \boldsymbol{x} \in \Omega,\ t_0 < t < T_q, && (1.1) \\ u(\boldsymbol{x}, t) &= 0, \quad \boldsymbol{x} \in \partial\Omega,\ t_0 < t < T_q, && (1.2) \\ u(\boldsymbol{x}, t_0) &= u_0(\boldsymbol{x}), \quad \boldsymbol{x} \in \Omega, && (1.3) \end{aligned}$$

where $\Omega \subset \mathbb{R}^n$ is a bounded connected domain with a piecewise smooth boundary $\partial\Omega$, $[t_0, T_q)$ is the maximal time interval of existence, and $d(\boldsymbol{x}) > 0$ represents the thermal diffusivity within the combustion chamber. The nonnegative function $\sigma(\boldsymbol{x})$ is the degeneracy function, with $\sigma(\boldsymbol{x}) = 0$ only for $\boldsymbol{x} \in \Omega_0 \subseteq \partial\Omega$, models particular heat transportation characteristics within the combustion chamber. The points in $\partial\Omega$ where the degeneracy $\sigma(\boldsymbol{x})$ vanishes are due to defects in the transportation of heat, whereas, the points where it becomes singular are viewed as defects in the diffusion of heat [77, 99].

The stochastic nonlinear reaction term $f(\varepsilon(\boldsymbol{x}), u)$ is singular at $u = U$ and monotonically increasing with respect to its second component, with the following properties

$$f(\varepsilon(\boldsymbol{x}), 0) = f_{\boldsymbol{x},0} > 0, \quad \lim_{u \to U^-} f(\varepsilon(\boldsymbol{x}), u) = \infty, \quad \int_0^U f(\varepsilon(\boldsymbol{x}), u)\, du = \infty$$

for each fixed $\boldsymbol{x} \in \Omega$ and $u \in [0, U)$. Further, $\varepsilon(\boldsymbol{x})$ is a stochastic spatial function such that,

$$f(\varepsilon(\boldsymbol{x}), u) > 0, \quad \int f(\varepsilon(\boldsymbol{x}), u)\, d\Omega < \infty,$$

for $\boldsymbol{x} \in \Omega$, $u \in [0, U)$.

Different semilinear parabolic initial-boundary value problems such as (1.1)-(1.3) have been studied intensively [4, 5, 22, 69, 77, 84, 85, 99, 121]. It has been shown that without stochastic influences, a well-posed continuous solution to (1.1)-(1.3) exists and is unique [4,5,69]. However, for certain domains, Ω, the existence, uniqueness, and well-posedness of the solution may be local in time [4, 33, 34, 36, 37]. In general, the stochastic influence may result in solutions which are only fractional Hölder continuous [46]. When $\sigma(\boldsymbol{x}) \equiv 1$, these results are a natural extension of the classical results for parabolic equations. However, special care must be taken for degenerate equations [23,71,86]. The conditions under which solutions to (1.1)-(1.3) exist locally and the behavior of these solutions are of great interest when considering these problems. Further, it has been shown that the solutions to Kawarada equations must be positive for appropriate nonnegative initial datum, as well as monotonically increasing with respect to time [33, 34, 36, 37, 69, 84]. While these properties are inherent to the solutions to (1.1)-(1.3), under the restrictions above, they are also necessary properties for the accurate modeling of solid-fuel combustion processes [22, 99].

The solution u of (1.1)-(1.3) is said to *quench* if $T_q < \infty$ and

$$\sup\{u_t(\boldsymbol{x}, t) \,:\, \boldsymbol{x} \in \Omega\} \to \infty \text{ as } t \to T_q^-. \tag{1.4}$$

T_q is then referred to as the *quenching time* for (1.1)-(1.3). When the solution is an increasing function in time, a necessary condition for quenching to occur is

$$\max\{u(\boldsymbol{x}, t) \,:\, \boldsymbol{x} \in \overline{\Omega}\} \to U^- \text{ as } t \to T_q^-. \tag{1.5}$$

for $T_q < \infty$ [4, 5, 26, 39, 84, 85, 93, 94]. In fact, for certain reaction terms, it has been shown that (1.4) and (1.5) are equivalent [36]. The points in Ω for which (1.5) occur are known as *quenching points*. For the problem (1.1)-(1.3), it has been shown that the quenching points are in a compact set [34, 36, 41]. Moreover, when

$n = 1$, $\Omega = (-a, a)$, $u_0 \equiv 0$, $\sigma \equiv 1$, and $f(\varepsilon, u) = (1-u)^{-1}$, it has been shown that quenching only occurs at one spatial point, namely, $x = 0$.

A domain Ω_* is called a *critical domain* of (1.1)-(1.3) if the solution of (1.1)-(1.3) exists globally when $\Omega \subseteq \Omega_*$ and (1.5) occurs when $\Omega_* \subseteq \Omega$. The computation of these critical domains has been an area of great interest [5,33,35,117,121]. When considering multidimensional problems, it is the case that both the *size* and *shape* of Ω will affect whether the solution quenches [37]. When $u_0 \equiv 0$, it is the case that by considering a family of nested domains with smooth boundaries, the critical domain of (1.1)-(1.3) can be determined by considering the steady-state problem associated to (1.1)-(1.3) [4,36]. In order to determine Ω_* uniquely, we can consider nested domains of the same shape [4,36,117]. Once the shape of the domain is fixed, then the domain is uniquely determined by its volume, thus, determining critical domains in this situation is reduced to determining the critical size [36, 117]. For completeness, we note that in [36], Chan and Ke defined two $n-$dimensional spatial domains Ω_1 and Ω_2 to have the same shape if there exists $\boldsymbol{y} \in \Omega_1 \cap \Omega_2$ and a constant $\lambda > 0$ such that

$$\Omega_2 = \{\boldsymbol{z} \,:\, \boldsymbol{z} = \boldsymbol{y} + \lambda(\boldsymbol{x} - \boldsymbol{y}) \text{ for } \boldsymbol{x} \in \Omega_1\}.$$

Thus, the critical domain is determined by taking the supremum over all domains of the same shape for which the steady-state problems admits a solution. The details of such computations may be found in [33, 35, 117].

In the case where $n = 1$, $\Omega = (-a, a)$, $u_0 \equiv 0$, $\sigma \equiv 1$, and $f(\varepsilon, u) = (1-u)^{-1}$, it was originally estimated that the critical value a^* was greater than $\sqrt{2}$ [69]. The estimate was improved to $a^* \in (0.7652, \pi/4)$ by Walter [121] and then $a^* \approx 0.765$ (to 3 significant digits) by Acker and Walter [5]. The result was further improved to be $a^* \approx 0.7652$ by Chan and Chen [35]. In fact, Walter [121] showed that $a^* = \kappa\sqrt{2}$, where

$$\kappa = \max_{0<\xi<\infty} \int_0^\xi e^{t^2-\xi^2}\, dt. \tag{1.6}$$

In Chan's study of multidimensional critical domains, he developed numerical algorithms to convert the given problem to a nonlinear integral equation via the Green's function [33]. He then used the monotone method (see [11, 40, 87], and the references therein) to find the minimal steady-state solution, which resulted in a stable computational method [33]. The computations are intensive for multidimensional cases, as the numerical procedure requires domain integration. However, Chan and Chen [35], Chan and Ke [36], and Tian [117] developed methods to further improve the efficiency and accuracy of such computations.

The unique quenching phenomenon exhibited by solutions to these quenching-combustion problems differ from the blow-up phenomenon observed in many other differential equations. A solution u is said to *blow-up* if u becomes unbounded in finite time [4, 41]. Based on this definition, it then follows that the derivative u_t is a solution to some blow-up problem. Quenching and blow-up problems are related and a quenching problem may be transformed into a blow-up problem under suitable conditions [41, 84]. Despite this relationship between the two problems, the quenching nature of the Kawarada equations presents many difficulties not seen in standard blow-up problems.

Developing numerical algorithms for solving Kawarada equations such as (1.1)-(1.3) has proven difficult due to the highly nonlinear singular stochastic reaction term. Much of the current research has involved developing algorithms which accurately predict key properties such as ignition temperature, ignition time, and critical domain size, while preserving the positive and monotone nature of the solution [33, 34, 39, 74, 75, 107]. These explorations have considered both uniform and nonuniform grids, as well as adaptive methods, but the numerical analysis of algorithms involving nonuniform grids to solve Kawarada equations is still incomplete. Moreover, most of the numerical analysis has involved the L_1 and L_∞ norms, rather than the preferable spectral norm [20, 75, 93–95].

Due to the multiple scales of the diffusion and reaction terms, algorithms for solving Kawarada equations have traditionally employed over-refined temporal grids to maintain stability and accuracy [39, 73–75, 108]. Grids of this nature are of little use in meaningful computations; *i.e.,* computations involving several spatial dimensions or cases with significantly increased quenching times. In order to rectify this issue, operator splitting methods and adaptive methods may be implemented [75, 79]. While there is still significant work to be completed in order to fully understand the implementation of these methods with Kawarada equations, it seems that combining splitting methods with certain adaptive methods may prove to be beneficial [19–21, 39, 73–75, 93–95, 105–109]

This dissertation studies the development and analysis of several numerical procedures for solving degenerate stochastic Kawarada equations on arbitrary grids. Chapter Two give a brief overview of the mathematical preliminaries necessary for the study of the developed numerical algorithms. Chapter Three presents an adaptive Crank-Nicholson scheme on arbitrary grids for solving the one-dimensional problem. Chapter Four concerns the solution of a two-dimensional model. A novel semi-discretized scheme is derived and the resulting system of differential equations and algorithm are both considered. We also present results concerning the nature of the nonlinear convergence of numerical solutions to singular problems. We consider a three-dimensional example in Chapter Five in order to present more general results for adaptive operator splitting methods. Throughout Chapters Three, Four, and Five, it is shown that the numerical algorithms developed preserve solution positivity, monotonicity, and stability under mild restrictions. Chapter Six outlines the contributions of the dissertation as well as outlining related projects and possible future endeavors. Numerical experiments and validations are provided throughout.

CHAPTER TWO

Mathematical Preliminaries

2.1 Finite Difference Methods on Arbitrary Grids

Finite difference methods have been widely used in mathematics and science. The notion of a finite difference is the cornerstone on which calculus was built due to its use to define the derivative. Finite differences are often used due to the simplicity of their implementation when uniform grids are employed [12, 38, 64, 70, 81, 101, 113]. However, it is often the case that the implementation of uniform grids can be quite costly in computations, so one wishes to employ nonuniform finite differences [93–95]. For example, if there are local regions of high variability such as is the case with shock wave, boundary layer, or singular problems, then it may be necessary to include a very fine mesh in such regions [19, 21, 63, 64, 73]. In these situations, it is often preferable to implement grids with nonuniform spacing between points. To that end, we present some basic results.

Definition 2.1. Let $\Omega \subset \mathbb{R}^n$ be a bounded, open, connected set with a piece-wise smooth boundary. A *grid* defined on Ω is a set $\mathbb{T} \subset \Omega$ such that

$$\mathbb{T} = \{(x_{1,i_1}, x_{2,i_2}, \ldots, x_{n,i_n}) \in \mathbb{R}^n \,:\, i_j = 0, 1, \ldots, N_j + 1,\ j = 1, 2, \ldots, n\},$$

where $x_{j,i_j+1} - x_{j,i_j} > 0,\ i_j = 0, \ldots, N_j,\ j = 1, \ldots, n$, and $(x_{1,i_1}, \ldots, x_{n,i_n}) \in \partial\Omega$ for any $i_j = 0,\ j = 1, \ldots, n$. The $n-$tuple $(x_{1,i_1}, \ldots, x_{n,i_n})$ is called a *grid point* of $\mathbb{T}$ and the value $h_{x_j,i_j} = x_{j,i_j+1} - x_{j,i_j},\ i_j = 0, \ldots, N_j,\ j = 1, \ldots n$ is the i_jth step size in the x_j-direction. $\mathbb{T}$ is called a *uniform grid* if $h_{x_j,i_j} = h_j > 0,\ i_j = 0, \ldots, N_j,\ j = 1, \ldots n$, otherwise $\mathbb{T}$ is a *nonuniform grid*.

In order to discuss finite difference methods involving nonuniform grids, we consider the space $\mathbb{H}$ consisting of all complex-valued sequences defined on a fixed

grid $\mathbb{T}$, denoted by $\{z_{i_1,\ldots,i_n}\},\ i_j = 0,\ldots,N_j+1,\ j=1,\ldots,n$ for fixed n and N. We then define the following linear operators on $\mathbb{H}$:

$$\Delta_{x_j,+} z_{i_1,\ldots,i_j,\ldots,i_n} = \frac{z_{i_1,\ldots,i_j+1,\ldots,i_n} - z_{i_1,\ldots,i_j,\ldots,i_n}}{h_{x_j,i_j}} \tag{2.1}$$

$$\Delta_{x_j,-} z_{i_1,\ldots,i_j,\ldots,i_n} = \frac{z_{i_1,\ldots,i_j,\ldots,i_n} - z_{i_1,\ldots,i_j-1,\ldots,i_n}}{h_{x_j,i_j}} \tag{2.2}$$

$$\Delta_{x_j,0} z_{i_1,\ldots,i_j,\ldots,i_n} = \frac{z_{i_1,\ldots,i_j+1/2,\ldots,i_n} - z_{i_1,\ldots,i_j-1/2,\ldots,i_n}}{h_{x_j,i_j}} \tag{2.3}$$

The operators (2.1), (2.2), and (2.3) are known as the forward, backward, and central difference operators, respectively [64]. These are examples of the standard nonuniform finite difference operators. We may further define the following finite difference operator

$$\begin{aligned}\Delta^2_{x_j,0} z_{i_1,\ldots,i_j,\ldots,i_n} = {} & \frac{2z_{i_1,\ldots,i_j+1,\ldots,i_n}}{h_{x_j,i_j}(h_{x_j,i_j-1}+h_{x_j,i_j})} - \frac{2z_{i_1,\ldots,i_j,\ldots,i_n}}{h_{x_j,i_j-1}h_{x_j,i_j}} \\ & + \frac{2z_{i_1,\ldots,i_j-1,\ldots,i_n}}{h_{x_j,i_j-1}(h_{x_j,i_j-1}+h_{x_j,i_j})}\end{aligned} \tag{2.4}$$

which results from a consecutive application of the operator $\Delta_{x_j,0}$ to an element of $\mathbb{H}$, that is $\Delta^2_{x_j,0} z_{i_1,\ldots,i_j,\ldots,i_n} = \Delta_{x_j,0}\left(\Delta_{x_j,0} z_{i_1,\ldots,i_j,\ldots,i_n}\right)$.

If we consider a sufficiently smooth function $f(\boldsymbol{x})$, then we may think of the range of f as a complex-valued sequence by making the association $f_{i_1,\ldots,i_n} = f(x_{1,i_1},\ldots,x_{n,i_n})$ for $(x_{1,i_1},\ldots,x_{n,i_n}) \in \mathbb{T}$. By simple Taylor expansion methods, if $\mathbb{T}$ is a nonuniform grid then it can then be verified that (2.1)-(2.3) are first-order approximations of $\partial_{x_j} f(x_{1,i_1},\ldots,x_{n,i_n})$ for $(x_{1,i_1},\ldots,x_{n,i_n}) \in \mathbb{T}$. Further (2.4) is a first-order approximation of $\partial^2_{x_j} f(x_{1,i_1},\ldots,x_{n,i_n})$ for $(x_{1,i_1},\ldots,x_{n,i_n}) \in \mathbb{T}$. When $\mathbb{T}$ is a uniform grid, (2.1)-(2.4) reduce to the uniform finite difference approximations on uniform grids with (2.3) and (2.4) increasing to second-order accurate [12, 38, 64, 70, 81, 101, 113].

2.2 The Matrix Exponential

Let $A \in \mathbb{C}^{N\times N}$ and $x_0 \in \mathbb{C}^N$. Then we may consider the following Cauchy problem

$$\begin{cases} x'(t) = Ax(t), & t > 0, \\ x(0) = x_0. \end{cases}$$

This Cauchy problem can be readily solved to obtain the solution $x(t) = E(tA)x_0$, $t \geq 0$, where $E(\cdot)$ is the matrix exponential defined as

$$E(A) = \sum_{n=0}^{\infty} \frac{1}{n!} A^n. \tag{2.5}$$

The properties of this matrix function are well explored and have been considered in the sense of matrix functions, linear operators, and semigroup operators (see [54, 78, 102, 124] and references therein). For the purposes of this dissertation, we will primarily be concerned with the properties of (2.5) as a matrix function and how to accurately and efficiently approximate this function.

2.2.1 Approximating the Matrix Exponential

The matrix exponential (2.5) is one of the most frequently utilized matrix functions in applications [54, 105, 106]. The theory of the matrix exponential has also been well studied and developed in response to these numerous applications [54, 89, 90, 105, 106]. There have been a multitude of proposed algorithms for computing the matrix exponential, but most are quite involved in nature [54, 90, 105, 106]. Each method has certain advantages and disadvantages. Herein, we will be concerned with approximating (2.5) via a Padé approximation.

It is known that if a function $g(z) \approx e^z$ for z contained in the spectrum of some $A \in \mathbb{C}^{N\times N}$ then we may approximate the matrix function $E(A)$ by $g(A)$ [54, 64, 90]. To that end, we consider the approximation

$$R_{pq}(z) = D_{pq}(z)^{-1} N_{pq}(z),$$

where

$$N_{pq} = \sum_{k=0}^{p} \frac{(p+q-k)!}{(p+q)!k!(q-k)!}(-z)^k$$

and

$$D_{pq} = \sum_{k=0}^{q} \frac{(p+q-k)!q!}{(p+q)!k!(q-k)!}(-z)^k.$$

Further, we call $R_{pq}(A)$ the $[p/q]$ Padé approximation of the matrix exponential, $E(A)$ [54, 64, 90].

By considering the above definition, we may derive the following, which are three of the most frequently used Padé approximants:

$$\begin{aligned} R_{10}(z) &= 1+z, \\ R_{01}(z) &= (1-z)^{-1}, \quad z \neq 1, \\ R_{11}(z) &= \left(1-\frac{z}{2}\right)^{-1}\left(1+\frac{z}{2}\right), \quad z \neq 2. \end{aligned}$$

Let $A \in \mathbb{C}^{N\times N}$ be a bounded matrix and $t \in \mathbb{R}$. Then R_{10}, R_{01}, and R_{11} may be used to approximate the matrix exponential as follows:

$$\begin{aligned} E(tA) &= R_{10}(tA) = 1+tA+\mathcal{O}(t^2), \quad t \to 0 \\ E(tA) &= R_{01}(tA) = (1-tA)^{-1}+\mathcal{O}(t^2), \quad t \to 0, \quad 1/t \notin \lambda(A) \\ E(tA) &= R_{11}(tA) = \left(1-\frac{tA}{2}\right)^{-1}\left(1+\frac{tA}{2}\right)+\mathcal{O}(t^3), \quad t \to 0, \quad 2/t \notin \lambda(A), \end{aligned}$$

as $t \to 0$, where $\lambda(A)$ is the spectrum of A [54, 64]. In the above, the notation $f(z) = g(z) + \mathcal{O}(z^p)$ is equivalent to $\|f(z) - g(z)\| \leq Cz^p$, for some induced norm $\|\cdot\|$ and the constant C is independent of z. These three approximations will be the approximations used throughout the analysis in this dissertation. We note that the primary disadvantage to such expansions is that the approximations are only guaranteed to be accurate near the origin [47, 54, 59, 64, 90]. This can be seen from the following identity:

$$E(tA) = R_{pq}(tA) + \frac{(-1)^q}{(p+q)!}(tA)^{p+q+1}D_{pq}(tA)^{-1}\int_0^1 s^p(1-s)^q E(t(1-s)A)\,ds.$$

However, we may rectify this issue by appropriately scaling the exponential [54, 59]. This may also be viewed as allowing the variable t to tend towards 0.

2.2.2 The Logarithmic Norm

Often, we are concerned with determining bounds for $\|E(tA)\|$, where $\|\cdot\|$ is any induced matrix norm. In application, this norm is typically the standard spectral or L_∞ norm for matrices. Via (2.5), we readily obtain the bound

$$\|E(tA)\| \leq E(t\|A\|),$$

for any matrix norm. However, this does not provide a uniform bound unless $\|A\| = 0$, as $E(t\|A\|) \to \infty$ as $t \to \infty$. When considering the spectral norm we have a useful computational tool for normal matrices. That is, if A is normal, then

$$\|E(tA)\|_2 = E(t\alpha(A)), \tag{2.6}$$

where $\alpha(A) = \max\{\mathrm{Re}(\lambda) : \lambda \in \lambda(A)\}$ [54, 64]. Thus, if the spectrum of A is in the left half of the complex plane, there is uniform decay of $\|E(tA)\|_2$ as $t \to \infty$. However, this is not the case if A is not normal [54, 90]. Further, in the case of non-normal matrices, (2.6) does not even hold and computation of the norm becomes much more involved.

Since we are often concerned with non-normal matrices that arise from the discretization of partial differential equations on arbitrary grids, herein, we consider a different approach for bounding $\|E(tA)\|$.

Definition 2.2. Let $A \in \mathbb{C}^{N\times N}$ and $\|\cdot\|$ be an induced matrix norm. Then the associated logarithmic norm $\mu : \mathbb{C}^{N\times N} \to \mathbb{R}$ of A is defined as

$$\mu(A) = \lim_{h\to 0^+} \frac{\|I_N + hA\| - 1}{h}.$$

Remark 2.3. For the spectral norm, $\mu_2(A) = \lambda_{\max}[(A + A^*)/2]$ [54, 106].

Remark 2.4. For the L_∞ norm, $\mu_\infty(A) = \sup_{i=1,\ldots,N}\{\mathrm{Re}(a_{ii}) + \sum_{j\neq i}|a_{ij}|\}$ [42].

Lemma 2.5. [54] *For $t \geq 0$ we have $\|E(tA)\| \leq E(t\mu(A))$.*

Proof. Consider the following linear first-order equation

$$\begin{aligned} x'(t) &= Ax(t), \quad t > t_0, \\ x(t_0) &= x_0 \end{aligned}$$

which has the solution $x(t) = E(tA)x_0$. Recall that the upper right Dini derivative for any function $x(t)$ with respect to t is defined as

$$\left(D_t^+ x\right)(t) = \limsup_{h\to 0^+} \frac{x(t+h) - x(t)}{h}$$

[67]. Using this fact and taking the norm, we obtain the differential inequality

$$D_t^+\|x(t)\| \;=\; \limsup_{h\to 0^+} \frac{\|E(hA)x(t)\| - \|x(t)\|}{h} \leq \mu(A)\|x(t)\| \tag{2.7}$$

where $\|\cdot\|$ is any induced matrix norm. Note that

$$\|x(t)\| \leq e^{t\mu(A)}\|x_0\|$$

is the solution to (2.7) [115]. Dividing by $\|x_0\|$ and taking the supremum of both sides over all x_0 such that $\|x_0\| \neq 0$ gives the desired result. ∎

2.2.3 Exponential Splitting

When solving partial differential equations, it is the case that certain spatial discretizations of the problem will result in a system of differential equations whose solution is given by a matrix exponential applied to some initial vector. As a motivating example, if $f(\varepsilon(\boldsymbol{x}), u) \equiv 0$ and $\sigma(\boldsymbol{x}) \equiv 1$ in (1.1)-(1.3), then a standard semi-discretization method results in the system

$$v'(t) \;=\; \sum_{i=1}^{n} A_i v(t), \quad t_0 < t < T_q, \tag{2.8}$$

$$v(t_0) \;=\; v_0. \tag{2.9}$$

By (1.1)-(1.3), it follows that the A_i are independent of t and v for $i = 1, \ldots, n$, the solution to (2.8),(2.9) is given by $v(t) = E\left(\sum_{i=1}^{n} A_i\right) v_0$, where this matrix exponential, in general, can be quite costly to compute [6, 64, 90, 113]. Thus, the goal of exponential splitting methods is to simplify the computation of such expressions.

Let $A_i \in \mathbb{C}^{N\times N},\ i = 1, \ldots, n,\ i \neq j$, where the matrices A_i and A_j may not commute for $i, j = 1, 2, \ldots, n$, and $M(t) = E(t(\sum_{i=1}^{n} A_i))$. The exponential splitting method approximates $M(t)$ with

$$S(t) = \sum_{j=1}^{K} \gamma_j E_j(t),$$

where the $E_j(t)$ are finite products of $E(\alpha_{n,j} t A_j)$, for $j = 1, 2, ..., n$. The $\alpha_{n,j}$ are constants which depend on the number of matrices involved and the γ_j depend on the $E_j(t)$ and K. Let

$$T(t) = \sum_{j=1}^{K} \gamma_j H_j(t),$$

where $H_j(t)$ is an appropriate approximation to $E_j(t)$. Then if

$$\|M(t) - T(t)\| \leq Ct^{p+1}, \quad t \to 0$$

we say that $T(t)$ is an order p approximation to the matrix exponential. That is, $S(t)$ is an order p exponential splitting method [65, 82, 88, 105, 106].

The simplest exponential splitting scheme is the first-order splitting, which, when considering two matrices, is given by

$$E(t(A_1 + A_2)) = E(tA_1)E(tA_2) + \mathcal{O}(t^2), \quad t \to 0.$$

This formula can be verified via Taylor expansion. The the first-order splitting formula for n matrices is given by

$$E\left(t \sum_{j=1}^{n} A_j\right) = \prod_{j=1}^{n} E\left(tA_j\right) + \mathcal{O}(t^2), \quad t \to 0.$$

The local truncation error can be verified by a straightforward inductive process. Other common splitting formulas are Strang splitting, which is given by

$$E\left(t\sum_{j=1}^{n}A_j\right)=\left[\prod_{j=1}^{n}E\left(\frac{t}{2}A_j\right)\right]\left[\prod_{j=1}^{n}E\left(\frac{t}{2}A_{n+1-j}\right)\right]+\mathcal{O}(t^3),\quad t\to 0,$$

and parallel splitting, which is given by

$$E\left(t\sum_{j=1}^{n}A_j\right)=\frac{1}{2}\left(\prod_{j=1}^{n}E(tA_j)+\prod_{j=1}^{n}E(tA_n+1-j)\right)+\mathcal{O}(t^3),\quad t\to 0$$

(c.f. [53, 64, 65, 83, 106, 112]).

There are several properties that an exponential splitting scheme should possess in order to be useful. One of the most restrictive properties is stability [29, 88, 112, 118, 119]. It has been shown that if restricted to the case where $\gamma_j > 0$, $\alpha_{n,j} \geq 0$, and $\gamma_j, \alpha_{n,j} \in \mathbb{R}$, which is a possible stability requirement in problems involving parabolic partial differential equations, then p cannot be greater than two. This is known as the Sheng-Suzuki barrier [25, 105, 106, 114]. It has recently been demonstrated that stable higher-order splitting schemes exist if one considers complex $\alpha_{n,j}$ with positive real parts and small arguments [31, 56, 57]. In this case, there are stable exponential splitting schemes with $p \geq 3$. For example, a third-order complex-valued splitting method is given by

$$E(t(A_1+A_2))=E(t\beta A_2)E(2t\beta A_1)E((t/2)A_2)E(2t\bar{\beta}A_1)E(t\bar{\beta}A_2)+\mathcal{O}(t^4),\quad t\to 0,$$

where $\beta=\frac{1}{4}-i\frac{\sqrt{3}}{12}$. Several other schemes, with orders higher than two, have been derived as well.

It may also be possible to breach the Sheng-Suzuki barrier by allowing some $\alpha_{n,j}$ to be negative [25, 105]. This type of splitting scheme may be stable when considering non-parabolic partial differential equations. It is also worth noting that the exponential operator may be approximated with higher order accuracy by considering operator splitting methods that are not exponential splitting methods, such as

extrapolated Alternating-Direction-Implicit (ADI) methods [17, 52, 103] or asymptotic splitting methods [6].

The order of the above indicate the local truncation error for the exponential splitting schemes and are valid for small values of t, which in numerical settings corresponds to small Courant-Friedrichs-Lewy conditions [106]. If one wants to consider global errors, we have the following generalized results from Sheng [105,106]. In the following results A_0 is the null matrix and $\mu(\cdot)$ is the logarithmic norm induced by the matrix norm.

Theorem 2.6 [106]. *Let $A_1, A_2, ..., A_n \in \mathbb{C}^{N\times N}$ and define*

$$E_{1,n}(t) = E\left(\sum_{j=1}^{n} A_j\right) - \prod_{j=1}^{n} E(tA_j).$$

Then for any $t > 0$ we have

$$\|E_{1,n}(t)\| \leq \frac{t^2}{2}\sum_{i=1}^{n-1}\left\|\left[A_i, \sum_{j=i+1}^{n} A_j\right]\right\| E\left(t\left[\sum_{j=1}^{i}\mu(A_j) + \mu\left(\sum_{j=i+1}^{n} A_j\right)\right]\right).$$

An important feature of this estimate is the fact that the estimate behaves much like the leading term in the truncation error estimate for $0 < t \ll 1$.

Theorem 2.7 [106]. *Let $A_1, A_2, ...A_n \in \mathbb{C}^{N\times N}$ and define*

$$E_{2,n}(t) = \left[\prod_{j=1}^{n} E\left(\frac{t}{2}A_j\right)\right]\left[\prod_{j=1}^{n} E\left(\frac{t}{2}A_{n+1-j}\right)\right] - E\left(t\sum_{j=1}^{n} A_j\right).$$

Then for any $t > 0$, there exist parameters $\theta_1, \theta_2, ...\theta_n$ with $0 < \theta_i < t,\ i = 1, 2, ..., n$, such that

$$\begin{aligned}\|E_{2,n}(t)\| \leq\ & \frac{t^3}{6}\sum_{i=1}^{n-1}\left\|\frac{1}{2}A_i + \sum_{j=i+1}^{n} A_j\right\|\left\|\left[A_i, \sum_{j=i+1}^{n} A_j\right]\right\| \\ & \times E\left(t\sum_{j=1}^{n}\mu(A_j)\right) E\left(\frac{\theta_i}{2}\mu\left(\frac{1}{2}A_i + \sum_{j=i+1}^{n} A_j\right)\right)\end{aligned}$$

Theorem 2.8 [106]. *Let $A_1, A_2 \in \mathbb{C}^{N\times N}$ and define*

$$E_3(t) = \frac{1}{2}\left(E(tA_1)E(tA_2) + E(tA_2)E(tA_1)\right) - E(t(A_1 + A_2)).$$

Then for any $t > 0$ we have

$$\|E_3(t)\| \leq \frac{t^3}{6}\|A_1 - A_2\|\|[A_1, A_2]\|E(t(\mu(A_1) + \mu(A_2))).$$

Next, we generalize the results in Theorem 2.8 to the case where $n \geq 2$ matrices are involved.

Theorem 2.9. *Let $A_1, A_2, ..., A_n \in \mathbb{C}^{N\times N}$ and define*

$$E_{3,n}(t) = \frac{1}{2}\left[\prod_{j=1}^{n} E(tA_j) + \prod_{j=1}^{n} E(tA_{n+1-j})\right] - E\left(t\sum_{j=1}^{n} A_j\right).$$

Then for any $t > 0$ we have

$$\begin{aligned}\|E_{3,n}(t)\| \quad \leq \quad & \frac{t^3}{6}\sum_{i=1}^{n-1}\left\|A_i - \sum_{j=i+1}^{n} A_j\right\|\left\|\left[A_i, \sum_{j=i+1}^{n} A_j\right]\right\| \\ & \times E\left(t\sum_{j=i}^{n}\mu(A_j)\right) E\left(2t\sum_{k=1}^{i-1}\mu(A_k)\right).\end{aligned}$$

Proof. We proceed by adding and subtracting in the appropriate terms which will allow us to make use of Theorem 2.8. Notice

$$\begin{aligned}E_{3,n}(t) \quad = \quad & \frac{1}{2}\left[\prod_{j=1}^{n} E(tA_j) + \prod_{j=1}^{n} E(tA_{n+1-j})\right] - E\left(t\sum_{j=1}^{n} A_j\right) \\ & + \sum_{i=2}^{n-1}\left[\prod_{j=0}^{i-1} E(tA_j)E\left(t\sum_{j=i}^{n} A_j\right)\prod_{j=0}^{i-1} E(tA_{i-j})\right] \\ & - \sum_{i=2}^{n-1}\left[\prod_{j=0}^{i-1} E(tA_j)E\left(t\sum_{j=i}^{n} A_j\right)\prod_{j=0}^{i-1} E(tA_{i-j})\right] \\ & + \frac{1}{2}\sum_{i=1}^{n-2}\left[\prod_{j=0}^{i} E(tA_j)\left(E\left(t\sum_{j=i+1}^{n} A_j\right) + E\left(t\sum_{j=i+1}^{n} A_j\right)\right)\prod_{j=0}^{i} E(tA_{i-j})\right] \\ & - \frac{1}{2}\sum_{i=1}^{n-2}\left[\prod_{j=0}^{i} E(tA_j)\left(E\left(t\sum_{j=i+1}^{n} A_j\right) + E\left(t\sum_{j=i+1}^{n} A_j\right)\right)\prod_{j=0}^{i} E(tA_{i-j})\right] \\ = \quad & \sum_{i=1}^{n-1}\left[\prod_{j=0}^{i-1} E(tA_j)\left(E\left(t\sum_{j=i}^{n} A_j\right)\right.\right. \\ & \left.\left. - \frac{1}{2}\left(E(tA_i)E\left(t\sum_{j=i+1}^{n} A_j\right) + E\left(t\sum_{j=i+1}^{n} A_j\right)E(tA_i)\right)\right)\prod_{j=0}^{i-1} E(tA_{i-j})\right]\end{aligned}$$

Taking the norm of both sides of the expression gives

$$\begin{aligned}
\|E_{3,n}(t)\| &\leq \sum_{i=1}^{n-1}\prod_{j=0}^{i-1} E(2t\mu(A_j)) \left\| E\left(t\sum_{j=i}^{n} A_j\right)\right. \\
&\quad \left. -\frac{1}{2}\left(E(tA_i)E\left(t\sum_{j=i+1}^{n} A_j\right) + E\left(t\sum_{j=i+1}^{n} A_j\right)E(tA_i)\right)\right\| \\
&\leq \frac{t^3}{6}\sum_{i=1}^{n-1}\left\|A_i - \sum_{j=i+1}^{n} A_j\right\|\left\|\left[A_i, \sum_{j=i+1}^{n} A_j\right]\right\| \\
&\quad \times E\left(t\sum_{j=i}^{n}\mu(A_j)\right) E\left(2t\sum_{k=1}^{i-1}\mu(A_k)\right)
\end{aligned}$$

which is the desired result. ∎

We note that this additional global error estimate has the desired qualities that were present in the previous results–that is, the commutator of the underlying matrices play an important role in the estimate, and if the matrices possess a negative logarithmic norm, then the error will decay exponentially as t increases.

CHAPTER THREE

The One-Dimensional Degenerate Stochastic Kawarada Equation

3.1 Introduction

Let $\Omega = (-a, a),\ \mathcal{D} = \Omega \times (t_0, T_q),\ \partial\Omega = \bar{\Omega} \setminus \Omega$ and $\mathcal{S} = \partial\Omega \times (t_0, T_q)$, where $a > 0,\ 0 \leq t_0 < T_q < \infty$. We are interested in the monotonically increasing positive solution of the degenerate stochastic Kawarada problem,

$$\sigma(x)u_t = u_{xx} + \varphi(\varepsilon)f(u), \quad (x,t) \in \mathcal{D}, \tag{3.1}$$

$$u(x,t) = 0, \quad (x,t) \in \mathcal{S}, \tag{3.2}$$

$$u(x,t_0) = u_0(x), \quad x \in \Omega, \tag{3.3}$$

where the degeneracy function $\sigma(x) \geq 0$ for $x \in \bar{\Omega}$, and the equality occurs only on $\partial\Omega$. The nonlinear source function, $f(u)$, is strictly increasing for $0 \leq u < 1$ with

$$f(0) = f_0 > 0, \quad \lim_{u \to 1^-} f(u) = +\infty,$$

and $\varphi(\varepsilon):\ 0 < \varphi_{\min} \leq \varphi \leq \varphi_{\max}$, is a stochastic inference function of the random variable, or white noise, $\varepsilon(x)$. The existence and uniqueness of the solution of (3.1)-(3.3) can be viewed as a generalization of the results given by Chan and Levine [36, 84]. It is also observed that solutions of the stochastic modeling problem (3.1)-(3.3) are in general only fractional order Hölder continuous [46].

We recall that the solution to (3.1)-(3.3) is said to quench if (1.4) occurs, with a corresponding necessary condition for quenching being (1.5). In this one-dimensional case, the critical domain may be explored more readily. It is known that a finite T_q exists only when a is greater than a certain *critical value* $a^* \ll \infty$. The interval Ω associated with such an a^* is defined as the *critical domain*, or *critical interval*, and denoted as Ω_*. Therefore, (1.5) occurs only when $\Omega_* \subseteq \Omega$, otherwise the monotone positive solution of (3.1)-(3.3) exists globally for $T_q \to \infty$ [4, 5, 84]. In the particular

circumstance when $\sigma(x), \varphi(\varepsilon) \equiv 1$ and $f(u) = (1-u)^{-1}$, we recall that the critical value is given by $a^* = \kappa\sqrt{2}$ [5, 69], where κ is defined in (1.6).

In order to demonstrate a method of approximating κ, we consider the case when $\sigma(x), \varphi(\varepsilon) \equiv 1$ and $f(u) = (1-u)^{-1}$, with homogeneous Dirichlet boundary conditions and a sufficiently small positive initial function. Then, by considering

$$\kappa = \max_{0<\xi<\infty} y(\xi) = \max_{0<\xi<\infty} \int_0^{\xi} e^{t^2-\xi^2} dt,$$

we can evaluate κ, since $y(\xi)$ satisfies the following initial value problem

$$y'(\xi) + 2\xi y(\xi) = 1, \quad y(0) = 0. \tag{3.4}$$

An explicit Euler approximation to (3.4) leads to

$$y_{k+1} = (1 - 2h\xi_k)y_k + h, \quad k = 0, 1, 2, \ldots; \quad y_0 = 0, \tag{3.5}$$

where $\xi_k = kh$, $k = 0, 1, 2, \ldots$, and with h being sufficiently small. Figure 3.1 depicts the approximated solution to (3.4) via (3.5) for $0 \le \xi \le 10$.

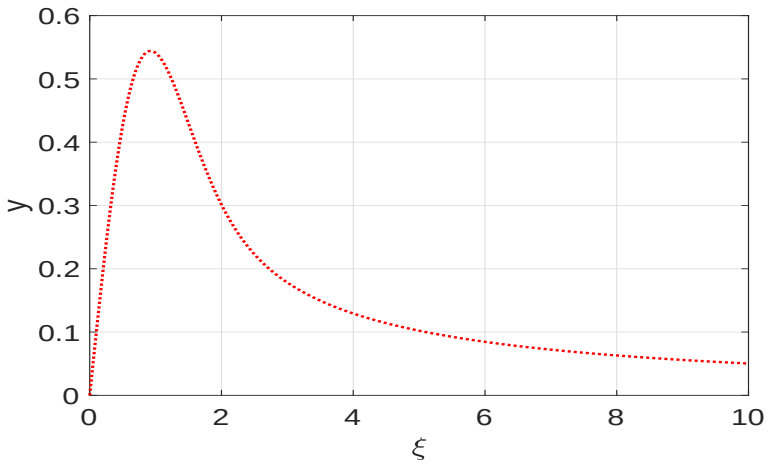

Figure 3.1: A plot of the Euler approximation of y for $0 \le \xi \le 10$. The peak represents the desired maximal value, *i.e.*, κ.

From the above we have $\kappa \approx 0.54413704$ and consequently,

$$a^* \approx 0.76952598.$$

We see that this simple procedure has provided an estimate that agrees with acceptable estimates up to the first two digits [5, 35, 121]. This estimate may be greatly improved by using a more accurate method for solving (3.4).

Kawarada partial differential equations have been intensively used for modeling numerous important phenomena in nature. They characterize not only ignitions of liquid fuels in combustion chambers, but also turbulent macro or micro flows between channel walls [22, 69, 74]. The latter is particularly meaningful for predicting and preventing oil pipeline decays [37]. Though computational results for (3.1)-(3.3) can be found in numerous recent publications, most of the numerical analysis presented relies heavily on the L_1 norm or L_∞ norm [20, 75, 93]. The numerical analysis in the current chapter implements the more preferred spectral norm. In addition, the influence of white noise associated to the source is considered. It should be noted, however, that impacts of nonsmooth sources are in general different from those due to nonsmooth initial data. In fact, while smooth solutions are still possible if nonsmooth initial data are dealt with appropriately, nonsmooth solutions are almost certain when a nonsmooth reaction term is utilized [24, 72].

This chapter examines a temporally adaptive Crank-Nicolson scheme for solving (3.1)-(3.3). Predetermined nonuniform grids are utilized in space and are chosen in order to ideally incorporate the effects of the quenching singularity and stochastic influences in space. The use of predetermined nonuniform spatial grids is practically preferable, especially in cases when quenching locations are predictable [74]. A further merit of such a semi-adaptive infrastructure is that it can be conveniently extended for solving multidimensional Kawarada problems. It also makes the subsequent numerical analysis much simpler and straightforward. Initial approaches of such an idea with uniform spatial grids can be found in [75].

It is crucial that the numerical solution acquired preserves fundamental features of the physical solution, such as the positivity, monotonicity, quenching time, and quenching location. To this end, our discussions will be organized as follows. In the next section, our adaptive Crank-Nicolson scheme for solving (3.1)-(3.3) is implemented and evaluated. Its positivity is investigated. In Section 3.3, constraints under which the numerical solution is monotonically increasing are determined. Our stability analysis is conducted in Section 3.4. We first consider a standard stability analysis for a fully linearized scheme. Then an extended stability analysis is fulfilled for a fully nonlinear method. In Section 3.5, several numerical examples are provided. These examples provide interesting insights into the effects of the degeneracy and stochastic functions on not only quenching times but also quenching locations.

3.2 Semi-adaptive Crank-Nicolson Scheme and its Positivity

Utilizing the transformation $\tilde{x} = x/a$ and reusing the original variable and other notations for simplicity, we may reformulate (3.1)-(3.3) as

$$u_t = \psi(x)u_{xx} + g(\varepsilon, u), \quad (x,t) \in \mathcal{D}, \tag{3.6}$$

$$u(-1,t) = u(1,t) = 0, \quad t > t_0, \tag{3.7}$$

$$u(x,t_0) = u_0(x), \quad x \in \Omega, \tag{3.8}$$

where $\Omega = (-1,1)$ and $\mathcal{D} = \Omega \times (t_0, T_q)$. Further, we have $\psi(x) = 1/(a^2\sigma(x))$ and $g(\varepsilon,u) = \varphi(\varepsilon)f(u)/\sigma(x)$. For a fixed $N \gg 1$, we inscribe over $\bar{\Omega}$ the variable grid:

$$\Omega = \{x_i \,:\, i = 0,\ldots,N+1;\ x_0 = -1,\ x_i < x_{i+1},\ x_{N+1} = 1\}.$$

Denote $h_i = x_{i+1} - x_i$ for $0 \le i \le N$. Let $u_i = u_i(t)$ be an approximation of $u(x_i,t)$ and adopt the nonuniform finite difference [75],

$$\partial_x^2 u(x_i,t) \;\approx\; \frac{2u_{i-1}}{h_{i-1}(h_{i-1}+h_i)} - \frac{2u_i}{h_{i-1}h_i} + \frac{2u_{i+1}}{h_i(h_{i-1}+h_i)}, \quad x_i \in \Omega^\circ,$$

where $\Omega^\circ = \Omega \setminus \{x_0, x_{N+1}\}$. Further, denote $v(t) = (u_1, u_2, \ldots, u_N)^\intercal \in \mathbb{R}^N$ and let $g(\varepsilon, v)$ be a discretization of the source term in (3.6). We obtain readily from

(3.6)-(3.8) the following semi-discretized problem

$$v'(t) = Mv(t) + g(\varepsilon, v(t)), \quad t_0 < t < T_q, \tag{3.9}$$

$$v(t_0) = v_0, \tag{3.10}$$

where $M = \frac{1}{a^2}BP \in \mathbb{R}^{N\times N}$, $B = \text{diag}\,(1/\sigma_1, \ldots, 1/\sigma_N) \in \mathbb{R}^{N\times N}$,

$$P = \text{tridiag}\,(l_i,\ m_i,\ n_i) = \begin{pmatrix} m_1 & n_1 & & & \\ l_1 & m_2 & n_2 & & \\ & \ldots & \ldots & \ldots & \\ & & l_{N-2} & m_{N-1} & n_{N-1} \\ & & & l_{N-1} & m_N \end{pmatrix} \in \mathbb{R}^{N\times N}, \tag{3.11}$$

and for the above

$$\begin{aligned} l_i &= \frac{2}{h_i(h_i + h_{i+1})},\ n_i = \frac{2}{h_i(h_{i-1} + h_i)}, \quad i = 1, \ldots, N-1, \\ m_i &= -\frac{2}{h_{i-1}h_i}, \quad i = 1, \ldots, N. \end{aligned}$$

The formal solution of (3.9), (3.10) can thus be written as

$$v(t) = E(tM)v_0 + \int_{t_0}^{t} E((t-s)M)g(\varepsilon, v(s))\, ds, \quad t_0 < t < T_q, \tag{3.12}$$

where $E(\cdot) = \exp(\cdot)$ is the matrix exponential [75]. We proceed by approximating (3.12) via a trapezoidal rule and a [1/1] Padé approximation [15, 64]; that is, $E(tM) = p(t) + \mathcal{O}\left(t^3\right),\ t \to 0$, where

$$p(t) = \left(I - \frac{t}{2}M\right)^{-1}\left(I + \frac{t}{2}M\right), \quad t_0 < t < T_q.$$

These lead to

$$v(t) = p(t)\left[v_0 + \frac{t}{2}g(\varepsilon, v_0)\right] + \frac{t}{2}g(\varepsilon, v(t)) + \mathcal{O}\left((t-t_0)^3\right), \quad |t - t_0| \to 0^+.$$

Based on the above, we obtain the following second-order in time semi-adaptive Crank-Nicolson scheme on variable spatial grids:

$$v_{\ell+1} = \left(I - \frac{\tau_\ell}{2}M\right)^{-1}\left(I + \frac{\tau_\ell}{2}M\right)\left(v_\ell + \frac{\tau_\ell}{2}g(\varepsilon, v_\ell)\right) + \frac{\tau_\ell}{2}g(\varepsilon, v_{\ell+1}), \tag{3.13}$$

where v_ℓ and $v_{\ell+1}$ are approximations of $v(t_\ell)$ and $v(t_{\ell+1})$, respectively, v_0 is the initial vector, $t_\ell = t_0 + \sum_{k=0}^{\ell-1} \tau_k,\ 0 < \tau_\ell \ll 1,\ \ell = 0, 1, 2, \ldots$, and $\{\tau_\ell\}_{\ell \geq 0}$ is a set of adaptive temporal steps. In order to avoid a fully implicit scheme, $g(\varepsilon, v_{\ell+1})$ may be approximated by $g(\varepsilon, w_\ell)$, where w_ℓ is an approximation to $v_{\ell+1}$, such as

$$w_\ell \ = \ v_\ell + \tau_\ell (M v_\ell + g(\varepsilon, v_\ell)), \quad 0 < \tau_\ell \ll 1, \tag{3.14}$$

in practical computations.

Recall (3.1). Due to the strong blow-up singularity of u_t as t approaches $T_q,\ a \geq a^*$, selecting the proper temporal steps τ_ℓ is vital for accurate computations. To this end, we may consider employing arc-length monitoring functions [50, 74, 75, 79], or allow the temporal steps to be inversely proportional to the source term or its gradient [20, 75, 93, 94]. A possible arc-length monitoring function is given by

$$m\left(\partial_t v, t\right) = \sqrt{1 + \left(\partial_t^2 v\right)^2}, \quad t_0 < t < T_q.$$

Using the discrete form of this monitoring function and setting the two maximal arc-lengths in neighboring intervals $[t_{k-2},\ t_{k-1}]$ and $[t_{k-1},\ t_k]$ equal, we acquire the following quadratic equations,

$$\tau_k^2 = \tau_{k-1}^2 + \left(\partial_t v_{k-1} - \partial_t v_{k-2}\right)^2 - \left(\partial_t v_k - \partial_t v_{k-1}\right)^2, \quad k = 1, 2, 3, \ldots,$$

with τ_0 given. In the above temporal adaptation procedures, we may consider a minimal temporal step size controller $\tilde{\tau}_0,\ 0 < \tilde{\tau}_0 \ll \tau_0$, to avoid sudden changes in grid movements or unnecessarily large numbers of computations.

Positivity is one of the most important characteristics that the solution of a Kawarada problem, such as (3.1)-(3.3) and (3.6)-(3.8) must possess [4, 5, 36, 84]. In order for our numerical solution to be valid, it is crucial that it preserves this property. To this end, we let $\wedge$ be one of the operations $<,\ \leq,\ >,\ \geq$ and $\alpha, \beta \in \mathbb{R}^{K_1 \times K_2}$. We assume the following notations in subsequent discussions:

(1) $\alpha \wedge \beta$ means $\alpha_{i,j} \wedge \beta_{i,j},\ i = 1, 2, \ldots, K_1;\ j = 1, 2, \ldots, K_2$;

(2) $a \wedge \alpha$ means $a \wedge \alpha_{i,j}, \quad i = 1, 2, \ldots, K_1;\ j = 1, 2, \ldots, K_2$, for any $a \in \mathbb{C}$.

Lemma 3.1. $\|P\|_2 \leq \max_{j=0,1,\ldots,N} \{4/h_i^2\}$.

Proof. Note that, in general, P is not symmetric. However, $\|P\|_2^2 = \rho(P^\intercal P)$, where $\rho(A)$ is the spectral radius of a matrix $A \in \mathbb{C}^{N\times N}$, and $P^\intercal P$ is symmetric with a bandwidth of five. Thus,

$$P^\intercal P = \begin{pmatrix} \tilde{m}_1 & \tilde{n}_1 & \tilde{N}_1 & & & & \\ \tilde{l}_1 & \tilde{m}_2 & \tilde{n}_2 & \tilde{N}_2 & & & \\ \tilde{L}_1 & \tilde{l}_2 & \tilde{m}_3 & \tilde{n}_3 & \tilde{N}_3 & & \\ & & \cdots & \cdots & \cdots & \cdots & \\ & & \tilde{L}_{N-4} & \tilde{l}_{N-3} & \tilde{m}_{N-2} & \tilde{n}_{N-2} & \tilde{N}_{N-2} \\ & & & \tilde{L}_{N-3} & \tilde{l}_{N-2} & \tilde{m}_{N-1} & \tilde{n}_{N-1} \\ & & & & \tilde{L}_{N-2} & \tilde{l}_{N-1} & \tilde{m}_N \end{pmatrix} \in \mathbb{R}^{N\times N},$$

where

$$\begin{aligned} \tilde{N}_j &= \tilde{L}_j = l_j n_{j+1}, \quad j = 1, \ldots, N-2, \\ \tilde{n}_j &= \tilde{l}_j = m_j n_j + m_{j+1} l_j, \quad j = 1, \ldots, N-1, \\ \tilde{m}_j &= \begin{cases} m_1^2 + l_1^2, & j = 1, \\ n_{j-1}^2 + m_j^2 + l_j^2, & j = 2, \ldots, N-1, \\ n_{N-1}^2 + m_N^2, & j = N. \end{cases} \end{aligned}$$

We may determine a bound on the spectral radius of $P^\intercal P$ by using Geršchgorin's circle theorem [64]. In fact, only the rows containing five nontrivial elements, *i.e.,* $j = 3, \ldots, N-2$, need to be considered. To this end,

$$|\lambda_j - \tilde{m}_j| \leq |\tilde{L}_{j-2}| + |\tilde{l}_{j-1}| + |\tilde{n}_j| + |\tilde{N}_j|, \quad j = 3, \ldots, N-2,$$

which gives

$$-|m_{j-1}n_{j-1} + m_j l_{j-1}| - |m_j n_j + m_{j+1} l_j|$$

$$-|l_{j-2}n_{j-1}| - |l_j n_{j+1}| + n_{j-1}^2 + m_j^2 + l_j^2 \;\leq\; \lambda_j \tag{3.15}$$

and

$$\begin{aligned}\lambda_j \;\leq\; & |m_{j-1}n_{j-1} + m_j l_{j-1}| + |m_j n_j + m_{j+1}l_j| \\ & + |l_{j-2}n_{j-1}| + |l_j n_{j+1}| + n_{j-1}^2 + m_j^2 + l_j^2. \end{aligned}\tag{3.16}$$

Let $h \equiv \min_{j=1,\ldots,N}\{h_j\}$. From (3.16) we acquire that

$$\begin{aligned}\lambda_j \;\leq\; & \frac{2}{h^2}\cdot\frac{2}{2h^2} + \frac{2}{h^2}\cdot\frac{2}{2h^2} + \frac{2}{h^2}\cdot\frac{2}{2h^2} + \frac{2}{h^2}\cdot\frac{2}{2h^4} + \frac{4}{4h^4} + \frac{4}{4h^2} \\ & + \left(\frac{2}{2h^2}\right)^2 + \left(\frac{2}{h^2}\right)^2 + \left(\frac{2}{2h^2}\right)^2 \;=\; \frac{16}{h^4}. \end{aligned}$$

Now, reverse (3.15) and by the same token,

$$\begin{aligned}-\lambda_j \;\leq\; & |m_{j-1}n_{j-1} + m_j l_{j-1}| + |m_j n_j + m_{j+1}l_j| + |l_{j-2}n_{j-1}| \\ & + |l_j n_{j+1}| - n_{j-1}^2 - m_j^2 - l_j^2 \\ \leq\; & |m_{j-1}n_{j-1} + m_j l_{j-1}| + |m_j n_j + m_{j+1}l_j| + |l_{j-2}n_{j-1}| \\ & + |l_j n_{j+1}| + n_{j-1}^2 + m_j^2 + l_j^2 \;\leq\; \frac{16}{h^4}\,, \end{aligned}$$

where, once again, $h \equiv \min_{j=1,\ldots,N}\{h_j\}$. Thus, combining the bounds we have

$$\|P\|_2 \leq \max_{j=1,\ldots,N}\left\{4/h_j^2\right\},$$

which is the desired result. ∎

For the following lemma we denote $\beta_{\min} = h^2/2\|B\|_2$ and $h = \min_{j=0,1,\ldots,N}\{h_i\}$. We first provide a definition and then prove the necessary lemma.

Definition 3.2 [58]. A matrix $A \in \mathbb{R}^{K_1\times K_2}$ is called monotone if $A\beta \geq 0$ implies that $\beta \geq 0$.

Lemma 3.3. *If*

$$\tau_\ell < a^2\beta_{\min}, \tag{3.17}$$

then $I - \frac{\tau_\ell}{2}M$ *and* $I + \frac{\tau_\ell}{2}M$ *are nonsingular. Further,* $I - \frac{\tau_\ell}{2}M$ *is monotone and inverse-positive, and* $I + \frac{\tau_\ell}{2}M$ *is nonnegative.*

Proof. First, we note that

$$\begin{aligned}\left\|\frac{\tau_\ell}{2}M\right\|_2 &\leq \frac{\tau_\ell}{2a^2}\|B\|_2\|P\|_2 \\ &\leq \frac{2\tau_\ell}{a^2}\|B\|_2\left(1/\min_{j=0,1,\ldots,N}\left\{h_i^2\right\}\right) \\ &= \frac{2\tau_\ell}{a^2h^2}\|B\|_2 \\ &< 1.\end{aligned}$$

Hence, $I + \frac{\tau_\ell}{2}M$ is nonsingular, and also nonnegative.

Next, we consider $A = I - \frac{\tau_\ell}{2}M$. A is clearly irreducible [58, 64]. Further, we have $A_{ij} \leq 0$ for $i \neq j$ and the weak row sum criterion is satisfied; hence A is monotone, and it follows that its inverse exists and is nonnegative. So, A must be inverse-positive [58]. This ensures the proof. ∎

The following lemma guarantees that our numerical solution will remain positive as long as (3.17) holds. This lemma will also be necessary for proving that the numerical solution is monotonically increasing with respect to time.

Lemma 3.4. *Let $A \in \mathbb{R}^{K_1 \times K_2}$ be nonsingular and nonnegative, and $\beta \in \mathbb{R}^{K_2}$ be positive. Then $A\beta > 0$.*

Proof. Let $A \in \mathbb{R}^{K_1 \times K_2}$ be nonsingular and nonnegative. In particular, this gives that each row of A must contain a nonzero element [54, 61]. Denote the rows of A as A_i for $i = 1, \ldots, K_1$. Let $\beta \in \mathbb{R}^{K_2}$ be positive. Note that the product $A\beta = (\alpha_1, \ldots, \alpha_{K_1})^\intercal$, where $\alpha_i = (A_i, \beta^\intercal)$ and $(\cdot, \cdot)$ is the standard Euclidean inner product on $\mathbb{C}^{K_2}$. Since each A_i has a positive element and β is positive, it follows that α_i is positive for $i = 1, \ldots, K_1$, giving the result. ∎

3.3 Monotonicity

Another fundamental feature which distinguishes a quenching solution from other blow-up type solutions is its monotonicity with respect to time $t \geq t_0$ [4, 5,

36, 74, 84]. It is therefore necessary to guarantee that a numerical solution preserves this important physical property when solving the Kawarada equation (3.1)-(3.3) or (3.6)-(3.8).

In order to commence, we need the following lemma.

Lemma 3.5. *If* $Mv_0 + g(\varepsilon, v_0) > 0$, *then it follows that* $Mv_\ell + g(\varepsilon, v_\ell) > 0$ *for all* $\ell \geq 0$.

Proof. First, we proceed be computing the following:

$$\begin{aligned}
Mv_{k+1} + g(\varepsilon, v_{k+1}) &= M\left[\left(I - \frac{\tau_k}{2}M\right)^{-1}\left(I + \frac{\tau_k}{2}M\right)\left(v_k + \frac{\tau_k}{2}g(\varepsilon, v_k)\right)\right. \\
&\qquad \left. + \frac{\tau_k}{2}g(\varepsilon, v_{k+1})\right] + g(\varepsilon, v_{k+1}) \\
&= M\left(I - \frac{\tau_k}{2}M\right)^{-1}\left[\left(I + \frac{\tau_k}{2}M\right)\left(v_k + \frac{\tau_k}{2}g(\varepsilon, v_k)\right)\right] \\
&\qquad + \left(I + \frac{\tau_k}{2}M\right)g(\varepsilon, v_{k+1}) \\
&> M\left(I - \frac{\tau_k}{2}M\right)^{-1}\left[\left(I + \frac{\tau_k}{2}M\right)\left(v_k + \frac{\tau_k}{2}g(\varepsilon, v_k)\right)\right] \\
&\qquad + \left(I + \frac{\tau_k}{2}M\right)g(\varepsilon, v_k) \\
&= \left(I - \frac{\tau_k}{2}M\right)^{-1}\left(I + \frac{\tau_k}{2}M\right)\left[Mv_k + \frac{\tau_k}{2}Mg(\varepsilon, v_k)\right. \\
&\qquad \left. + \left(I - \frac{\tau_k}{2}M\right)g(\varepsilon, v_k)\right] \\
&= \left(I - \frac{\tau_k}{2}M\right)^{-1}\left(I + \frac{\tau_k}{2}M\right)\left[Mv_k + g(\varepsilon, v_k)\right],
\end{aligned}$$

where the inequality follows from the fact that $f(u)$ is strictly increasing and Lemma 3.4. Second, we proceed by induction. Letting $k = 0$ we have

$$Mv_1 + g(\varepsilon, v_1) > \left(I - \frac{\tau_0}{2}M\right)^{-1}\left(I + \frac{\tau_0}{2}M\right)\left[Mv_0 + g(\varepsilon, v_0)\right] > 0$$

by the assumption and Lemmas 3.3 and 3.4. Third, we assume that the inequality holds for $k = \ell - 1$. It follows that

$$Mv_\ell + g(\varepsilon, v_\ell) > \left(I - \frac{\tau_{\ell-1}}{2}M\right)^{-1}\left(I + \frac{\tau_{\ell-1}}{2}M\right)\left[Mv_{\ell-1} + g(\varepsilon, v_{\ell-1})\right] > 0,$$

by the inductive assumption and Lemmas 3.3 and 3.4. Thus, we have the result by induction. ∎

We now show that the scheme (3.13) produces a monotonically increasing sequence of vectors under reasonable assumptions.

Lemma 3.6. *If* (3.17) *holds,* $\tau_k \geq 0$ *are sufficiently small for all* $0 \leq k \leq \ell$, *and* $Mv_0 + g(\varepsilon, v_0) > 0$, *then* $v_{\ell+1} \geq v_\ell$ *for all* $\ell \geq 0$. *That is, the sequence* $\{v_\ell\}_{\ell=0}^{\infty}$ *is monotonically increasing.*

Proof. From (3.13) we observe that

$$\begin{aligned}
v_{k+1} - v_k &= \left(I - \frac{\tau_k}{2}M\right)^{-1}\left(I + \frac{\tau_k}{2}M\right)\left(v_k + \frac{\tau_k}{2}g(\varepsilon, v_k)\right) + \frac{\tau_k}{2}g(\varepsilon, v_{k+1}) - v_k \\
&> \left(I - \frac{\tau_k}{2}M\right)^{-1}\left(I + \frac{\tau_k}{2}M\right)\left(v_k + \frac{\tau_k}{2}g(\varepsilon, v_k)\right) + \frac{\tau_k}{2}g(\varepsilon, v_k) - v_k \\
&= \left(I - \frac{\tau_k}{2}M\right)^{-1}\left\{\left(I + \frac{\tau_k}{2}M\right)\left[v_k + \frac{\tau_k}{2}g(\varepsilon, v_k)\right]\right. \\
&\qquad \left. - \left(I - \frac{\tau_k}{2}M\right)\left[v_k - \frac{\tau_k}{2}g(\varepsilon, v_k)\right]\right\} \\
&= \left(I - \frac{\tau_k}{2}M\right)^{-1}\left(I + \frac{\tau_k}{2}M\right)\left[\tau_k\left(Mv_k + g(\varepsilon, v_k)\right)\right] \\
&> 0,
\end{aligned}$$

by the assumption and Lemmas 3.3, 3.4, and 3.5. Since the result holds for all $k \geq 0$, we have that the sequence $\{v_\ell\}_{\ell \geq 0}$ is monotonically increasing as desired. ∎

Lemma 3.7. *Let* $x = (1, 1, \ldots, 1)^\intercal \in \mathbb{R}^N$. *Then for any* $\tau_\ell \geq 0$ *we have*

$$\left(I - \frac{\tau_\ell}{2}M\right)x \geq x.$$

Proof. Consider

$$w \;=\; \left(I - \frac{\tau_\ell}{2}M\right)x \;=\; (w_1, w_2, \ldots, w_N)^\intercal.$$

First, we observe that

$$\begin{aligned}
w_1 &= \left(1 - \frac{\tau_\ell}{2}\cdot\frac{-2}{a^2\sigma_1 h_0 h_1}\right) - \frac{\tau_\ell}{2}\cdot\frac{2}{a^2\sigma_1 h_1(h_0 + h_1)} \\
&= 1 + \frac{\tau_\ell}{a^2\sigma_1}\left(\frac{1}{h_0 h_1} - \frac{1}{h_1(h_0 + h_1)}\right) \\
&> 1.
\end{aligned}$$

Secondly, for $i = 2, \ldots, N-1$, we have

$$\begin{aligned} w_i &= -\frac{\tau_\ell}{2} \cdot \frac{2}{a^2\sigma_i h_{i-1}(h_{i-1}+h_i)} + \left(1 - \frac{\tau_\ell}{2} \cdot \frac{-2}{a^2\sigma_i h_{i-1} h_i}\right) - \frac{\tau_\ell}{2} \cdot \frac{2}{a^2\sigma_i h_i (h_{i-1}+h_i)} \\ &= 1 + \frac{\tau_\ell}{a^2\sigma_i}\left[\frac{-h_i + (h_{i-1}+h_i) - h_{i-1}}{h_{i-1}h_i(h_{i-1}+h_i)}\right] \\ &= 1. \end{aligned}$$

Finally, we observe that

$$\begin{aligned} w_N &= -\frac{\tau_\ell}{2} \cdot \frac{2}{a^2\sigma_N h_{N-1}(h_{N-1}+h_N)} + \left(1 - \frac{\tau_\ell}{2} \cdot \frac{-2}{a^2\sigma_N h_{N-1} h_N}\right) \\ &= 1 + \frac{\tau_\ell}{a^2\sigma_N}\left[\frac{1}{h_N(h_{N-1}+h_N)}\right] \\ &> 1. \end{aligned}$$

Hence, we may conclude that $w_i \geq 1,\ i = 1, \ldots, N$. Therefore $w \geq x$. ∎

In the next lemma we show that numerical quenching, *i.e.,* one or more components of v_ℓ reaching or exceeding unity, cannot occur immediately after the first time step under appropriate constraints.

Lemma 3.8. *Let x be the vector defined in Lemma 3.7 and $v_0 \equiv 0$. If* (3.17) *holds and*

$$\bar{h}^2 < 2\|B\|_2 / [a^2 \varphi_{\max} f(\tau_0 \varphi_{\max} f_0 / \sigma_{\min})],$$

where $\bar{h} = \max_{i=1,\ldots,N}\{h_i\}$, then $v_1 < x$.

Proof. Recall (3.13). For $v_0 \equiv 0$ we have

$$v_1 = \left(I - \frac{\tau_0}{2}M\right)^{-1}\left(I + \frac{\tau_0}{2}M\right)\frac{\tau_0}{2}g(\varepsilon, 0) + \frac{\tau_0}{2}g(\varepsilon, v_1).$$

Using

$$g(\varepsilon, v_1) \approx g(\varepsilon, w_0) = g(\varepsilon, v_0 + \tau_0(Mv_0 + g(\varepsilon, v_0))) = g(\varepsilon, \tau_0 f_0 \gamma),$$

where $\gamma = (\varphi_1/\sigma_1, \ldots, \varphi_N/\sigma_N)^\intercal \in \mathbb{R}^N$, we have

$$\left(I - \frac{\tau_0}{2}M\right)\left(v_1 - \frac{\tau_0}{2}g(\varepsilon, \tau_0 f_0 \gamma)\right) = \left(I + \frac{\tau_0}{2}M\right)\frac{\tau_0}{2}f_0\gamma. \tag{3.18}$$

Based on (3.18) we observe that

$$\begin{aligned} v_1 - x &= \left(I - \frac{\tau_0}{2}M\right)^{-1} \left[\left(I + \frac{\tau_0}{2}M\right)\frac{\tau_0}{2}f_0\gamma \right. \\ &\qquad \left. + \left(I - \frac{\tau_0}{2}M\right)\left(\frac{\tau_0}{2}g(\varepsilon, \tau_0 f_0\gamma) - x\right)\right] \\ &= \left(I - \frac{\tau_0}{2}M\right)^{-1}\left(s^+ + s^-\right), \end{aligned}$$

where

$$s^+ = \frac{\tau_0}{2}\left(I + \frac{\tau_0}{2}M\right) f_0\gamma + \frac{\tau_0}{2}\left(I - \frac{\tau_0}{2}M\right) g(\varepsilon, \tau_0 f_0\gamma)$$

and

$$s^- = -\left(I - \frac{\tau_0}{2}M\right) x.$$

It can be seen that

$$\begin{aligned} \left|s^+\right| &= \frac{\tau_0}{2}\left|\left(I + \frac{\tau_0}{2}M\right) f_0\gamma + \left(I - \frac{\tau_0}{2}M\right) g(\varepsilon, \tau_0 f_0\gamma)\right| \\ &\leq \frac{\tau_0}{2}\max\left\{\left|f_0\gamma\right|, \left|g(\varepsilon, \tau_0 f_0\gamma)\right|\right\}\left\|\left(I + \frac{\tau_0}{2}M\right) + \left(I - \frac{\tau_0}{2}M\right)\right\|_2 \\ &< \frac{\bar{h}^2}{2\|B\|_2}a^2\varphi_{\max} f(\tau_0\varphi_{\max} f_0/\sigma_{\min}), \end{aligned}$$

and the above indicates that

$$s^+ \leq \frac{a^2\bar{h}^2\varphi_{\max} f(\tau_0\varphi_{\max} f_0)}{2\|B\|_2}x.$$

By Lemma 3.7 we conclude that $s^- \leq -x$, and therefore,

$$s^+ + s^- \leq \left[\frac{a^2\bar{h}^2\varphi_{\max} f(\tau_0\varphi_{\max} f_0/\sigma_{\min})}{2\|B\|_2} - 1\right]x.$$

Since we again wish each component of the above vector to be negative, we need

$$\frac{a^2\bar{h}^2 f(\tau_0\varphi_{\max} f_0/\sigma_{\min})}{2\|B\|_2} - 1 < 0$$

or

$$\bar{h}^2 < \frac{2\|B\|_2}{a^2 f(\tau_0\varphi_{\max} f_0/\sigma_{\min})}.$$

Hence $v_1 - x \leq 0$ follows immediately from the assumptions. ∎

Combining above results we obtain immediately the following.

Theorem 3.9. *Assume that for* $\ell_0 \geq 0$,

(i) $\bar{h}^2 < \dfrac{2\|B\|_2}{a^2\varphi_{\max} f(\tau_{\ell_0}\varphi_{\max} f_{\ell_0}/\sigma_{\min})}$, *where* $\bar{h} = \max_{i=1,\ldots,N}\{h_i\}$,

(ii) $Mv_{\ell_0} + g(\varepsilon, v_{\ell_0}) > 0$,

If (3.17) *holds for all* $\ell \geq \ell_0$, *then the sequence* $\{v_\ell\}_{\ell\geq\ell_0}$ *produced by the semi-adaptive nonuniform scheme* (3.13) *increases monotonically until unity is reached or exceeded by one or more components of the solution vector, i.e., until quenching occurs.*

3.4 Stability

Nonlinear stability has been an extremely challenging issue when Kawarada equations are concerned [4, 20, 74, 75, 93, 94]. On the other hand, linear stability analysis may uncover crucial information for underlying schemes locally and asymptotically [74, 100]. In this section, we will carry out a standard stability analysis in the von Neumann sense for (3.13) with its nonlinear source term frozen. The analysis will then be extended to circumstances where the nonlinear term is not frozen.

In the following $\mu_2(A)$, where $A \in \mathbb{R}^{N\times N}$, represents the logarithmic norm of the matrix A associated to the spectral norm.

Lemma 3.10. *Let* P *be as in* (3.11). *Then* P *is congruent to a symmetric matrix. In particular,*

$$P = D^{-1/2} S D^{1/2} \in \mathbb{R}^{N\times N},$$

where

$$D = \operatorname{diag}(\delta_1, \ldots, \delta_N), \;\; S = \operatorname{tridiag}(\alpha_i, m_i, \alpha_i)$$

for which

$$\delta_j = \frac{h_{j-1} + h_j}{h_0 + h_1} \quad \textit{and} \quad \alpha_k = \sqrt{n_k l_k}.$$

Proof. The proof is clear by the definitions [19]. ∎

Lemma 3.11. *$\rho(P) \in (-\infty, 0]$, where $\rho(A) = \lambda_{\max}(AA^\intercal)$ for any $A \in \mathbb{R}^{N\times N}$.*

Proof. By Lemma 3.10 we have that P is congruent to a symmetric matrix, hence all eigenvalues of P are real [61]. Since P is diagonally dominant with negative diagonal elements, the result follows immediately from Geršhgorin's circle theorem [58, 64]. ∎

Lemma 3.12. *$\lambda(M) \subset (-\infty, 0)$ and $\mu_2(B^{1/2}PB^{1/2}) < 0$.*

Proof. Since $M = BP = B^{1/2}B^{1/2}P$, we have $B^{-1/2}M = B^{1/2}P$. Hence

$$B^{-1/2}M(B^{1/2})^\intercal = B^{1/2}PB^{1/2} = B^{1/2}P(B^{1/2})^\intercal$$

because B is diagonal. Further,

$$B^{-1/2}MB^{1/2} = B^{-1/2}BPB^{1/2} = B^{1/2}PB^{1/2}$$

is congruent to a symmetric matrix. Thus matrices $B^{-1/2}MB^{1/2}$ and P are congruent. Since the eigenvalues of P are real and negative, the eigenvalues of $B^{-1/2}MB^{1/2}$ and M must be real and negative.

Since we have $B^{-1/2}MB^{1/2} = B^{1/2}PB^{1/2}$, then the eigenvalues of $B^{1/2}PB^{1/2}$ are real and negative, which gives the result via Remark 2.3. ∎

Lemma 3.13. *If $\tau_k \geq 0$ for $0 \leq k \leq \ell$, then we have*

$$\left\| \prod_{k=0}^{\ell} E(\tau_k M) \right\|_2 \leq \sqrt{\kappa(B)} \equiv \sqrt{\|B^{-1}\|_2 \|B\|_2}.$$

Proof. We first show $E(\tau_k M) = B^{1/2}E(\tau_k B^{1/2}PB^{1/2})B^{-1/2}$ for $\tau_k \geq 0$. To this end, we have

$$B^{-1/2}E(\tau_k M)B^{1/2} = \sum_{j=0}^{\infty} \frac{\left(\tau_k B^{1/2}PB^{1/2}\right)^j}{j!} = E(\tau_k B^{1/2}PB^{1/2}). \tag{3.19}$$

It then follows from (3.19) and Lemma 2.5,

$$\left\| \prod_{k=0}^{\ell} E(\tau_k M) \right\|_2 = \left\| \prod_{k=0}^{\ell} \left(B^{1/2}E(\tau_k B^{1/2}PB^{1/2})B^{-1/2} \right) \right\|_2$$

$$
\begin{aligned}
&= \left\| B^{1/2} \left(\prod_{k=0}^{\ell} E(\tau_k B^{1/2} P B^{1/2}) \right) B^{-1/2} \right\|_2 \\
&\leq \|B^{1/2}\|_2 \|B^{-1/2}\|_2 \prod_{k=0}^{\ell} E(\tau_k \mu(B^{1/2} P B^{1/2})) \\
&\leq \sqrt{\kappa(B)}.
\end{aligned}
$$

∎

Lemma 3.14. *If* (3.17) *holds and* $\tau_k \geq 0$ *are sufficiently small for all* $0 \leq k \leq \ell$*, then*

$$
\left\| \prod_{k=0}^{\ell} \left(I - \frac{\tau_k}{2} M \right)^{-1} \left(I + \frac{\tau_k}{2} M \right) \right\|_2 \leq C,
$$

where C *is a constant independent of* ℓ *and* $\tau_k,\ 0 \leq k \leq \ell$*.*

Proof. Recalling the [1/1] Padé, we have

$$
\left(I - \frac{\tau_k}{2} M \right)^{-1} \left(I + \frac{\tau_k}{2} M \right) \ = \ E(\tau_k M) + \mathcal{O}\left(\tau_k^3\right), \quad \tau_k \to 0^+.
$$

for τ_k sufficiently small. By the definition of P and $\{\tau_\ell\}_{\ell \geq 0}$, we have $\sum_{k=0}^{\ell} \tau_k \leq T_q$ and $\tau = \max_{0 \leq k \leq \ell} \{\tau_k\} \leq 1$. Now, based on Lemma 3.13,

$$
\begin{aligned}
\left\| \prod_{k=0}^{\ell} \left(I - \frac{\tau_k}{2} M \right)^{-1} \left(I + \frac{\tau_k}{2} M \right) \right\|_2 &= \left\| \prod_{k=0}^{\ell} E(\tau_k M) + \mathcal{O}\left(\tau_k^3\right) \right\|_2 \\
&\leq \left\| \prod_{k=0}^{\ell} E(\tau_k M) \right\|_2 + c\tau^2 \sum_{k=0}^{\ell} \tau_k \\
&\leq \sqrt{\kappa(B)} + cT_q \\
&\leq C,
\end{aligned}
$$

which yields the desired bound. ∎

Combining the above results gives the following theorem.

Theorem 3.15. *If* (3.17) *holds and* $\tau_k \geq 0$ *are sufficiently small for all* $0 \leq k \leq \ell$*, then the semi-adaptive nonuniform method* (3.13) *with the stochastic source term*

frozen is unconditionally stable in the von Neumann sense under the spectral norm, that is,

$$\|z_{\ell+1}\|_2 \leq C\|z_0\|_2, \quad \ell \geq 0,$$

where $z_0 = v_0 - \tilde{v}_0$ is an initial error, $z_{\ell+1} = v_{\ell+1} - \tilde{v}_{\ell+1}$ is the $(\ell+1)$th perturbed error vector, and $C > 0$ is a constant independent of ℓ and τ_k for each $0 \leq k \leq \ell$.

Proof. When the nonlinear stochastic source term is frozen, $z_{\ell+1}$ takes the form of

$$z_{\ell+1} = \left(I - \frac{\tau_\ell}{2}M\right)^{-1}\left(I + \frac{\tau_\ell}{2}M\right) z_\ell, \quad \ell \geq 0. \tag{3.20}$$

Iterating (3.20) gives

$$z_{\ell+1} = \prod_{k=0}^{\ell}\left(I - \frac{\tau_k}{2}M\right)^{-1}\left(I + \frac{\tau_k}{2}M\right) z_0. \tag{3.21}$$

Taking the norm of both sides of (3.21), it follows that

$$\begin{aligned}\|z_{\ell+1}\|_2 &\leq \left\|\prod_{k=0}^{\ell}\left(I - \frac{\tau_k}{2}M\right)^{-1}\left(I + \frac{\tau_k}{2}M\right)\right\|_2 \|z_0\|_2 \\ &\leq C\|z_0\|_2,\end{aligned}$$

where C is a positive constant independent of ℓ and τ_k for each $0 \leq k \leq \ell$. ∎

We now consider the case without freezing the nonlinear stochastic source term in (3.13). In the following, let t_Q be the time at which numerical quenching occurs, that is, $\|v_Q\|_\infty \geq 1$, and recall that $t_m = t_0 + \sum_{k=0}^{m-1}\tau_k$ for any $m \geq 0$. Also, let

$$\Phi_k = \left(I - \frac{\tau_k}{2}M\right)^{-1}\left(I + \frac{\tau_k}{2}M\right), \ 0 \leq k \leq \ell.$$

Further, we need the following definition

Definition 3.16. If $v, w \in \mathbb{R}^N$, we define $\mathcal{L}(v, w)$ to be the set of line segments directed from v to w. That is, $\mathcal{L}(v, w) = \{v + t(w - v) \, : \, 0 \leq t \leq 1\}$. A vector $\xi \in \mathcal{L}(v, w)$ if and only if there exists some $t^* \in [0, 1]$ such that $\xi = v + t^*(w - v)$.

Theorem 3.17. *If* (5.14) *holds and* $\tau_k \geq 0$ *are sufficiently small for all* $0 \leq k \leq \ell$, *then the semi-adaptive nonuniform method* (3.13) *is unconditionally stable in the von Neumann sense, that is, for every* $t_m < t_Q$ *there exists a constant* $C(t_m) > 0$ *such that*

$$\|z_{\ell+1}\|_2 \leq C(t_m)\|z_0\|_2, \quad 0 \leq \ell \leq m,$$

where $z_0 = v_0 - \tilde{v}_0$ *is an initial error,* $z_{\ell+1} = v_{\ell+1} - \tilde{v}_{\ell+1}$ *is the* $(\ell+1)$*th perturbed error vector, and* $C(t_m) > 0$ *is a constant independent of* ℓ *and* τ_k *for each* $0 \leq k \leq \ell$.

Proof. By definition we have

$$v_{\ell+1} = \Phi_\ell \left(v_\ell + \frac{\tau_\ell}{2} g(\varepsilon, v_\ell) \right) + \frac{\tau_\ell}{2} g(\varepsilon, v_{\ell+1}), \quad \ell \geq 0.$$

It follows that

$$\begin{aligned} z_{\ell+1} &= \Phi_\ell z_\ell + \frac{\tau_\ell}{2}\Phi_\ell (g(\varepsilon, v_\ell) - g(\varepsilon, \tilde{v}_\ell)) + \frac{\tau_\ell}{2}(g(\varepsilon, v_{\ell+1}) - g(\varepsilon, \tilde{v}_{\ell+1})) \\ &= \Phi_\ell z_\ell + \frac{\tau_\ell}{2}\Phi_\ell g_v(\varepsilon, \xi_\ell) z_\ell + \frac{\tau_\ell}{2} g_v(\varepsilon, \xi_{\ell+1}) z_{\ell+1}, \end{aligned}$$

where $\xi_k \in \mathcal{L}(v_k, \tilde{v}_k),\ k = \ell, \ell+1$. Rearranging the above equality, we have

$$\left(I - \frac{\tau_\ell}{2} g_v(\varepsilon, \xi_{\ell+1}) \right) z_{\ell+1} = \Phi_\ell \left(I + \frac{\tau_\ell}{2} g_v(\varepsilon, \xi_\ell) \right) z_\ell.$$

Further, it follows that for τ_k being sufficiently small,

$$\left(I - \frac{\tau_k}{2} g_v(\varepsilon, \xi) \right)^{-1} = E\left(\frac{\tau_k}{2} g_v(\varepsilon, \xi) \right) + \mathcal{O}\left(\tau_k^2\right), \quad \tau_k \to 0^+$$

and

$$I + \frac{\tau_k}{2} g_v(\varepsilon, \xi) = E\left(\frac{\tau_k}{2} g_v(\varepsilon, \xi) \right) + \mathcal{O}\left(\tau_k^2\right), \quad \tau_k \to 0^+.$$

Thus, for $\tau_k \to 0^+$, we have

$$\begin{aligned} z_{\ell+1} &= \left(I - \frac{\tau_\ell}{2} g_v(\varepsilon, \xi_{\ell+1}) \right)^{-1} \Phi_\ell \left(I + \frac{\tau_\ell}{2} g_v(\varepsilon, \xi_\ell) \right) z_\ell \\ &= \left\{ \prod_{k=0}^{\ell} \left[E\left(\frac{\tau_k}{2} g_v(\varepsilon, \xi_{k+1}) \right) + \mathcal{O}\left(\tau_k^2\right) \right] \Phi_k \left[E\left(\frac{\tau_k}{2} g_v(\varepsilon, \xi_k) \right) + \mathcal{O}\left(\tau_k^2\right) \right] \right\} z_0 \end{aligned}$$

$$= \left\{ \prod_{k=0}^{\ell} \left[E\left(\frac{\tau_k}{2} g_v(\varepsilon, \xi_{k+1}) \right) \right] \Phi_k \left[E\left(\frac{\tau_k}{2} g_v(\varepsilon, \xi_k) \right) \right] + \mathcal{O}\left(\sum_{k=0}^{\ell} \tau_k^2 \right) \right\} z_0.$$

Setting $G(t_m) = \max_{0 \le k \le m} \|g_v(\varepsilon, \xi_k(t))\|_2$ and $\tilde{P} = B^{1/2} P B^{1/2}$ we have

$$\begin{aligned}
\|z_{\ell+1}\|_2 &\le \left\{ \left\| \prod_{k=0}^{\ell} E\left(\frac{\tau_k}{2} g_v(\varepsilon, \xi_{k+1}) \right) \Phi_k E\left(\frac{\tau_k}{2} g_v(\varepsilon, \xi_k) \right) \right\|_2 + c_1 \sum_{k=0}^{\ell} \tau_k^2 \right\} \|z_0\|_2 \\
&\le \left\{ \left\| \prod_{k=0}^{\ell} E\left(\frac{\tau_k}{2} g_v(\varepsilon, \xi_{k+1}) \right) E(\tau_k M) E\left(\frac{\tau_k}{2} g_v(\varepsilon, \xi_k) \right) \right\|_2 + c_2 \sum_{k=0}^{\ell} \tau_k^2 \right\} \|z_0\|_2 \\
&\le \left\{ \|\Psi_\ell\|_2 + c_3 \tau \sum_{k=0}^{\ell} \tau_k \right\} \|z_0\|_2 \\
&\le \left\{ \|\Psi_\ell\|_2 + c_3 \tau T_q \right\} \|z_0\|_2, \qquad (3.22)
\end{aligned}$$

where c_1, c_2, c_3 are constants independent of ℓ and $\tau_k,\ k = 0, 1, \ldots, \ell$, $\sum_{k=0}^{\ell} \tau_k \le T_q$, $\tau = \max_{k=0,\ldots,\ell}\{\tau_k\}$, and

$$\Psi_\ell = \prod_{k=0}^{\ell} E\left(\frac{\tau_k}{2} g_v(\varepsilon, \xi_{k+1}) \right) E(\tau_k M) E\left(\frac{\tau_k}{2} g_v(\varepsilon, \xi_k) \right).$$

It then follows that

$$\begin{aligned}
\|\Psi_\ell\|_2 &= \left\| \prod_{k=0}^{\ell} E\left(\frac{\tau_k}{2} g_v(\varepsilon, \xi_{k+1}) \right) E(\tau_k M) E\left(\frac{\tau_k}{2} g_v(\varepsilon, \xi_k) \right) \right\|_2 \\
&\le \left\| \prod_{k=0}^{\ell} E\left(\frac{\tau_k}{2} g_v(\varepsilon, \xi_{k+1}) \right) B^{1/2} E(\tau_k \tilde{P}) B^{-1/2} E\left(\frac{\tau_k}{2} g_v(\varepsilon, \xi_k) \right) \right\|_2 \\
&= \left\| \prod_{k=0}^{\ell} B^{1/2} E\left(\frac{\tau_k}{2} g_v(\varepsilon, \xi_{k+1}) \right) E(\tau_k \tilde{P}) E\left(\frac{\tau_k}{2} g_v(\varepsilon, \xi_k) \right) B^{-1/2} \right\|_2 \\
&= \left\| B^{1/2} \left[\prod_{k=0}^{\ell} E\left(\frac{\tau_k}{2} g_v(\varepsilon, \xi_{k+1}) \right) E(\tau_k \tilde{P}) E\left(\frac{\tau_k}{2} g_v(\varepsilon, \xi_k) \right) \right] B^{-1/2} \right\|_2 \\
&\le \sqrt{\kappa(B)} \prod_{k=0}^{\ell} \left\| E\left(\frac{\tau_k}{2} g_v(\varepsilon, \xi_{k+1}) \right) \right\|_2 \left\| E(\tau_k \tilde{P}) \right\|_2 \left\| E\left(\frac{\tau_k}{2} g_v(\varepsilon, \xi_k) \right) \right\|_2 \\
&\le \sqrt{\kappa(B)} \prod_{k=0}^{\ell} E(\tau_k G(t_m)) \\
&\le \sqrt{\kappa(B)} E\left(G(t_m) \sum_{k=0}^{\ell} \tau_k \right) \\
&\le \sqrt{\kappa(B)} E(G(t_m) T_q). \qquad (3.23)
\end{aligned}$$

Let

$$C(t_m) = \sqrt{\kappa(B)}E(G(t_m)T_q) + c_2\tau T_q.$$

Since $t_m < t_Q$, it follows that $G(t_m) < \infty$ for all $t_m < t_Q$. Combining (3.22) and (3.23) yields the desired stability. ∎

Remark 3.18. The nonuniform constant $G(t_m)$ is anticipated to be large within the interval $[t_0, t_m] \subset [t_0, t_Q)$. However, we observe in experiments that its values remain well-manageable as long as proper stopping criteria are adopted when implementing the algorithm. This allows for the claimed numerical stability.

3.5 Numerical Experiments

We consider the following degenerate stochastic Kawarada model problem in the first three experiments:

$$\sigma(x)u_t = \frac{1}{a^2}u_{xx} + \frac{\varphi(\varepsilon)}{(1-u)^\theta}, \quad -1 < x < 1,\ t_0 < t < T_q, \tag{3.24}$$

$$u(-1,t) = u(1,t) = 0, \quad t > t_0, \tag{3.25}$$

$$u(x,t_0) = u_0(x), \quad -1 < x < 1, \tag{3.26}$$

where $T_q < \infty,\ \theta > 0,\ u_0 \in C[-1,1]$, and $0 \le u_0 \ll 1$.

Without loss of generality, we set $\theta = 1$, $t_0 = 0$, $u_0(x) = 0.001(1 - \cos(2\pi x))$, $-1 \le x \le 1$, and let our temporal adaptations start once $v(t) = \max_{-1\le x\le 1} u(x,t)$ reaches a certain value v^*. In most computational procedures, we adopt $v^* = 0.90$ for such a triggering criterion [74]. The main purposes of our computations are to examine the numerical method developed, and to explore impacts of varying physical parameters used in the equation. In the first experiment we will focus on the consequences due to variations in domain sizes. Quenching behaviors and possible temporal blow-up times are recorded. The second experiment will illustrate impacts of the degeneracy on quenching profiles. The third experiment will explore the effects that a stochastic component may have on the numerical solution and quenching

criteria. Our semi-adaptive algorithm (3.13) coupled with (3.25), (3.26) is shown to be satisfactorily reliable, effective, and accurate. Finally, we extend our pursuits with a two-dimensional stochastic Kawarada equation problem to demonstrate the usability and effectiveness of our semi-adaptive infrastructure in higher-dimensional applications. For this two-dimensional extension, a typical LOD [110] strategy is used to mimic the one-dimensional structure.

Experiment 1

Letting $\sigma(x), \varphi(\epsilon) \equiv 1$ be fixed, we vary the value of the parameter a to study its effects on the quenching phenomenon. Since quenching, if it exists, must occur at $x_q = 0$ [74, 75], we may consider herein a set of symmetric grids for the simplicity of computations. We generate the nonuniform grids in the following way. Consider a parabola designed to have a prescribed minimum at $x_{\lfloor (N+2)/2 \rfloor}$ and a prescribed maximum at x_0 and x_{N+1}. Then a standard arc-length adaptation procedure based on the curvature [20] produces the nonuniform grid, which is scaled to fit $[-1, 1]$.

To commence, we adopt $a = 0.5$ and plot $u_0(x)$ and its reference temporal derivative in Figure 3.2 We note that the locations of the twin peaks of the initial function chosen and triple peaks of the temporal derivative are symmetric with respect to the origin.

Let $T_q = 1.0479$. In Figure 3.3, the left and right graphics show the two-dimensional heat flow of u and its velocity, u_t, respectively. It can be observed in the former that the heat flows smoothly and monotonically from the left to right. However, the multiple-peak maximal values quickly merge into one and the flow tends to be steady as time increases. Temporal locations of the slices in Figure 3.4 are chosen by evenly dividing the arc-length of the function $L(t) = \max_{-1 \le x \le 1} u(x, t)$. These plots again indicate that the solution u tends to be steady with limited changes, while the rate of change function quickly tapers and then diminishes when t tends

to T_q. Both the numerical solution u and temporal derivative u_t preserve symmetry about $x = 0$ as expected. The temporal adaptation is never activated as the maximum of the solution stays far below unity. The experimental results presented are consistent with existing results [74, 75, 84].

It is noticed in this experiment that u exists globally. More detailed profiles of the maximal values of u and u_t at different time levels are shown in Figure 3.5 for $0 \leq t \leq T_q$. Embedded figures are for u and u_t in terminal positions at $t = T_q$. It is again observed that while the solution u increases monotonically, the temporal derivative function u_t decreases after some initial disturbances. In the terminal position $T_0 = 1.05290729$, we have

$$\max_{-1\leq x\leq 1} u(x, T_0) \approx 0.14181367$$

and

$$\max_{-1\leq x\leq 1} u_t(x, T_0) \approx 1.46892335 \times 10^{-4}.$$

In the next experiment, we choose $a = 2$ in order to witness a quenching case for which the physical solution should exist only for finite time. We show three-dimensional profiles of the numerical solution u and its temporal derivative u_t in Figure 3.6 for $0 \leq t \leq T^*$ and $T^0 \leq t \leq T^*$, where $T^0 = 0.50928649$, respectively. A quenching time of $T^* \approx 0.50939149$ is observed. The sole purpose of using the temporal interval $[T^0, T^*]$ is to witness the explosive feature of u_t immediately prior to quenching. This corresponds to the last 105 time steps in computations. The curvature functions are again selected via the arc-length of the maximal value function of u. It is evident that while u quenches peacefully as $t \to T^*$, the function u_t blows up simultaneously.

More details of the maximal value profiles of u and u_t can be found in Figure 3.7. For additional information, we embed the terminal solution u and corresponding derivative u_t into the main frames. A logarithmic scale is used for u_t in order

to provide a better illustration of the explosive feature of the derivative function. The temporal adaptation is triggered automatically once $\max_{-1\leq x\leq 1} u \approx 0.90$, and remains activated throughout the remainder of computations.

Figure 3.8 shows the effect of domain size on quenching time. The numerical solutions based on 1000 different values of $a \in [0.7652281, 10.7552281]$ are computed, compared, and analyzed. The reason for choosing $a_1 = 0.7652281$ is that it is slightly larger than the theoretical critical size of $a^* \approx 0.76522804$ [36, 74]. The experiments indicate that the quenching time is longer when a is close to a_1, with a maximum $T^*_{a_1} = 9.75235001$. The quenching time then sharply decreases. These results firmly support theoretical expectations that the quenching time should approach infinity as the domain size decreases to a^*.

We also observe that the quenching time seems to have a lower threshold. Although the data acquired exhibit slight oscillations, the vibrations should not be caused by round-off errors, since various error-reduction measurements are utilized in our calculations. For example, we let the temporal step minimum $\tau_{\min} = c \times 10^{-6}$, where $c > 0$ is an usual floating point number. When a temporal derivative value is evaluated, we reformulate the original formula through modifications such as

$$v'_\ell \approx \frac{10^6(v_{\ell+1} - v_\ell)}{10^6 \tau_{min}} = \frac{v_{\ell+1} - v_\ell}{c} \times 10^6$$

which effectively reduces the risk of unfavorable round-off errors. Consequently, we obtain a final value of $T^*_{a_{1000}} \approx 0.51598431$.

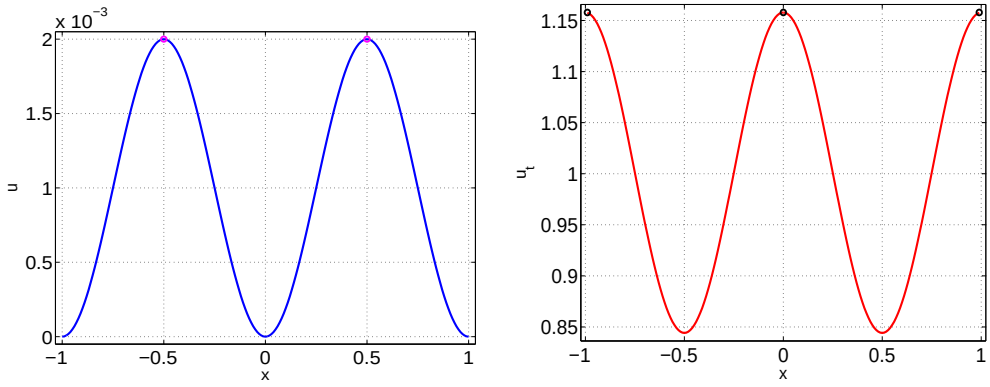

Figure 3.2: Initial function $u_0(x) = 0.001(1 - \cos(2\pi x))$ [LEFT] and its estimated temporal derivative via (3.24) [RIGHT]. Locations of multiple maximal values of the functions concerned are symmetric with respect to the origin.

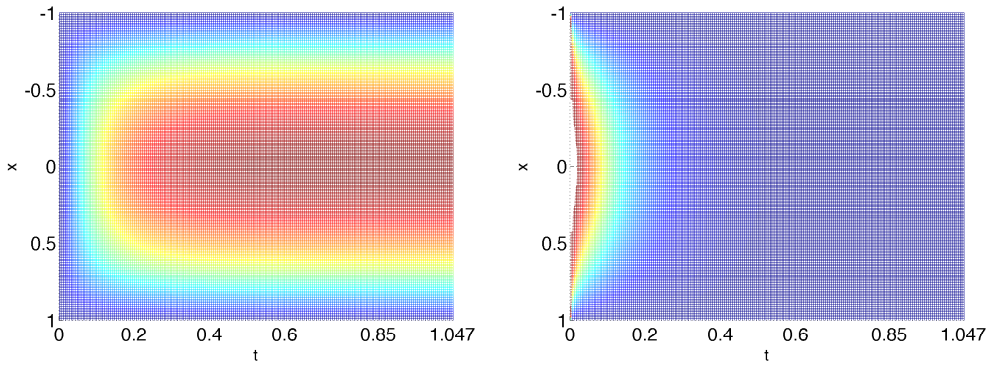

Figure 3.3: Two-dimensional thermal flow plots of the numerical solution u [LEFT] and u_t [RIGHT] for $t \in [0, T_q]$. It is observed that while the heat flows from the left to the right smoothly, symmetrically and increases monotonically in the first figure, the flow speed decreases rapidly but monotonically as time goes on. There is no quenching found in this situation.

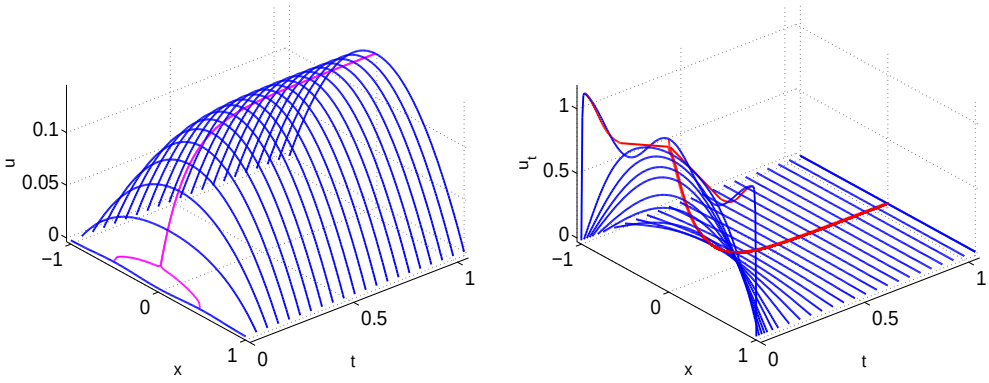

Figure 3.4: Three-dimensional plots of the numerical solution curvatures of u [LEFT] and u_t [RIGHT] for $t \in [0, T_q]$. The magenta curve represents the maximal value trajectory of u [LEFT], and the red curve is for that of u_t [RIGHT] at different t-levels for $0 < t \leq T_q$.

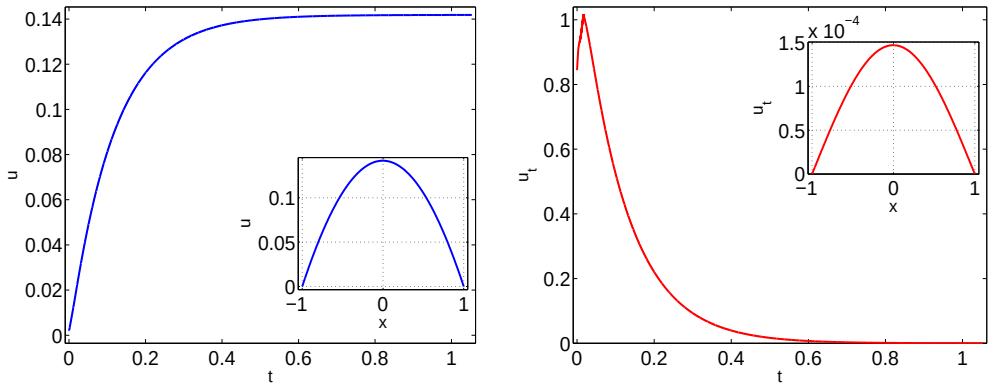

Figure 3.5: Curves in the main frames are for profiles of the maximal values of u [LEFT] and u_t (RIGHT). That is, they are plots of $\max_{-1\leq x\leq 1} u$, $0 \leq t \leq T_q$, and $\max_{-1\leq x\leq 1} u_t$, $0 < \epsilon \leq t \leq T_q$, respectively. The embedded graphics represent profiles of u [LEFT] and u_t [RIGHT] at time $t = T_q$. Up to 200,000 temporal steps have been executed. Temporal adaptation is never activated in this circumstance since no quenching is generated.

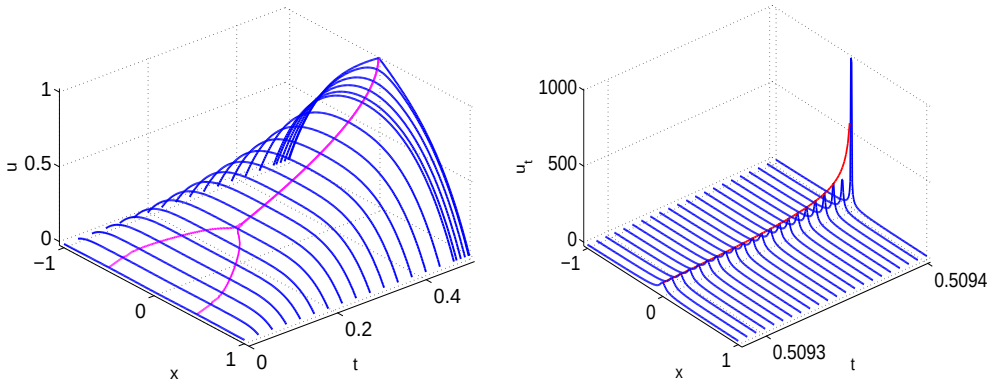

Figure 3.6: Three-dimensional curvature views of u, $0 \leq t \leq T^*$, [LEFT] and u_t, $T^0 \leq t \leq T^*$, [RIGHT] where $T^0 = 0.50928649$ and $T^* = 0.50939149$ are used. The magenta and red curves represent functions $\max_{-1\leq x\leq 1} u$ and $\max_{-1\leq x\leq 1} u_t$, respectively. The temporal derivative values concentrates about the quenching point with $\max_{-1\leq x\leq 1} u_t(x, T^*) > 985 \gg 1$.

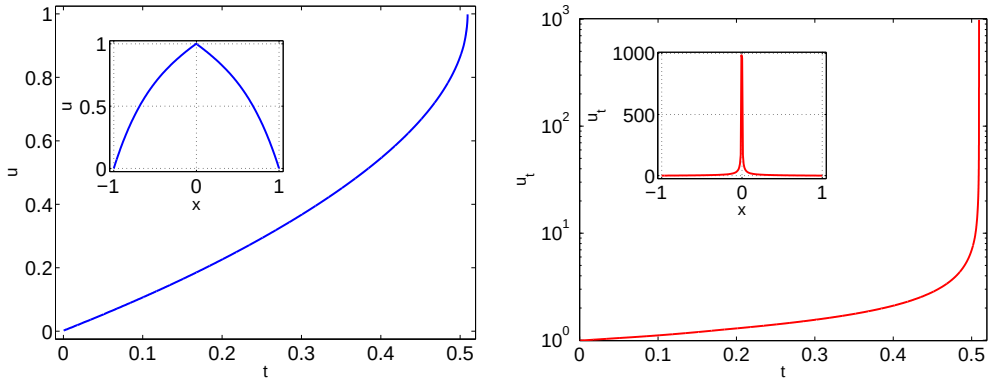

Figure 3.7: Maximal value profiles of the numerical solution u [LEFT] and u_t [RIGHT]. The mainframe curves are for $\max_{-1\leq x\leq 1} u$ and $\max_{-1\leq x\leq 1} u_t$ for $0 \leq t \leq 0.50939149$. The embedded graphics represent profiles of u and u_t immediately prior to quenching. The quenching time is observed to be $T^* \approx 0.50939149$.

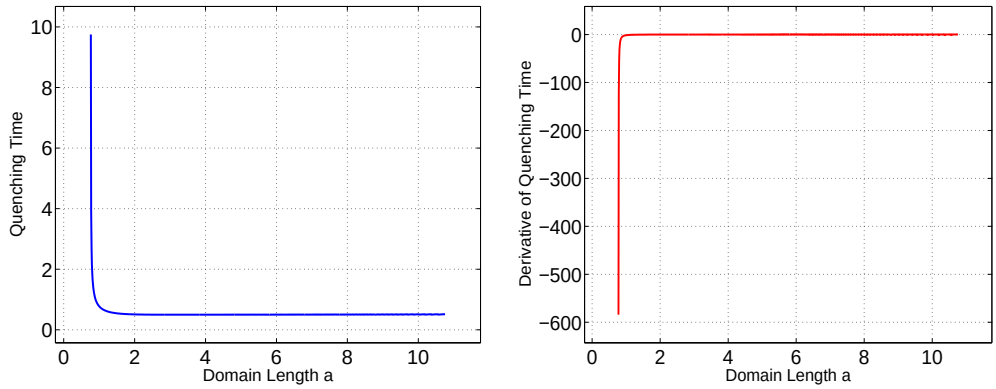

Figure 3.8: Illustrations of the dynamic connection between quenching times and domain sizes a [LEFT], and the rate of change of the quenching time with respect to a [RIGHT]. As a increases beyond a_1, quenching time declines rapidly until its minimal value $T^*_{a_{307}} \approx 0.49936094$, where $a_{307} = 3.8321581$. Once a increases beyond a_{307} the quenching time increases in a slightly oscillatory manner to reach $T^*_{a_{1000}}$.

Experiment 2

Let us consider $a = 2,\ \varphi(\varepsilon) \equiv 1$ and utilize the same initial function $u_0(x) = 0.001(1 - \cos(2\pi x))\ \ -1 \leq x \leq 1$. We now set our degenerate function to be $\sigma(x) = (x+1)^p(1-x)^{1-p},\ \ -1 \leq x \leq 1,\ 0 \leq p \leq 1$. Note that $\sigma(x)$ creates a degeneracy near each of the spatial boundaries of the problem (3.24)-(3.26). We commence by using the golden ratio $p = (\sqrt{5}-1)/2$.

We may observe in Figures 3.9 and 3.10 how the maximal values have shifted away from the center due to the degeneracy. The velocity map of u_t matches that of u in the thermal plots. To view more clearly the explosive profile of u_t, a time interval $[0.90543368, 0.90554168]$ is adopted in the second frames. Note that the temporal derivative u_t reaches its maximum at the quenching point with $\max_{x,t} u_t \approx 475.59028634$. Further, in Figures 3.10 and 3.11, we can observe that there is a remarkable shift of the local maximal values to the left of the origin when approaching quenching, as compared to cases without a degeneracy. The temporal adaptation is activated once $\max_{-1\leq x\leq 1} u \approx 0.90$ and remains active throughout the remainder of the computations.

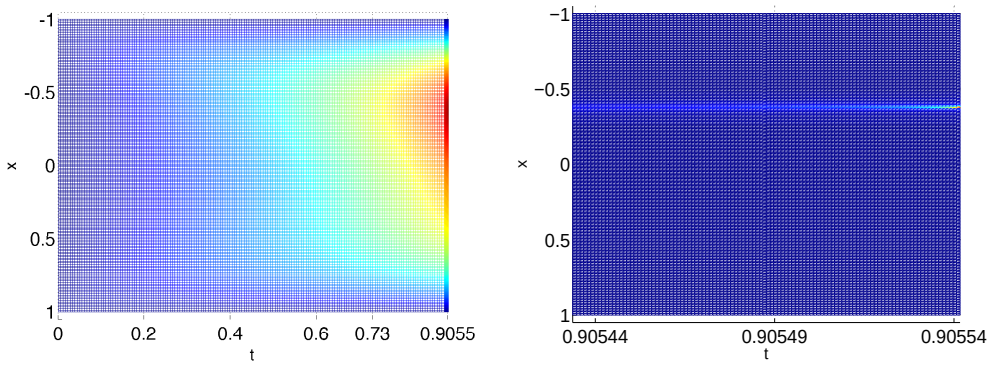

Figure 3.9: Two-dimensional thermal flows of the numerical solution u for $t \in [0, T_q]$ [LEFT], and u_t for $t \in [0.90543368, 0.90554168]$ [RIGHT]. In the former case, the heat flows smoothly and monotonically increases until quenching at $P = (-0.37870754, 0.90554168)$. Numerical solutions in last 105 temporal steps immediately before quenching are used for estimating u_t.

Figure 3.12 is designed to show possible relations between the quenching location and p, as well as the connections between the quenching time and p. Values of p are specified through the given degeneracy function $\sigma(x)$. It is found in our numerical experiments that the quenching position decays monotonically as p increases. Extreme values,

$$x^* = -0.55223881,$$

and

$$x^* = 0.55223881,$$

are taken for $p = 0,\ 1$, respectively. As expected, the quenching location is at the origin when $p = 1/2$. However, the decay of quenching location function is apparently nonlinear and exhibits a pattern of antisymmetry. It seems that the impact of p on quenching locations is relatively more significant for $p \in [0.4, 0.6]$.

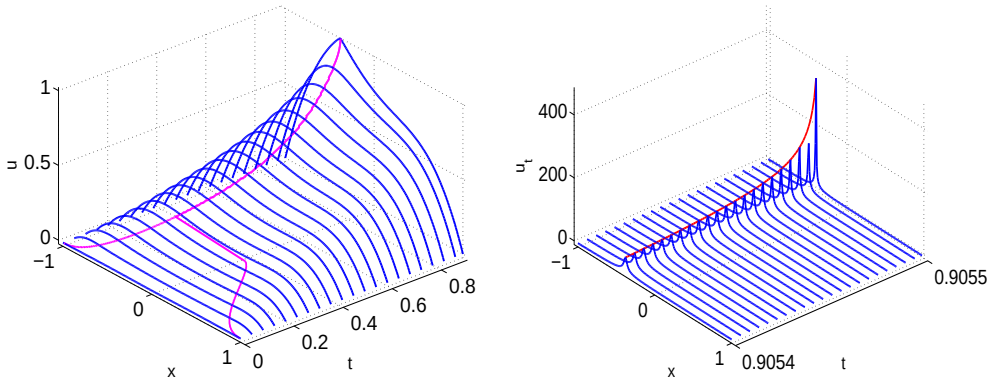

Figure 3.10: Three-dimensional views of u [LEFT] and u_t [RIGHT]. The blue three-dimensional curvature plots represent profiles of u and u_t at different times, respectively. While the magenta curves indicate $\max_{-1\leq x\leq 1} u$, the red curves are for $\max_{-1\leq x\leq 1} u_t$.

Further, for the range of p values used, we may observe that the minimal quenching time,

$$T^* \approx 0.39406344,$$

occurs as p approaches either 0^+ or 1^-. On the other hand, the maximum quenching time,

$$T^* \approx 0.964575643$$

can be witnessed at $p = 0.5$. The quenching time function is symmetric about $p = 0.5$ but again nonlinear. The impact of p on the quenching time is relatively more pronounced when p is closer to the end of its defined interval, that is, when $p \in [0, 0.12]$ or $p \in [0.88, 1]$.

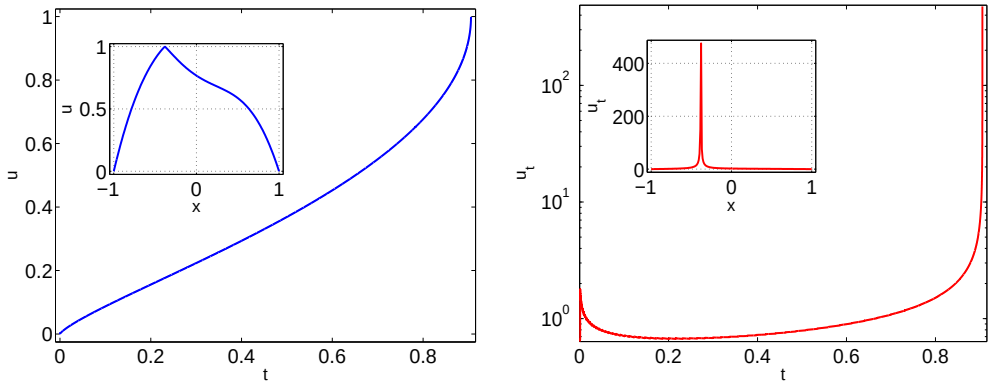

Figure 3.11: Profiles of the maximal values of the numerical solution u [LEFT] and its derivative u_t [RIGHT]. The two embedded pictures are for u and u_t in the last position immediately before quenching. The quenching location is $x^* = -0.37870754$ and the quenching time is $T_q \approx 0.90554168$ in the experiments which are well-agreeable with known results [4, 36, 74, 75].

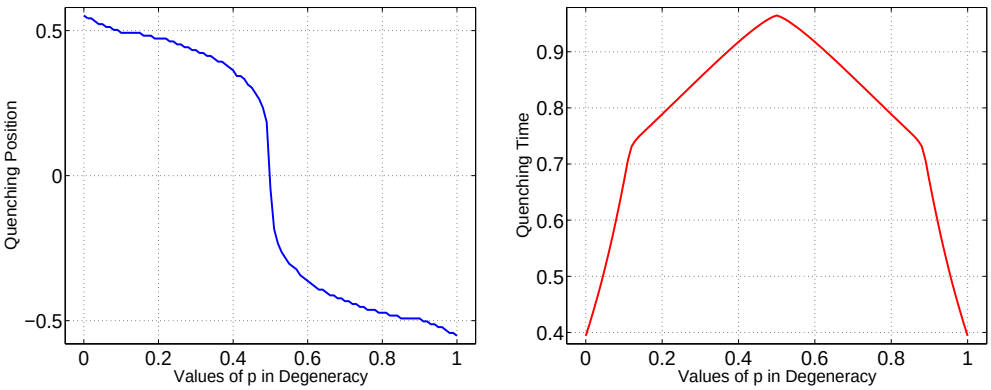

Figure 3.12: The left figure displays the relationship between quenching position and values of p in the degeneracy function $\sigma(x)$. The right picture, on the other hand, shows the connection between the quenching time and values of p in $\sigma(x)$. As expected, quenching position and time distribution should be symmetric about the value $p = 0.5$ [20, 22, 75].

Experiment 3

We proceed with $a = 2$ and $\sigma(x) \equiv 1$ in this particular exploration. In order to study the effects of the stochastic influence we consider the function $\varphi(\varepsilon) = \varepsilon^2,\ 0.01 \leq \varepsilon \leq 1$. In this example we explore the numerical solutions resulting from two different white noise vectors $\varepsilon(x)$. The purpose of these considerations is to investigate how slight changes in the vector $\varepsilon(x)$ can result in drastically different solutions profiles.

The two different random function outputs used in this experiment are displayed in Figure 3.13. Note that the vector $\varepsilon(x) = (\varepsilon_1, \ldots, \varepsilon_N)^\intercal$ is generated randomly, with each component consisting of a uniformly distributed random number $\varepsilon_i \in [0.01, 1],\ i = 1, \ldots, N$. Three-dimensional curvature views of the numerical solution u for $t \in [0, T_1]$ and and u_t for $t \in [T_1^0, T_1]$ corresponding the left random variable function are given in Figure 3.13. Values of $T_1^0 = 1.84873839$ and $T_1 = 1.84884339$ are used in the second frame. Again, the heat monotonically increases from left to right until quenching at

$$P = (0.02065323, 1.84884339).$$

On the other hand, the velocity u_t maximum trajectory matches that of u and explodes at the aforementioned quenching position P in an extremely short period of time. Numerical solutions in last 105 temporal steps immediately before quenching are displayed.

Note from Figures 3.14 and 3.15 how the location of quenching has shifted, just as in the degeneracy case, but this solution is slightly to the right of the origin. The most notable feature is the lack of an initial smoothness in the solution profile of u. The temporal adaptation is triggered once $\max_{-1 \leq x \leq 1} u \approx 0.90$ and remains active throughout the remainder of computations. Quenching occurs at $x^* = 0.06658575$ and the quenching time is $T_1^* \approx 1.84884339$.

Figures 3.16 and 3.17 are for the case when the second random output in Figure 3.13 is selected. $T_2^0 = 2.15900314$ and $T_2 = 2.15910814$ are utilized for u_t. The heat u flows smoothly and increases monotonically until quenching occurs at $P = (0.02065323, 2.15910814)$. On the other hand, the trajectory of the maximal velocity of u_t matches that of u. The temporal derivative explodes at the aforementioned quenching position P, with the maximal value reaching its peak here. Numerical solutions in last 105 temporal steps immediately before quenching are employed for the plot of u_t. It can also be seen that the stochastic source term causes the maximum value of the solution to shift drastically. The temporal adaptation is activated once $\max_{-1\leq x\leq 1} u \approx 0.90$ and remains active throughout the remainder of the computations.

To conclude this experiment, we reconsider the second case and generate the surface plots of the last 105 t-level numerical solutions before quenching in Figure 3.18. Note that in all sets of figures concerning stochastic influence, the quenching time is considerably longer. This is due to the fact that the constraints on ε dampen the effects of the source term, thereby increasing the amount of time for a solution component to reach unity. Further, note how small differences in the random function $\varphi(\varepsilon)$ can shift the quenching location to either side of the origin. It can also be observed in Figures 3.14-3.18 that the solution u becomes quite non-smooth near the quenching point. We may also note how differently the maximum values of the solution u flows with respect to time in Figures 3.14, 3.16, and 3.18. While the maximal values converge to the appropriate spatial position fairly quickly, their paths to that point are extremely different and erratic.

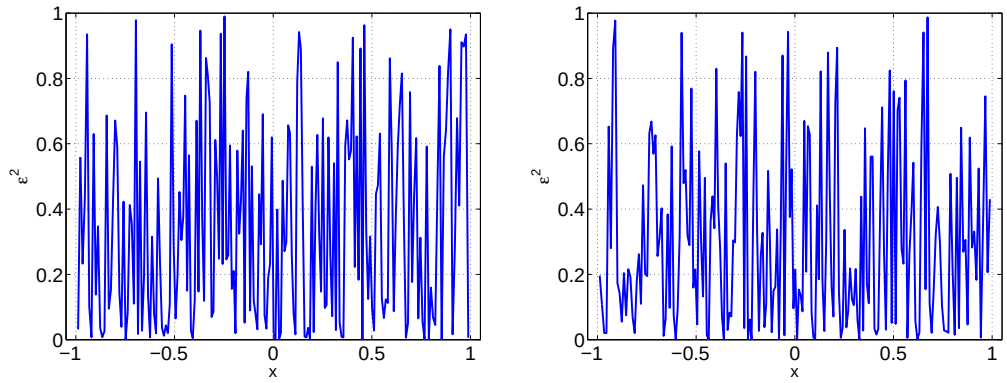

Figure 3.13: Plots of two different stochastic function values corresponding to $\varphi(\varepsilon) = \varepsilon^2$ are shown. Herewith we have $0.01 \leq \varepsilon \leq 1$.

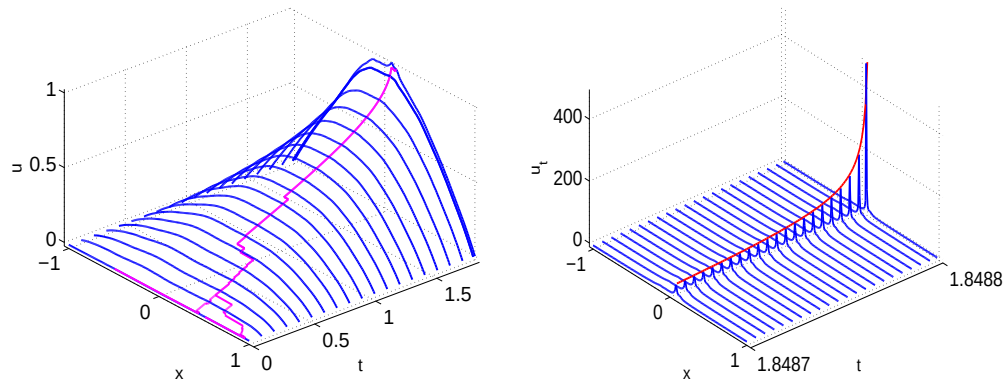

Figure 3.14: Three-dimensional curvature views of u [LEFT] and u_t [RIGHT] corresponding to the first set of random values. The blue lines represent profiles of u and u_t at different times, while the magenta and red lines represent $\max_{-1\leq x\leq 1} u$ and $\max_{-1\leq x\leq 1} u_t$, respectively. The temporal derivative has its largest values concentrated about the quenching point with $\max u_t \approx 484.14167207$.

Since the Lax equivalence theorem does not apply to nonlinear schemes such as (3.13), rigorous tests on the nonlinear convergence are in general important and need to be completed. But our experiments are carried out in cases when nonlinear source terms are linearized, similar to those in [19, 20, 74]. This linearization allows for the problem to be locally considered linear, and in this sense, convergence can be ensured through the numerical stability. Note that such an argument is only valid in the local sense, a global convergence analysis of the numerical method (3.13) must be conducted via chemical-physical energy conservation methods. Such an endeavor has been in our agenda and will be discussed carefully in future works. A numerical exploration of such nonlinear convergence phenomenon will be given in the following chapter.

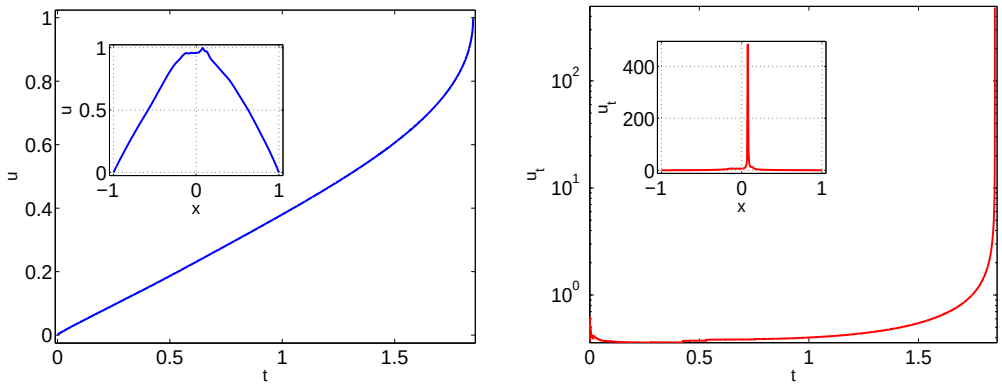

Figure 3.15: Profiles of the maximal values of the numerical solution u [LEFT] and its derivative u_t [RIGHT]. The two embedded pictures are for u and u_t in the last position immediately before quenching.

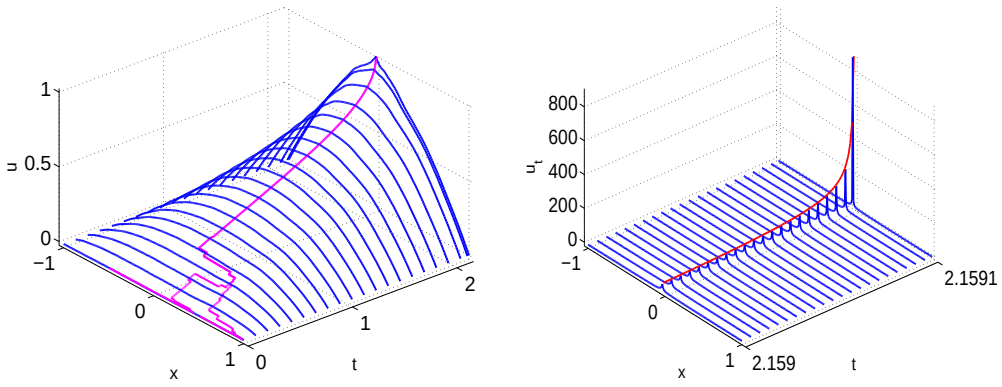

Figure 3.16: Three-dimensional curvature views of u [LEFT] and u_t [RIGHT]. The blue lines represent profiles of u and u_t at different times, while the magenta and red lines represent $\max_{-1\le x\le 1} u$ and $\max_{-1\le x\le 1} u_t$, respectively. The temporal derivative has its largest values concentrated about the quenching point with $\max u_t \approx 885.07977535$.

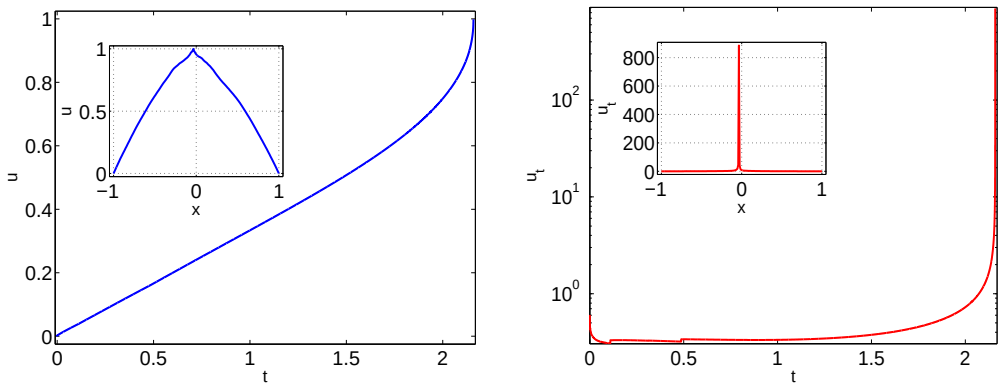

Figure 3.17: Profiles of the maximal values of the numerical solution u [LEFT] and its derivative u_t [RIGHT]. The two embedded pictures are for u and u_t in the last position immediately before quenching. The quenching location is $x^* = -0.04359769$ and the quenching time is $T_2^* \approx 2.15910814$.

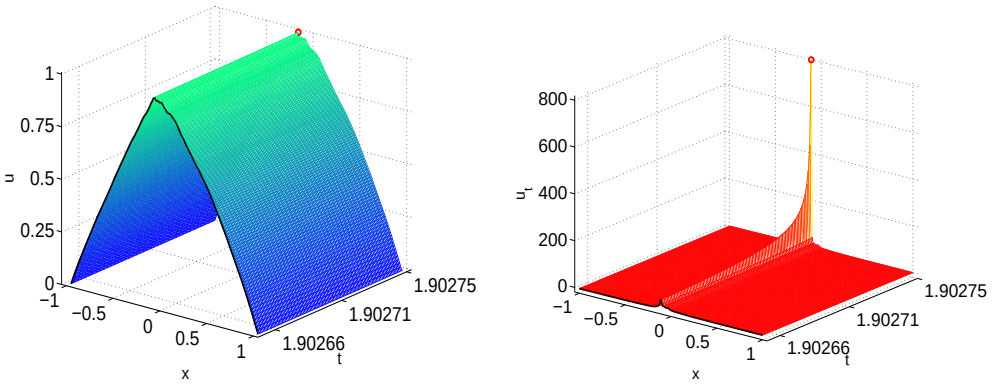

Figure 3.18: More detailed three-dimensional surface views of u [LEFT] and u_t [RIGHT]. Both surfaces increase monotonically with respect to the time. The function u and its temporal derivative have their largest values concentrated about the quenching point with $\max u \approx 0.99888386$ and $\max u_t \approx 799.51622462$. Quenching time $T^* \approx 1.90275250$.

Experiment 4

We now consider the following two-dimensional problem:

$$\sigma(x,y)u_t = \frac{1}{a^2}u_{xx} + \frac{1}{b^2}u_{yy} + \frac{\varphi(\varepsilon)}{(1-u)^\theta}, \quad -1 < x,y < 1,\ t_0 < t \le T_q, \tag{3.27}$$

$$u(-1,y,t) = u(1,y,t) = u(x,-1,t) = u(x,1,t) = 0, \quad t > t_0, \tag{3.28}$$

$$u(x,y,t_0) = u_0(x,y), \quad -1 < x,y < 1, \tag{3.29}$$

where $T_q < \infty,\ \theta > 0,\ u_0(x,y) \in C[[-1,1]\times[-1,1]]$, and $0 \le u_0 \ll 1$. Without loss of generality, we choose $a = b = 2$, $\theta = 1$, $t_0 = 0$, and $u_0(x,y) = 0.001(1-\cos(2\pi x))(1-\cos(2\pi y))$, $1 \le x,y \le 1$. For simplicity we once again set $\sigma(x,y) \equiv 1,\ -1 \le x,y \le 1$, and $\varphi(\varepsilon) = \varepsilon^2,\ 0.01 \le \varepsilon \le 1$. We wish to demonstrate that the stochastic effects exhibited in the previous experiment are still present in a significant manner in the two-dimensional case. To this end, we first approximate (3.27)-(3.29) via a standard nonuniform LOD method [19, 20, 93, 94, 110].

Figure 3.19 depicts the three-dimensional profiles of the solution u and its derivative u_t, immediately prior to quenching. Note that $T_q \approx 2.56418014$ is the observed quenching time. As in the previous experiment, we have experienced a

Table 3.1: Experimental quenching locations $P_k^* = (x_k^*, y_k^*),\ k = 1, \ldots, 5$, due to stochastic influences. Drifting effects can be clearly observed.

k	x_k^*	y_k^*
1	0.03482587	-0.01492537
2	0.03703703	-0.06172839
3	0.01234568	-0.01234568
4	0.08641975	0.06172840
5	-0.01234568	0.01234568

slight increase in quenching times as compared to existing results for , $\sigma(x, y), \varphi(\varepsilon) \equiv 1$ [19, 20, 74].

Projections of $\max_{-1\le y\le 1} u(x, y, t)$ and $\max_{-1\le x\le 1} u_t(x, y, t)$, respectively, are depicted in Figure 3.20. In the absence of stochastic influences, the theoretical spatial quenching location should be $P = (0, 0)$. We observe that the spatial quenching position has shifted to

$$P^* = (0.03482587, -0.01492537)$$

under the influence of the present stochastic source term. Repeated experiments with varying stochastic influence functions suggest a similar phenomenon. We list results of five randomly selected stochastic functions in Table 3.1 as an illustration. The purpose of such repeated experiments are to explore the extent of the influence that a stochastic source term may have on quenching position. We note similarities between the plots in Figure 3.20 and those for one-dimensional cases, in the sense that the quenching location has been disturbed. This is to be expected, as the results demonstrate that the propagation of the nonsmooth feature is not limited to one-dimensional situations only.

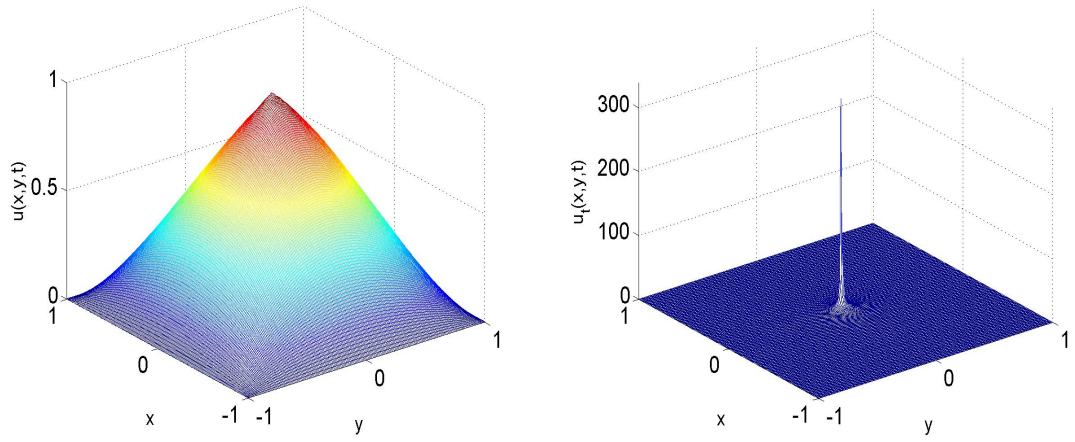

Figure 3.19: Three-dimensional views of u [LEFT] and u_t [RIGHT] immediately prior to quenching. Quenching is observed to occur at $T_q \approx 2.56418014$. The temporal derivative is observed to reach a maximal value $\max u_t \approx 331.04812435$. The blow-up of u_t is concentrated around the observed spatial quenching point.

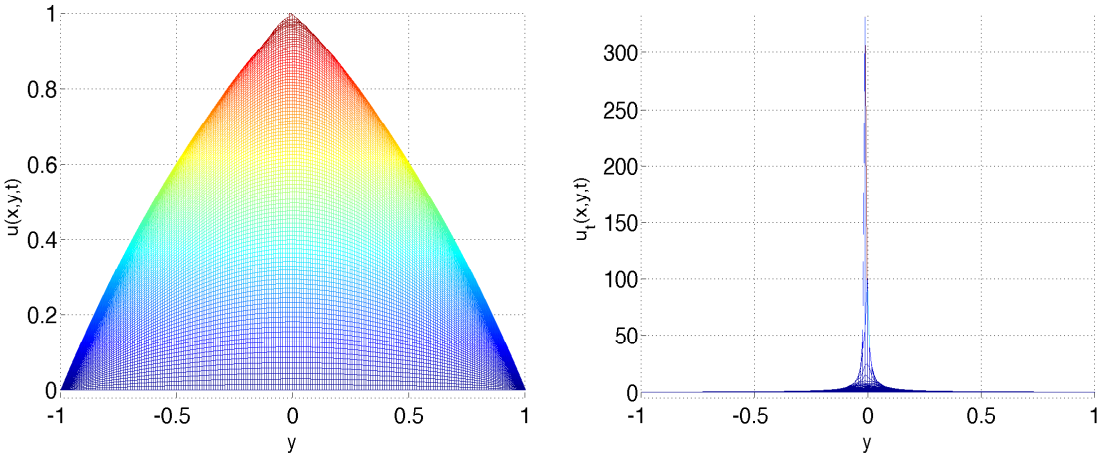

Figure 3.20: Projections of u [LEFT] and u_t [RIGHT] onto the xu-plane and xu_t-plane immediately prior to quenching, respectively. A slight shift of the location of maximum values is observed. It is evident that the solution smoothness is once again affected slightly by the presence of the stochastic influence in reactions.

CHAPTER FOUR

The Two-Dimensional Degenerate Stochastic Kawarada Equation

4.1 Introduction

Let $\Omega = (-a, a)\times(-b, b) \subset \mathbb{R}^2$ be an idealized combustion chamber, $\partial\Omega = \bar{\Omega}\backslash\Omega$ be its boundary, and $\mathcal{D} = \Omega \times (t_0, T_q)$, $\mathcal{S} = \partial\Omega \times (t_0, T_q)$, where $a, b > 0$, $0 \le t_0 < T_q < \infty$ with T_q being the terminal time. Further, let $U > 0$ be the ignition temperature. If $u(x, y, t)$ denotes the temperature distribution within the chamber, we have the following two-dimensional model generalized from the original Kawarada configuration [69]:

$$\mathscr{L}u = f(\varepsilon, u), \quad (x, y, t) \in \mathcal{D}, \tag{4.1}$$

$$u(x, y, t) = 0, \quad (x, y, t) \in \mathcal{S}, \tag{4.2}$$

$$u(x, y, t_0) = u_0(x, y) \ll c, \quad (x, y) \in \Omega, \tag{4.3}$$

where

$$\mathscr{L} := \sigma(x, y)\partial_t - \Delta,$$

and Δ is the standard two-dimensional Laplacian. The degeneracy function $\sigma(x, y)$ is nonnegative for $x \in \bar{\Omega}$ that vanishes only for $(x, y) \in \partial\Omega_0 \subseteq \partial\Omega$. The nonlinear stochastic reaction term, $f(\varepsilon, u)$ with a bounded stochastic influence $\varepsilon(x, y)$, satisfies the following properties

$$f(\varepsilon, 0) = f_0(\varepsilon) > 0, \quad f_u(\varepsilon, u) > 0, \quad \lim_{u\to U^-} f(\varepsilon, u) = \infty, \quad \int_0^U f(\varepsilon, u)\, du = \infty$$

for each fixed $(x, y) \in \Omega$ and $u \in [0, U)$. The stochastic influence is characterized by

$$0 < f^{\varepsilon}_{\min} \le \min_{x,y}\{f(\varepsilon, u)\} \quad \text{and} \quad \max_{x,y}\{f(\varepsilon, u)\} \le f^{\varepsilon}_{\max} \ll \infty$$

for each $u \in [0, U)$. Once again, we recall the definition of quenching, (1.4), and its associated necessary condition (1.5). We may note that quenching is a mathematical

interpretation of the fuel ignition/combustion process in physics. Since $T_q < \infty$ only when certain spatial references, such as the size and shape of Ω, reach their critical limits, a domain Ω_* is called a *critical domain* of (4.1)-(4.3) if the solution of (4.1)-(4.3) exists globally for $\Omega \subseteq \Omega_*$ and (1.5) occurs as $\Omega_* \subseteq \Omega$. We recall that such critical domains are not unique in multidimensional circumstances, since both the *size* and *shape* of Ω affect whether or not combustion occurs [20, 21, 37, 39]. Hence, any explorations of the critical domain may only proceed after first fixing the shape of the domain.

Highly effective and efficient algorithms for solving Kawarada equations such as (4.1)-(4.3) have been difficult to obtain due to the highly nonlinear mechanism inherent to the problem. There has been much effort to develop algorithms that may accurately predict the ignition location and time, solution profiles, and critical domain characteristics, while reasonably conserving the solution positivity and monotonicity [33, 34, 39, 74, 75, 107]. While explorations have been carried out on both uniform and nonuniform grids, as well as via adaptive grids, rigorous analysis of different schemes involving nonuniform grids has remained incomplete. To improve computational efficiency, splitting strategies have been introduced and incorporated into numerical procedures while taking advantage of adaptive temporal grid structures [21, 75, 79]. The success of such combinations has also become a key motivation for the study to be presented in this chapter.

Rigorous mathematical analysis is developed for a highly vibrant method based upon semi-discretization for solving (4.1)-(4.3) in this chapter. In the next section, we verify carefully the order of accuracy of the scheme proposed. In Sections 4.3 and 4.4, we prove that the solution of the semi-discretized system, as well as the corresponding scheme, preserve the expected solution positivity and monotonicity under reasonable restrictions. Section 4.5 is devoted to standard and reinforced stability analysis of the numerical method. Experimental results to validate our analysis and

explore global nonlinear convergence of the singular stochastic Kawarada solutions are presented in Section 4.6.

4.2 Derivation of Scheme

Throughout this chapter, we set $U = 1$. Utilizing transformations $\tilde{x} = x/a,\ \tilde{y} = y/b$, and reusing the original variables for notation simplicity, we may reformulate (4.1)-(4.3) as

$$u_t = \frac{1}{a^2\sigma}u_{xx} + \frac{1}{b^2\sigma}u_{yy} + g(\varepsilon, u), \quad (x, y, t) \in \mathcal{D}, \tag{4.4}$$

$$u(x, y, t) = 0, \quad (x, y, t) \in \mathcal{S}, \tag{4.5}$$

$$u(x, y, t_0) = u_0(x, y) \ll 1, \quad (x, y) \in \Omega, \tag{4.6}$$

where $\Omega = (-1, 1)\times(-1, 1) \subset \mathbb{R}^2$ and $g(\varepsilon, u) = f(\varepsilon, u)/\sigma(x, y)$. For fixed $N_x, N_y \gg 1$ we define

$$\begin{aligned}\Omega_h &= \{(x_i, y_j) : 0 \le i \le N_x + 1;\ 0 \le j \le N_y + 1\},\\ \Omega_h^\circ &= \{(x_i, y_j) : 0 < i < N_x + 1;\ 0 < j < N_y + 1\},\end{aligned}$$

where $x_0 = y_0 = -1,\ x_{i+1} - x_i = h_{x,i} > 0,\ y_{j+1} - y_j = h_{y,j} > 0$ for $0 \le i \le N_x,\ 0 \le j \le N_y$, and $x_{N_x+1} = y_{N_y+1} = 1$. Let $u_{i,j}(t)$ denote an approximation of the solution of (4.4)-(4.6) at $(x_i, y_j, t) \in \Omega_h \times [t_0, T_q)$. We consider the following nonuniform finite difference formulas [75],

$$\partial_x^2 u(x_i, y_j, t) \approx \frac{2u_{i-1,j}(t)}{h_{x,i-1}(h_{x,i-1} + h_{x,i})} - \frac{2u_{i,j}(t)}{h_{x,i-1}h_{x,i}} + \frac{2u_{i+1,j}(t)}{h_{x,i}(h_{x,i-1} + h_{x,i})}, \tag{4.7}$$

$$\partial_y^2 u(x_i, y_j, t) \approx \frac{2u_{i,j-1}(t)}{h_{y,j-1}(h_{y,j-1} + h_{y,j})} - \frac{2u_{i,j}(t)}{h_{y,j-1}h_{y,j}} + \frac{2u_{i,j+1}(t)}{h_{y,j}(h_{y,j-1} + h_{y,j})}, \tag{4.8}$$

for $(x_i, y_j) \in \Omega_h^\circ$. Further, for a standard lexicographical ordering, we denote $v(t) = (u_{1,1}, u_{2,1}, \ldots,\ u_{N_x,1}, u_{1,2}, \ldots, u_{N_x,N_y})^\intercal \in \mathbb{R}^{N_xN_y}$, and let $g(\varepsilon, v)$ be a suitable discretization of the nonlinear reaction term in (4.4). We derive from from (4.4)-(4.6) the following semi-discretized system

$$v'(t) = Mv(t) + g(\varepsilon, v(t)), \quad t_0 < t < T_q, \tag{4.9}$$

$$v(t_0) \;=\; v_0. \tag{4.10}$$

Denote $h_{\min} = \min_{1\le i\le N_x;1\le j\le N_y}\{h_{x,i-1}h_{x,i}, h_{y,j-1}h_{y,j}\}$ and

$$M_x = \frac{1}{a^2}B(I_{N_y}\otimes P_x),\ M_y = \frac{1}{b^2}B(P_y\otimes I_{N_x}),\ M = M_x + M_y,$$

where $\otimes$ stands for the Kronecker product, $I_{N_\alpha}\in\mathbb{R}^{N_\alpha\times N_\alpha},\ \alpha = x, y$, are identity matrices. Further, let

$$\begin{aligned} B &= \operatorname{diag}\left(\sigma_{1,1}^{-1},\sigma_{2,1}^{-1},\ldots,\sigma_{N_x,1}^{-1},\sigma_{1,2}^{-1},\ldots,\sigma_{N_x,N_y}^{-1}\right)\in\mathbb{R}^{N_xN_y\times N_xN_y},\\ P_\alpha &= \operatorname{tridiag}\left(h_{\min}^{-1}l_{\alpha,i}, h_{\min}^{-1}m_{\alpha,i}, h_{\min}^{-1}n_{\alpha,i}\right)\in\mathbb{R}^{N_\alpha\times N_\alpha},\quad \alpha = x, y, \end{aligned}$$

and for the above,

$$\begin{aligned} l_{\alpha,j} &= \frac{2h_{\min}}{h_{\alpha,j}(h_{\alpha,j}+h_{\alpha,j+1})},\quad n_{\alpha,j} = \frac{2h_{\min}}{h_{\alpha,j}(h_{\alpha,j-1}+h_{\alpha,j})},\quad j = 1,\ldots,N_\alpha-1,\\ m_{\alpha,j} &= -\frac{2h_{\min}}{h_{\alpha,j-1}h_{\alpha,j}},\quad j = 1,\ldots,N_\alpha;\ \alpha = x, y. \end{aligned}$$

The formal solution of (4.9), (4.10) is

$$v(t) = E(tM)v_0 + \int_{t_0}^{t} E((t-s)M)g(\varepsilon, v(s))\,ds,\quad t_0 < t < T_q, \tag{4.11}$$

where $E(\cdot)$ is the corresponding matrix exponential [54,64,75]. An aim of this chapter is to investigate a highly efficient numerical procedure for solving the problem (4.9)-(4.11).

To this end, we consider the following realization of (4.11) on variable temporal grids:

$$v_{k+1} = E(\tau_k M)v_k + \int_{t_k}^{t_{k+1}} E((t_{k+1}-s)M)g(\varepsilon, v(s))\,ds,\quad k = 0,1,\ldots \tag{4.12}$$

where v_k and v_{k+1} are approximations to $v(t_k)$ and $v(t_{k+1})$, respectively, v_0 is the initial vector, $t_k = t_0 + \sum_{j=0}^{k-1}\tau_j$, $0 < \tau_k \ll 1$, $k = 0,1,2,\ldots$, and $\{\tau_k\}_{k\ge 0}$ is a set of adaptive temporal steps. In fact, a fast temporal step refinement mechanism must be triggered robotically as t_k approaches the quenching time, since u_t may grow

exponentially and affect computations near quenching points [36, 84, 99]. On the other hand, an overly refined grid should also be avoided for the sake of efficiency and accuracy [17,50,73]. In light of these concerns, a standard arc-length monitoring function may be implemented to generate the temporal steps and handle the strong nonlinearity at quenching [19,39,50,74,75,79]. Such monitoring functions have been discussed in Section 3.2.

Further, to avoid the need for nonlinear iterative methods to solve the derived nonlinear algebraic systems, in computations we replace $g(\varepsilon, v_{k+1})$ by $g(\varepsilon, w_k)$, where w_k is a suitable approximation to v_{k+1} with the proper order of accuracy [20,93,94]. However, no such approximation is utilized in the following analysis.

We have the following weighted approximation.

Lemma 4.1. *Assume that $f(\varepsilon, u) \in C_c^2(\mathcal{D})$ and $\tau_k \to 0^+$. Then for $\theta \in [0, 1]$ we have*

$$\int_{t_k}^{t_{k+1}} E((t_{k+1} - s)M)g(\varepsilon, v(s))\, ds - M^{-1}[E(\tau_k M) - I][\theta g(\varepsilon, v_k) + (1 - \theta)g(\varepsilon, v_{k+1})],$$

is order p, where $p = 2$ when $\theta = 1/2$, and $p = 1$ otherwise.

Proof. We begin with the following difference

$$\begin{aligned} \eta_k &= \int_{t_k}^{t_{k+1}} E((t_{k+1} - s)M)g(\varepsilon, v(s))\, ds \\ &\qquad - \int_{t_k}^{t_{k+1}} E((t_{k+1} - s)M)[\theta g(\varepsilon, v_k) + (1 - \theta)g(\varepsilon, v_{k+1})]\, ds. \end{aligned}$$

Replace the first integral by a trapezoidal rule and integrate the second directly to obtain

$$\begin{aligned} \eta_k &= \frac{\tau_k}{2}\left[g(\varepsilon, v_{k+1}) + E(\tau_k M)g(\varepsilon, v_k)\right] \\ &\qquad - M^{-1}[E(\tau_k M) - I][\theta g(\varepsilon, v_k) + (1 - \theta)g(\varepsilon, v_{k+1})] \end{aligned}$$

to order three, as $\tau_k \to 0^+$. We now consider local expansions of each of the terms.

$$E(\tau_k M)g(\varepsilon, v_k) = g(\varepsilon, v_k) + \tau_k M g(\varepsilon, v_k) + \frac{\tau_k^2}{2} M^2 g(\varepsilon, v_k) + \mathcal{O}\left(\tau_k^3\right), \quad \tau_k \to 0^+$$

$$
\begin{aligned}
g(\varepsilon, v_{k+1}) &= g(\varepsilon, v_k) + g_v(\varepsilon, v_k)(v_{k+1} - v_k) + \frac{1}{2} g_{vv}(\varepsilon, v_k)(v_{k+1} - v_k)^2 \\
&\qquad + \mathcal{O}\left(\|v_{k+1} - v_k\|^3\right), \quad \tau_k \to 0^+ \\
&= g(\varepsilon, v_k) + \tau_k g_v(\varepsilon, v_k) v_k' \\
&\qquad + \frac{\tau_k^2}{2} g_{vv}(\varepsilon, v_k)(v_k')^2 + \mathcal{O}\left(\|\tau_k v_k'\|^3\right), \quad \tau_k \to 0^+ \\
&= g(\varepsilon, v_k) + \tau_k g_v(\varepsilon, v_k) v_k' + \mathcal{O}\left(\tau_k^2\right), \quad \tau_k \to 0^+
\end{aligned}
$$

$$
M^{-1}[E(\tau_k M) - I][\theta g(\varepsilon, v_k)] = \tau_k \theta g(\varepsilon, v_k) + \frac{\tau_k^2 \theta}{2} M g(\varepsilon, v_k) + \mathcal{O}\left(\tau_k^3\right), \quad \tau_k \to 0^+
$$

$$
\begin{aligned}
&M^{-1}[E(\tau_k M) - I][(1-\theta) g(\varepsilon, v_{k+1})] \\
&\quad = (1-\theta)\left[\tau_k + \frac{\tau_k^2}{2} M\right] g(\varepsilon, v_k) + \tau_k^2 (1-\theta) g_v(\varepsilon, v_k) v_k' + \mathcal{O}\left(\tau_k^3\right), \quad \tau_k \to 0^+
\end{aligned}
$$

In the above we have used the notation $(v_{k+1} - v_k)^2$ and $(v_k')^2$ to represent $(v_{k+1} - v_k) \otimes (v_{k+1} - v_k)$ and $(v_k') \otimes (v_k')$, respectively. A direct comparison then leads to.

$$
\eta_k = \frac{\tau_k^2}{2} g_v(\varepsilon, v_k) v_k' - (1-\theta)\tau_k^2 g_v(\varepsilon, v_k) v_k' + \mathcal{O}\left(\tau_k^3\right), \quad \tau_k \to 0^+,
$$

and apparently, the approximation is first-order unless $\theta = 1/2$, in which case the approximation is second-order. ∎

Let $\Phi_{x,k} \equiv E(\tau_k M_x/2)$, $\Phi_{y,k} \equiv E(\tau_k M_y)$, and $\Phi_k \equiv \Phi_{x,k}\Phi_{y,k}\Phi_{x,k}$. We further denote $F(\varepsilon, v_k, v_{k+1}, \theta) \equiv \theta g(\varepsilon, v_k) + (1-\theta) g(\varepsilon, v_{k+1})$. Thus, from (4.12) and Lemma 4.1 we acquire that

$$
\begin{aligned}
v_{k+1} &= E(\tau_k M) v_k + \int_{t_k}^{t_{k+1}} E((t_{k+1} - s) M) F(\varepsilon, v_k, v_{k+1}, \theta)\, ds + \mathcal{O}\left(\tau_k^{p+1}\right) \\
&= E(\tau_k M) v_k + M^{-1}\left[E(\tau_k M) - I\right] F(\varepsilon, v_k, v_{k+1}, \theta) + \mathcal{O}\left(\tau_k^{p+1}\right) \\
&= \Phi_k v_k + M^{-1}\left[\Phi_k - I\right] F(\varepsilon, v_k, v_{k+1}, \theta) + \mathcal{O}\left(\tau_k^{p+1}\right), \quad \tau_k \to 0^+, \qquad (4.13)
\end{aligned}
$$

where $\theta \in [0, 1]$ is a fixed parameter, and $p \in \{1, 2\}$ depending upon the choice of θ. We note that the stochastic influences are completely contained in the vector-valued function $F(\varepsilon, v_k, v_{k+1}, \theta)$.

Before proceeding, we would like to note that, in general, (4.7) and (4.8) are first-order approximations [64,75]. The following lemma demonstrates that in certain cases the accuracy can be increased to second-order.

Lemma 4.2. *If the nonuniform grid Ω_h is the image of a uniform grid on Ω via a smooth mapping, then* (4.7) *and* (4.8) *are in fact second-order.*

Proof. We consider the case for (4.7) and note that the result for (4.8) follows in a similar manner. Assume that $u \in C^4(\Omega)$ and Ω_h is generated via a smooth mapping $g^{(x)}$ defined as

$$x_i = g^{(x)}(\omega_i^{(x)}),\ i = 0, \ldots, N+1 \tag{4.14}$$

where $\omega_i^{(x)} = -1 + ik_1,\ i = 0, \ldots, N+1$, with $k = 2/(N+1)$. Thus, $u(x, y, t) = u(g^{(x)}(\omega^{(x)}), y, t)$. We now consider the local truncation error, $\psi_{i,j}^{(x)}(t)$, of (4.7) at a point $(x_i, y_j, t) \in \Omega_h \times [t_0, T_q)$:

$$\begin{aligned}
\psi_{i,j}^{(x)}(t) &= \partial_x^2 u(x_i, y_j) - \left[\frac{2u_{i-1,j}(t)}{h_{x,i-1}(h_{x,i-1}+h_{x,i})} - \frac{2u_{i,j}(t)}{h_{x,i-1}h_{x,i}} + \frac{2u_{i+1,j}(t)}{h_{x,i}(h_{x,i-1}+h_{x,i})}\right] \\
&= 2\partial_x^3 u(x_i, y_j)(h_{x,i-1} - h_{x,i}) + \mathcal{O}\left(\frac{h_{x,i}^3}{h_{x,i-1}+h_{x,i}}\right), \quad h_{x,i-1}, h_{x,i} \to 0^+ \\
&= 2\partial_x^3 u(x_i, y_j)[(x_i - x_{i-1}) - (x_{i+1} - x_i)] \\
&\qquad + \mathcal{O}(\max\{h_{x,i-1}^2, h_{x,i}^2\}), \quad h_{x,i-1}, h_{x,i} \to 0^+.
\end{aligned} \tag{4.15}$$

For general nonuniform grids, (4.15) is first-order, however, due to (4.14), we have

$$\begin{aligned}
(x_i - x_{i-1}) - (x_{i+1} - x_i) &= -k_1^2 \frac{x_{i-1} - 2x_i + x_{i+1}}{k_1^2} \\
&= -k_1^2 \partial_{\omega^{(x)}}^2 g^{(x)}(\omega_i^{(x)}) + \mathcal{O}(k_1^2), \quad k_1 \to 0^+.
\end{aligned} \tag{4.16}$$

Note that for $\xi_i = \epsilon\omega_i + (1-\epsilon)\omega_{i-1},\ \epsilon \in [0, 1]$, we have

$$\begin{aligned}
h_{x,i-1} &= x_i - x_{i-1} \\
&= g^{(x)}(\omega_i) - g^{(x)}(\omega_{i-1}) \\
&= \partial_\omega g^{(x)}(\xi_i) k_1
\end{aligned}$$

which gives that

$$k_1 = (g_\omega^{(x)}(\xi_i))^{-1} h_{x,i-1} = \mathcal{O}(h_{x,i-1}), \quad h_{x,i-1} \to 0^+.$$

A similar process also gives $k_1 = \mathcal{O}(h_{x,i}),\ h_{x,i} \to 0^+$. These facts combined with (4.15) and (4.16) gives the desired result. ∎

4.3 Positivity

As discussed before, solutions to (4.1)-(4.3) remain positive within their domains of existence; *i.e*, for $t \in [t_0, T_q)$ [4,5,36,84]. Once again, this is also a key characteristics of a healthy physical solution no matter whether an ignition, or quenching, occurs [19, 99]. The property must be properly preserved by (4.13), and likewise, by our semi-discretized problem (4.9), (4.10). As in the previous chapter, all vector inequalities are to be interpreted componentwise. Further, we will use Lemma 3.4, from the previous chapter, in the ensuing analysis.

Lemma 4.3. *The matrix $E(\tau_k M)$ is positive for all $\tau_k \geq 0$.*

Proof. Note that $M = M_x + M_y$ is such that $M_{ij} \geq 0$ for $i \neq j$. Let $N = M + \beta I$, where $\beta = 8/h_{\min} \min\{a^2, b^2\}$. Then N is a positive matrix and

$$E(\tau_k M) = E(\tau_k (N - \beta I)) = E(-\tau_k \beta I) E(\tau_k N).$$

Since βI is a diagonal matrix, it follows that $E(-\tau_k \beta I)$ is a diagonal matrix, with $(E(-\tau_k \beta I))_{ij} = e^{-\tau_k \beta} > 0$ for $i \neq j$ and 0 elsewhere. Further, $E(\tau_k N)$ is a positive matrix by the definition of the matrix exponential and the fact that N is a positive matrix. ∎

Lemma 4.4. *The solution to* (4.9),(4.10) *is positive for all $t_0 < t < T_q$ and $0 \leq u < 1$.*

Proof. Note that the solution to (4.9),(4.10) is given by (4.11) and that $E(tM)v_0$ is positive for all positive v_0, by Lemmas 3.4 and 4.3. Similarly, $E((t-s)M)g(\varepsilon, v(s))$

is positive for all $t_0 \leq s \leq t$ since by construction $g(\varepsilon, v(s))$ is a positive vector and by Lemma 3.4. Since the integral of positive vectors is positive, it follows that $v(t)$ is positive. ∎

Lemma 4.5. *The matrices $\Phi_{x,k}$ and $\Phi_{y,k}$ are positive for all $\tau_k \geq 0$. Further, Φ_k is positive for all $\tau_k \geq 0$.*

Proof. Consider $\Phi_{y,k} = E(\tau_k M_y)$. Note that M_y is such that $(M_y)_{ij} \geq 0$ for $i \neq j$. Let $N_y = M_y + \beta I$, where $\beta = 4/h_{\min} \min\{b^2\}$. Then N_y is a positive matrix and

$$E(\tau_k M_y) = E(\tau_k(N_y - \beta I)) = E(-\tau_k \beta I) E(\tau_k N_y).$$

Since βI is a diagonal matrix, it follows that $E(-\tau_k \beta I)$ is a diagonal matrix, with $(E(-\tau_k \beta I))_{ij} = e^{-\tau_k \beta} > 0$ for $i \neq j$ and 0 elsewhere. Further, $E(\tau_k N_y)$ is a positive matrix by the definition of the matrix exponential and the fact that N_y is a positive matrix. Thus, $\Phi_{y,k}$ is positive for all $\tau_k \geq 0$. The proof is similar for the matrix $\Phi_{x,k}$. ∎

In the remainder of this section, we consider the matrix $M^{-1}[\Phi_k - I]$ and show that the matrix is positive under appropriate restriction on τ_k.

Lemma 4.6. *For any $\tau_k \geq 0$, we have $\|\Phi_{x,k}\|_\infty \leq 1$ and $\|\Phi_{y,k}\|_\infty \leq 1$.*

Proof. The proof follows by applying Lemma 2.4 and using Remark 2.3 to compute the logarithmic norm of each matrix. That fact that each matrix is diagonally dominant gives $\mu_\infty(M_\sigma) \leq 0$, $\sigma = x, y$. ∎

Now, we wish to determine a bound for $\|M^{-1}\|_\infty$ under suitable conditions on our nonuniform spatial grids. To that end, we denote

$$\begin{aligned} c_\alpha(h) \;=\; & \min_{i=1,\ldots,N_\alpha} \left\{ \frac{h_{\alpha,i}(2 + h_{\alpha,i})}{h_{\alpha,i-1}(h_{\alpha,i-1} + h_{\alpha,i})} + \frac{h_{\alpha,i+1}(h_{\alpha,i+1} - 2)}{h_{\alpha,i}(h_{\alpha,i-1} + h_{\alpha,i})} \right. \\ & \left. + 2(h_{\alpha,i+1} - h_{\alpha,i}) \sum_{j=1}^{i} h_{\alpha,j} \right\}, \end{aligned}$$

$$k(h) \;=\; [a^{-2}c_x(h) + b^{-2}c_y(h)]/4, \tag{4.17}$$

where $\alpha = x, y$. Let $\sigma_{\max} = \max_{1\le i\le N_x; 1\le j\le N_y} \sigma_{i,j}$.

Lemma 4.7. *Assume $k(h) \ge 1$. Then $\|M^{-1}\|_\infty \le \sigma_{\max}/2$, where $\sigma_{\max} = \max_{i,j}\sigma_{i,j}$.*

Proof. Let $\tilde{M} = B^{-1}M = a^{-2}(I_{N_y} \otimes P_x) + b^{-2}(P_y \otimes I_{N_x})$. We have

$$\|M^{-1}\|_\infty \le \|\tilde{M}^{-1}\|_\infty \|B^{-1}\|_\infty \le \sigma_{\max}\|\tilde{M}^{-1}\|_\infty.$$

Thus, we only need to consider the case with $\tilde{M}$. To this end, we let $f_{i,j}$ be any mesh function defined on Ω_h. Define $u_{i,j} = -\tilde{M}^{-1}f_{i,j}$, where $u_{i,j}$ solves the equation $-\tilde{M}u_{i,j} = f_{i,j}$ on Ω_h and satisfies the homogeneous Dirichlet boundary conditions $u_{i,j} = 0,\ (x_i, y_j) \in \partial\Omega_h$. For $w(x,y) = [x^2+y^2]/4$, we define $w_{i,j}$ on $\overline{\Omega}_h$ by

$$w_{i,j} = \frac{1}{4}\left[\left(-1 + \sum_{k=1}^{i} h_{x,k}\right)^2 + \left(-1 + \sum_{k=1}^{j} h_{y,k}\right)^2\right].$$

Clearly, $\Delta w = w_{xx} + w_{yy} = 1$. We consider $\tilde{M}w_{i,j}$ by examining $\overline{\Delta}_{x,h}w_{i,j} \equiv 4(I_{N_y} \otimes P_x)w_{i,j}$ and $\overline{\Delta}_{y,h}w_{i,j} \equiv 4(P_y \otimes I_{N_x})w_{i,j}$ separately. Thus, we have

$$\begin{aligned}
\overline{\Delta}_{x,h}w_{i,j} &= l_{x,i-1}\left[\left(-1 + \sum_{k=1}^{i-1} h_{x,k}\right)^2\right] + m_{x,i}\left[\left(-1 + \sum_{k=1}^{i} h_{x,k}\right)^2\right] \\
&= l_{x,i-1}\left[\left(-1 - h_{x,i} + \sum_{k=1}^{i} h_{x,k}\right)^2\right] + m_{x,i}\left[\left(-1 + \sum_{k=1}^{i} h_{x,k}\right)^2\right] \\
&\quad + n_{x,i}\left[\left(-1 + \sum_{k=1}^{i+1} h_{x,k}\right)^2\right] + n_{x,i}\left[\left(-1 + h_{x,i+1} + \sum_{k=1}^{i} h_{x,k}\right)^2\right] \\
&= l_{x,i-1}h_{x,i}\left(-2\sum_{k=1}^{i} h_{x,k} + 2 + h_{x,i}\right) \\
&\qquad + n_{x,i}h_{x,i+1}\left(2\sum_{k=1}^{i} h_{x,k} - 2 + h_{x,i+1}\right) \\
&= \left(l_{x,i-1}h_{x,i}^2 + n_{x,i}h_{x,i+1}^2\right) + 2(n_{x,i}h_{x,i+1} - l_{x,i-1}h_{x,i})\left(\sum_{k=1}^{i} h_{x,k} - 1\right)
\end{aligned}$$

$$
\begin{aligned}
&= \frac{h_{x,i}(2+h_{x,i})}{h_{x,i-1}(h_{x,i-1}+h_{x,i})} + \frac{h_{x,i+1}(h_{x,i+1}-2)}{h_{x,i}(h_{x,i-1}+h_{x,i})} + 2(h_{x,i+1}-h_{x,i})\sum_{j=1}^{i} h_{x,i} \\
&\geq c_x(h).
\end{aligned}
$$

A similar argument indicates that

$$\overline{\Delta}_{y,h} w_{i,j} \geq c_y(h).$$

Combining these results gives that $\tilde{M} w_{i,j} \geq k(h)\boldsymbol{x}$, where $\boldsymbol{x} = (1, 1, \ldots, 1)^{\intercal} \in \mathbb{R}^{N_x N_y}$.

Note that $w_{i,j}$ is nonnegative on $\overline{\Omega}_h$ and $\|w_{i,j}\|_\infty = 1/2$. It follows therefore

$$\tilde{M}(\|f_{i,j}\|_\infty w_{i,j} + u_{i,j}) \geq \|f_{i,j}\|_\infty k(h)\boldsymbol{x} - f_{i,j} \geq 0,$$

based on our earlier assumptions. Hence, by the Discrete Maximum Principle [113], $\|f_{i,j}\|_\infty w_{i,j} + u_{i,j}$ achieves its maximum on $\partial\Omega_h$. Since $u_{i,j} = 0$ on $\partial\Omega_h$, we have

$$
\begin{aligned}
u_{i,j} &\leq \|f_{i,j}\|_\infty w_{i,j} + u_{i,j} \\
&\leq \|f_{i,j}\|_\infty \|w_{i,j}\|_\infty \\
&\leq \frac{\|f_{i,j}\|_\infty}{2}
\end{aligned}
$$

for $(x_i, y_j) \in \Omega_h$. Similarly, we have

$$\tilde{M}(\|f_{i,j}\|_\infty w_{i,j} - u_{i,j}) \geq \|f_{i,j}\|_\infty k(h)\boldsymbol{x} + f_{i,j} \geq 0,$$

which gives

$$
\begin{aligned}
-u_{i,j} &\leq \|f_{i,j}\|_\infty w_{i,j} - u_{i,j} \\
&\leq \|f_{i,j}\|_\infty \|w_{i,j}\|_\infty \\
&\leq \frac{\|f_{i,j}\|_\infty}{2}.
\end{aligned}
$$

A combination of the above results gives

$$\frac{\|u_{i,j}\|_\infty}{\|f_{i,j}\|_\infty} = \frac{\|-\tilde{M}^{-1} f_{i,j}\|_\infty}{\|f_{i,j}\|_\infty} \leq \frac{1}{2}.$$

It follows naturally that $\|\tilde{M}^{-1}\|_\infty \leq 1/2$ since $f_{i,j}$ are arbitrary. This completes our proof. ∎

We note that our restriction on $k(h)$ is reasonable and has no negative impact on desired computations. In fact, $k(h) \geq 1$ can be readily observed if uniform or symmetric nonuniform grids are utilized. Moreover, for certain nonuniform grids we have the following corollary.

Corollary 4.8. *If the nonuniform grid Ω_h is the image of a uniform grid on Ω via a smooth mapping, then we have*

$$\|M^{-1}\|_\infty \leq \sigma_{\max}/2 + \mathcal{O}(\max_{i,j}\{h_{x,i}^2, h_{y,j}^2\})$$

for $h_{x,i}, h_{y,j} \to 0^+$.

Proof. Assume that $u \in C^4(\Omega)$ and Ω_h is generated via smooth mappings $g^{(x)}$ and $g^{(y)}$ with

$$x_i = g^{(x)}(\omega_i^{(y)}) \quad \text{and} \quad y_i = g^{(y)}(\omega_j^{(y)}),$$

where $\omega_i^{(x)} = -1 + ik_1,\ i = 0, \ldots, N_x + 1$ and $\omega_j^{(y)} = -1 + ik_2,\ j = 0, \ldots, N_y + 1$. Using the Taylor expansions of the functions $g^{(x)}$ and $g^{(y)}$ in (4.17) yields $k(h) = 1 + \mathcal{O}(\max\{k_1^2, k_2^2\}),\ k_1, k_2 \to 0^+$. Just as in Lemma 4.2, we may deduce that $k_1 = \mathcal{O}(h_{x,i}),\ h_{x,i} \to 0^+$ and $k_2 = \mathcal{O}(h_{y,j}),\ h_{y,j} \to 0^+$, which gives $k(h) = 1 + \mathcal{O}(\max_{i,j}\{h_{x,i}^2, h_{y,j}^2\}),\ h_{x,i}, h_{y,j} \to 0^+$. Using this fact in the proof of Lemma 4.7 gives the desired result. ∎

Lemma 4.9. *Assume that $k(h) \geq 1$. For $\tau_k \geq 0$ sufficiently small, $M^{-1}[\Phi_k - I]$ is positive.*

Proof. Note that

$$M^{-1}[\Phi_k - I] \;=\; \int_{t_k}^{t_{k+1}} w_k(s)\, ds, \tag{4.18}$$

where

$$w_k(s) \;=\; M^{-1}\left[\frac{1}{2} M_x E_1(s) E_2(s) E_1(s)\right.$$

$$+E_1(s)M_yE_2(s)E_1(s) + \frac{1}{2}E_1(s)E_2(s)M_xE_1(s)\Big],$$

with

$$E_1(s) = E\left(\frac{t_{k+1}-s}{2}M_x\right)$$

and

$$E_2(s) = E((t_{k+1}-s)M_y).$$

By [106] it follows that

$$w_k(s) \;=\; E_1(s)E_2(s)E_1(s) + M^{-1}\mathcal{E}(s), \tag{4.19}$$

where

$$\begin{aligned}
\mathcal{E}(s) &= [E_1(s), M_y]E_2(s)E_1(s) + \frac{1}{2}E_1(s)[E_2(s), M_x]E_1(s) \\
&= \left(-\frac{1}{2}\int_{t_{k+1}}^{t_{k+1}-s} E_1(s-\xi)[M_x, M_y]E_1(\xi)\,d\xi\right)E_2(s)E_1(s) \\
&\qquad + -\frac{1}{2}E_1(s)\left(\int_{t_{k+1}}^{t_{k+1}-s} E_2(s-\xi)[M_y, M_x]E_2(\xi)\,d\xi\right)E_1(s) \\
&= \left(\frac{1}{2}\int_{t_{k+1}-s}^{t_{k+1}} E_1(s-\xi)[M_x, M_y]E_1(\xi)\,d\xi\right)E_2(s)E_1(s) \\
&\qquad + \frac{1}{2}E_1(s)\left(\int_{t_{k+1}-s}^{t_{k+1}} E_2(s-\xi)[M_y, M_x]E_2(\xi)\,d\xi\right)E_1(s).
\end{aligned}$$

Note that

$$\int_{t_k}^{t_{k+1}} E_1(s)E_2(s)E_1(s)\,ds$$

is positive by Lemmas 3.4 and 4.5, so it only remains to show that the norm of the remaining terms may be made sufficiently small. To that end

$$\begin{aligned}
\left\|M^{-1}\int_{t_k}^{t_{k+1}} \mathcal{E}(s)\,ds\right\|_\infty &\leq \|M^{-1}\|_\infty \int_{t_k}^{t_{k+1}} \|E_1(s)\|_\infty^2\|E_2(s)\|_\infty\|[M_x, M_y]\|_\infty s\,ds \\
&= \frac{t_{k+1}^2 - t_k^2}{2}\|M^{-1}\|_\infty\|E_1(s)\|_\infty^2\|E_2(s)\|_\infty\|[M_x, M_y]\|_\infty \\
&\leq \frac{(t_{k+1}+t_k)\tau_k}{2}\|M^{-1}\|_\infty\|[M_x, M_y]\|_\infty
\end{aligned}$$

$$\leq \frac{T_q \sigma_{\max} \tau_k^2}{2} \|[M_x, M_y]\|_\infty.$$

Thus, for τ_k sufficiently small the desired result follows. ∎

Remark 4.10. Lemma 4.9 holds for all $\tau_k \geq 0$ in many realistic situations where $\|[M_x, M_y]\|_\infty = 0$. The equality is apparently true for cases with a symmetric degeneracy term on symmetric nonuniform grids. Numerical experiments show that $\|[M_x, M_y]\|_\infty$ remains well-bounded.

4.4 Monotonicity

As has been discussed in the previous chapter, the solution to (4.1)-(4.3) must be monotone with respect to time [4, 5, 36, 74, 84]. Solutions to Kawarada problems are monotonically increasing with respect to time on their domain of existence. Thus, it is important that this is rigorously observed in (4.13) as well as (4.9),(4.10).

In the following results, there are additional restrictions place on the stochastic nonlinear reaction term in order to guarantee monotonicity. Further, our results are similar to those one would expect in the non-stochastic case. We first consider (4.9), (4.10).

Lemma 4.11. *If* $Mv_0 + g(\varepsilon, v_0) > 0$, *then the solution to* (4.9),(4.10) *is monotonically increasing with respect to time for all* $t_0 < t < T_q$ *and* $0 \leq u < 1$.

Proof. Recall (4.9), (4.10). Let $w(t) = v'(t)$ and consider

$$w'(t) = [M + g_v(\varepsilon, v(t))]w(t), \quad t_0 < t < T_q, \tag{4.20}$$

$$w(t_0) = Mv_0 + g(\varepsilon, v_0) \equiv w_0. \tag{4.21}$$

The solution to (4.20), (4.21) is given by

$$w(t) = E\left(\int_{t_0}^{t} [M + g_v(\varepsilon, v(s))]\, ds\right) w_0.$$

Note that $g_v(\varepsilon, v(t))$ is a diagonal matrix and since $f_u \geq 0$, it follows that g_v is a nonnegative matrix. Letting

$$A(t) = \int_{t_0}^{t} [M + g_v(\varepsilon, v(s))]\, ds$$

it follows that $A_{ij} \geq 0$ for $i \neq j$. Thus, by Lemma 4.3, we have that $E(A(t))$ is positive for $t_0 \leq t < T_q$. By Lemma 3.4, since $w_0 > 0$, we have that $w(t) > 0$ for $t_0 < t < T_q$. Thus, $v'(t) > 0$ for $t_0 < t < T_q$ and we have that the solution is monotonically increasing with respect to time. ∎

Lemma 4.12. *Consider* (4.13). *If* $Mv_0 + g(\varepsilon, v_0) > 0$, *then it follows that* $Mv_k + g(\varepsilon, v_k) > 0$ *for all* $k \geq 0$.

Proof. Assume that $Mv_0 + g(\varepsilon, v_0) > 0$ for (4.13). Next, note that

$$\begin{aligned} Mv_{k+1} &= M\left\{\Phi_k v_k + M^{-1}[\Phi_k - I]\,[\theta g(\varepsilon, v_k) + (1-\theta) g(\varepsilon, v_{k+1})]\right\} \\ &= \Phi_k\,[Mv_k + [\theta g(\varepsilon, v_k) + (1-\theta) g(\varepsilon, v_{k+1})]] \\ &\qquad - [\theta g(\varepsilon, v_k) + (1-\theta) g(\varepsilon, v_{k+1})] \end{aligned}$$

which gives

$$\begin{aligned} Mv_{k+1} + g(\varepsilon, v_{k+1}) &= \Phi_k\,[Mv_k + [\theta g(\varepsilon, v_k) + (1-\theta) g(\varepsilon, v_{k+1})]] \\ &\qquad - [\theta g(\varepsilon, v_k) + (1-\theta) g(\varepsilon, v_{k+1})] + g(\varepsilon, v_{k+1}) \\ &> \Phi_k\,[Mv_k + [\theta g(\varepsilon, v_k) + (1-\theta) g(\varepsilon, v_k)]] \\ &\qquad - [\theta g(\varepsilon, v_{k+1}) + (1-\theta) g(\varepsilon, v_{k+1})] + g(\varepsilon, v_{k+1}) \\ &= \Phi_k[Mv_k + g(\varepsilon, v_k)] \quad > \quad 0 \end{aligned}$$

by the inductive assumption, Lemmas 3.4 and 4.5, and the fact that $f(\varepsilon, u)$ is monotonically increasing. ∎

Lemma 4.13. *Consider* (4.13). *Let* $\tau_k \geq 0$ *be sufficiently small and* $Mv_0 + g(\varepsilon, v_0) > 0$. *Then* $v_{k+1} > v_k$ *for all* $k \geq 0$. *That is, the sequence* $\{v_k\}_{k\geq 0}$ *is monotonically increasing for* (4.13).

Proof. We begin by considering (4.13). We have

$$\begin{aligned}
v_{k+1} - v_k &= \Phi_k v_k + M^{-1}[\Phi_k - I]g(\varepsilon, v_k)[\theta g(\varepsilon, v_k) + (1-\theta)g(\varepsilon, v_{k+1})] - v_k \\
&= [\Phi_k - I]v_k + M^{-1}[\Phi_k - I][\theta g(\varepsilon, v_k) + (1-\theta)g(\varepsilon, v_{k+1})] \\
&= M^{-1}\left\{M[\Phi_k - I]v_k + [\Phi_k - I][\theta g(\varepsilon, v_k) + (1-\theta)g(\varepsilon, v_{k+1})]\right\} \\
&= M^{-1}\left\{[\Phi_k - I]Mv_k + [\Phi_k - I][\theta g(\varepsilon, v_k) + (1-\theta)g(\varepsilon, v_{k+1})]\right\} \\
&= M^{-1}[\Phi_k - I]\{Mv_k + [\theta g(\varepsilon, v_k) + (1-\theta)g(\varepsilon, v_{k+1})]\} \\
&> M^{-1}[\Phi_k - I]\{Mv_k + [\theta g(\varepsilon, v_k) + (1-\theta)g(\varepsilon, v_k)]\} \\
&= M^{-1}[\Phi_k - I]\{Mv_k + g(\varepsilon, v_k)\} \\
&> 0
\end{aligned}$$

by Lemmas 4.9 and 4.12. ∎

We may generalize the above results to obtain the following theorem.

Theorem 4.14. *Assume that* $k_0 \geq 0$ *and* $Mv_{k_0} + g(\varepsilon, v_{k_0}) > 0$. *Then the sequence* $\{v_k\}_{k \geq k_0}$ *produced by the semi-discretized nonuniform scheme* (4.13) *increases monotonically until unity is reached or exceeded by one or more components of the solution vector, i.e., until quenching occurs.*

4.5 Stability

Stability of different schemes for solving singular and stochastic Kawarada equations such as (4.1)-(4.3) has been a highly nontrivial and challenging concern [4,20,74,75,93,94]. This difficulty is mostly attributed to the fact that near quenching the temporal derivative of the solution may blow up faster than an exponential rate [19, 39]. Most existing investigations simply consider a linear stability analysis, and later the results are reconfirmed through rigorous computational experiments [20, 21, 74, 75]. Since such considerations have been proven to be highly effective in localized computations [39, 100], in this section, we will first carry out a standard

linear stability analysis for (4.13). The study will then be extended to a nonlinear case by including contributions from the singular nonlinear stochastic reaction term. This extension of the analysis ensures that the singular and stochastic nature of the differential equation is incorporated near the quenching point as quenching is approached.

Lemma 4.15. *P_x and P_y are congruent to symmetric matrices. In particular,*

$$P_\alpha = D_\alpha^{-1/2} S_\alpha D_\alpha^{1/2} \in \mathbb{R}^{N_\alpha \times N_\alpha},\ \alpha = x, y,$$

where

$$P_\alpha = \text{diag}\left(\delta_{\alpha,1}, \ldots, \delta_{\alpha,N}\right),\ S_\alpha = \text{tridiag}\left(\gamma_{\alpha,i}, m_{\alpha,i}, \gamma_{\alpha,i}\right)$$

for which

$$\delta_{\alpha,i} = \frac{h_{\alpha,i-1} + h_{\alpha,i}}{h_{\alpha,0} + h_{\alpha,1}} \quad \textit{and} \quad \gamma_{\alpha,i} = \sqrt{n_{\alpha,i} l_{\alpha,i}}.$$

Proof. The proof is similar to that in [19]. ∎

Lemma 4.16. *$\rho(P_\alpha) \in (-\infty, 0],\ \alpha = x, y,$ where $\rho(A) = \lambda_{\max}(AA^\intercal)$ for any $A \in \mathbb{R}^{N \times N}$.*

Proof. Consider P_x. By Lemma 4.13 we have that P_x is congruent to a symmetric matrix, hence all eigenvalues of P_x are real. Since P_x is diagonally dominant with negative diagonal elements, the result follows immediately [61]. A similar argument gives the result for P_y ∎

Lemma 4.17. *All eigenvalues of M_x and M_y are real and negative. Further, we have $\mu_2(B^{1/2} P_x B^{1/2}) < 0$ and $\mu_2(B^{1/2} P_y B^{1/2}) < 0$.*

Proof. We first consider M_x. Since $M_x = BP_x = B^{1/2} B^{1/2} P_x$, we have $B^{-1/2} M_x = B^{1/2} P_x$. Hence

$$B^{-1/2} M_x (B^{1/2})^\intercal = B^{1/2} P_x B^{1/2} = B^{1/2} P_x (B^{1/2})^\intercal$$

because B is diagonal. Further,

$$B^{-1/2}M_xB^{1/2} = B^{-1/2}BP_xB^{1/2} = B^{1/2}P_xB^{1/2}$$

is congruent to a symmetric matrix, since P_x is congruent to a symmetric matrix. Thus, the matrices $B^{-1/2}M_xB^{1/2}$ and P_x are congruent. Since the eigenvalues of P_x are real and negative, the eigenvalues of $B^{-1/2}M_xB^{1/2}$ and M_x must be real and negative.

Since we have $B^{-1/2}M_xB^{1/2} = B^{1/2}P_xB^{1/2}$, then the eigenvalues of $B^{1/2}P_xB^{1/2}$ are real and negative, which gives the result. A similar argument gives the results for $P_y,\ M_y,$ and $B^{1/2}P_yB^{1/2}$. Remark 2.3 and the fact that a matrix and its transpose share eigenvalues gives $\mu_2(B^{1/2}P_xB^{1/2}) < 0$ and $\mu_2(B^{1/2}P_yB^{1/2}) < 0$. ∎

Lemma 4.18. *For $\tau_j \geq 0$ we have $\left\|\prod_{j=0}^{k}\Phi_j\right\|_2 \leq \sqrt{\kappa(B)} = \sqrt{\max\sigma_{i,j}/\min\sigma_{i,j}}$.*

Proof. We first show $\Phi_{y,j} = B^{1/2}E(\tau_jB^{1/2}P_yB^{1/2})B^{-1/2}$ for $\tau_j \geq 0$. To this end, we have

$$\begin{aligned} B^{-1/2}\Phi_{y,j}B^{1/2} &= \sum_{n=0}^{\infty}\frac{\left(\tau_jB^{1/2}P_yB^{1/2}\right)^n}{n!} \\ &= E(\tau_jB^{1/2}P_yB^{1/2}) \\ &\equiv \tilde{\Phi}_{y,j}. \end{aligned} \tag{4.22}$$

Similarly, we have

$$\begin{aligned} B^{-1/2}\Phi_{x,j}B^{1/2} &= \sum_{n=0}^{\infty}\frac{\left((\tau_j/2)B^{1/2}P_xB^{1/2}\right)^n}{n!} \\ &= E((\tau_j/2)B^{1/2}P_xB^{1/2}) \\ &\equiv \tilde{\Phi}_{x,j}. \end{aligned} \tag{4.23}$$

It then follows from (4.22), (4.23), and Lemmas 2.4 and 4.15

$$\left\|\prod_{j=0}^{k}\Phi_j\right\|_2 = \left\|\prod_{j=0}^{k}\Phi_{x,j}\Phi_{y,j}\Phi_{x,j}\right\|_2$$

$$
\begin{aligned}
&= \left\| \prod_{j=0}^{k} \left(B^{1/2} \tilde{\Phi}_{x,j} B^{-1/2} \right) \left(B^{1/2} \tilde{\Phi}_{y,j} B^{-1/2} \right) \left(B^{1/2} \tilde{\Phi}_{x,j} B^{-1/2} \right) \right\|_2 \\
&= \left\| B^{1/2} \left(\prod_{j=0}^{k} \tilde{\Phi}_{x,j} \tilde{\Phi}_{y,j} \tilde{\Phi}_{x,j} \right) B^{-1/2} \right\|_2 \\
&\leq \|B^{1/2}\|_2 \|B^{-1/2}\|_2 \prod_{j=0}^{k} E(\tau_j(\mu_2(B^{1/2} P_x B^{1/2}) + \mu_2(B^{1/2} P_y B^{1/2}))) \\
&\leq \sqrt{\kappa(B)},
\end{aligned}
$$

where $\kappa(B)$ is the condition number of the matrix B. ∎

Combining the above results gives the following theorem.

Theorem 4.19. *For $\tau_k \geq 0$ sufficiently small, the semi-adaptive nonuniform method* (4.13) *with the nonlinear stochastic reaction term frozen is unconditionally stable in the von Neumann sense under the spectral norm. that is,*

$$\|z_{k+1}\|_2 \leq C \|z_0\|_2, \quad k \geq 0,$$

where $z_0 = v_0 - \tilde{v}_0$ is an initial error, $z_{k+1} = v_{k+1} - \tilde{v}_{k+1}$ is the $(k+1)$th perturbed error vector, and $C > 0$ is a constant independent of k and τ_j for each $0 \leq j \leq k$.

Proof. Recall (4.13). When the nonlinear reaction term is frozen, z_{k+1} takes the form of

$$z_{k+1} = \Phi_k z_k, \quad k \geq 0. \tag{4.24}$$

Iterating (4.24) gives

$$z_{k+1} = \prod_{j=0}^{k} \Phi_j z_0. \tag{4.25}$$

Taking the norm of both sides of (4.25), it follows that

$$\|z_{k+1}\|_2 \leq \left\| \prod_{j=0}^{k} \Phi_j \right\|_2 \|z_0\|_2 \leq \sqrt{\kappa(B)} \|z_0\|_2.$$

Letting $C \equiv \sqrt{\kappa(B)}$ gives the desired result. ∎

We now consider the case without freezing the nonlinear stochastic reaction term in (4.13). In the following, we let t_Q be the time at which numerical quenching occurs, that is, the first time for which $\|v_Q\|_\infty \geq 1$.

Theorem 4.20. *For $\tau_k \geq 0$ sufficiently small, the semi-adaptive nonuniform method (4.13) is unconditionally stable in the von Neumann sense, that is, for every $t_m < t_Q$ there exists a constant $C(t_m) > 0$ such that*

$$\|z_{k+1}\|_2 \leq C(t_m)\|z_0\|_2, \quad 0 \leq k \leq m,$$

where $z_0 = v_0 - \tilde{v}_0$ is an initial error, $z_{k+1} = v_{k+1} - \tilde{v}_{k+1}$ is the $(k+1)$th perturbed error vector, and $C(t_m) > 0$ is a constant independent of k and τ_j for each $0 \leq j \leq k$.

Proof. Recalling (4.13), we have

$$v_{k+1} = \Phi_k v_k + M^{-1}[\Phi_k - I][\theta g(\varepsilon, v_k) + (1-\theta)g(\varepsilon, v_{k+1})], \quad k \geq 0,\ \theta \in [0,1].$$

It follows that

$$\begin{aligned} z_{k+1} &= \Phi_k z_k + M^{-1}[\Phi_k - I][\theta(g(\varepsilon, v_k) - g(\varepsilon, \tilde{v}_k)) \\ &\qquad + (1-\theta)(g(\varepsilon, v_{k+1}) - g(\varepsilon, \tilde{v}_{k+1}))] \\ &= \Phi_k z_k + M^{-1}[\Phi_k - I][\theta g_v(\varepsilon, \xi_k) z_k + (1-\theta) g_v(\varepsilon, \xi_{k+1}) z_{k+1}] \\ &= \Phi_k z_k + \left(\int_{t_k}^{t_{k+1}} w_k(s)\, ds\right)[\theta g_v(\varepsilon, \xi_k) z_k + (1-\theta) g_v(\varepsilon, \xi_{k+1}) z_{k+1}], \quad (4.26) \end{aligned}$$

where $\xi_j = \epsilon v_j + (1-\epsilon)\tilde{v}_j,\ \epsilon \in [0,1],\ j = k, k+1$, and $k \geq 0,\ \theta \in [0,1]$. Recall (4.19). By utilizing a left-endpoint quadrature to approximate the integral in (4.26), we observe that

$$\begin{aligned} z_{k+1} &= \Phi_k z_k + \left(\tau_k \Phi_k + \mathcal{O}\left(\tau_k^2\right)\right)[\theta g_v(\varepsilon, \xi_k) z_k + (1-\theta) g_v(\varepsilon, \xi_{k+1}) z_{k+1}], \\ \Gamma_{1,k+1} z_{k+1} &= \Phi_k \Gamma_{2,k} z_k, \\ z_{k+1} &= \Gamma_{1,k+1}^{-1} \Phi_k \Gamma_{2,k} z_k, \quad (4.27) \end{aligned}$$

as $\tau_k \to 0^+$, where

$$\Gamma_{1,k+1} = I - \tau_k(1-\theta)\left(I + \mathcal{O}\left(\tau_k\right)\right) g_v(\varepsilon, \xi_{k+1}), \quad \tau_k \to 0^+$$

and

$$\Gamma_{2,k} = I + \tau_k\theta\left(I + \mathcal{O}\left(\tau_k\right)\right) g_v(\varepsilon, \xi_k), \quad \tau_k \to 0^+.$$

It follows therefore that, by employing the standard [1/0] and [0/1] Padé approximations, respectively,

$$\begin{aligned}
\Gamma_{1,k+1}^{-1} &= E\left(\tau_k(1-\theta)\left(I + \mathcal{O}\left(\tau_k\right)\right) g_v(\varepsilon, \xi_{k+1})\right) + \mathcal{O}\left(\tau_k^2\right), \quad \tau_k \to 0^+, \\
\Gamma_{2,k} &= E\left(\tau_k\theta\left(I + \mathcal{O}\left(\tau_k\right)\right) g_v(\varepsilon, \xi_k)\right) + \mathcal{O}\left(\tau_k^2\right), \quad \tau_k \to 0^+.
\end{aligned}$$

Let

$$\Psi_k = \Gamma_{1,k+1}^{-1}\Phi_k\Gamma_{2,k}.$$

Applying the above to (4.27), We obtain

$$\begin{aligned}
z_{k+1} &= \left\{\Psi_k + \mathcal{O}\left(\tau_k^2\right)\right\} z_k, \quad \tau_k \to 0^+ \\
&= \left\{\prod_{j=0}^{k}\left[\Psi_j + \mathcal{O}\left(\tau_j^2\right)\right]\right\} z_k, \quad \tau_j \to 0^+,\ j = 0, 1, \ldots, k \\
&= \left\{\prod_{j=0}^{k}\Psi_j + \sum_{j=0}^{k}\mathcal{O}\left(\tau_j^2\right)\right\} z_0, \quad \tau_j \to 0^+,\ j = 0, 1, \ldots, k.
\end{aligned}$$

Now, let $G(t_m) = \max_{0\le j\le m}\left\|g_v(\varepsilon, \xi_j)\right\|_2$. Taking the norm of both sides of the above expression yields

$$\left\|z_{k+1}\right\|_2 \le \left\{\left\|\prod_{j=0}^{k} e^{\tau_j(1-\theta)(1+c_2\tau_j)G(t_m)}\Phi_j e^{\tau_j\theta(1+c_3\tau_j)G(t_m)}\right\|_2 + c_1\sum_{j=0}^{k}\tau_j^2\right\}\left\|z_0\right\|_2,$$

where $c_1,\ c_2,$ and c_3 are positive constants independent of τ_j and j for $j = 0, 1, \ldots, k$. Thus, for $\tau_j \ge 0$ sufficiently small,

$$\left\|z_{k+1}\right\|_2 \le \left\{\left\|\prod_{j=0}^{k} e^{2\tau_j(1-\theta)G(t_m)}\Phi_j e^{2\tau_j\theta G(t_m)}\right\|_2 + c\sum_{j=0}^{k}\tau_j\right\}\left\|z_0\right\|_2$$

$$\leq \left\{ e^{2T_q G(t_m)} \sqrt{\kappa(B)} + T_q \right\} \|z_0\|_2$$
$$\leq C(t_m)\|z_0\|_2,$$

where c is a positive constant independent of $\tau_j, j,\ j = 0, 1, \ldots, k$, and we have used the fact that $\sum_{j=0}^{k} \tau_j \leq T_q$. It follows that $G(t_m) < \infty$ for all $t_m < t_Q$. This completes our proof. ∎

4.6 Numerical Experiments

We consider the following degenerate stochastic Kawarada model problem

$$\sigma(x,y)u_t = \frac{1}{a^2}u_{xx} + \frac{1}{b^2}u_{yy} + \frac{\varphi(\varepsilon)}{1-u}, \quad -1 < x, y < 1, \tag{4.28}$$
$$u(-1,y,t) = u(1,y,t) = 0, \quad -1 \leq y \leq 1, \tag{4.29}$$
$$u(x,-1,t) = u(x,1,t) = 0, \quad -1 \leq x \leq 1, \tag{4.30}$$
$$u(x,y,t_0) = u_0(x,y), \quad -1 < x, y < 1, \tag{4.31}$$

where $0 \leq t_0 < t \leq T_q < \infty$, $u_0 \in C^2([-1,1] \times [-1,1])$, and $0 \leq u_0 \ll 1$.

Without loss of generality, we set $t_0 = 0$, $a = b = 2$, and choose $u_0(x,y) = 0.001(1-\cos(2\pi x))(1-\cos(2\pi y)),\ -1 \leq x, y \leq 1$. Temporal adaptations are initiated once

$$\max_{1 \leq i \leq N_x;\, 1 \leq j \leq N_y} u_{i,j}(t) \geq \epsilon_0 = 0.90,$$

since quenching is expected to occur in the situation [20, 33, 36, 39, 95]. We fix the parameter $\theta = 1/2$ in (4.13). We primarily focus on the capability of the scheme (4.13) to recover anticipated numerical solutions and, at the same time, explore the nonlinear numerical convergence of the semi-adaptive semi-discretized scheme. Our first experiment will serve as a baseline approach, where nonlinear convergence results at different time levels in the absence of degenerate or stochastic influences will be presented. Degenerate and stochastic influences on the convergence will be closely observed in the second experiment. Standard [1/1] Padé approximants will be utilized for matrix exponential evaluations [15, 64]. Appropriate restrictions are

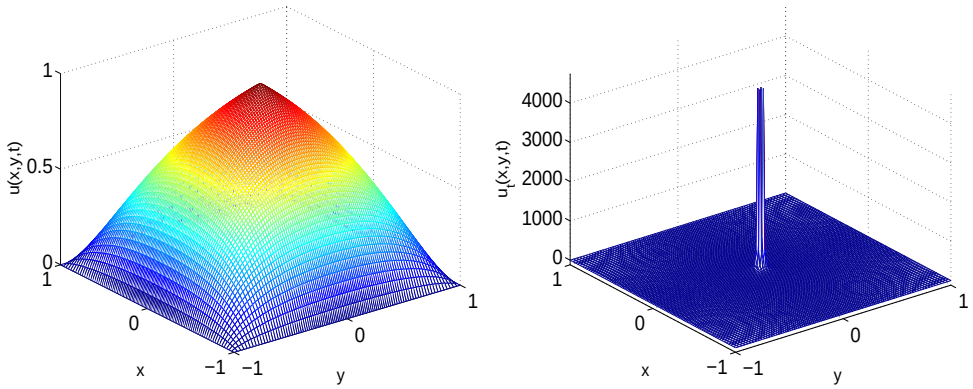

Figure 4.1: Solution u [LEFT] and its temporal derivative u_t [RIGHT] immediately prior to quenching.

realized for guaranteeing the required positivity and monotonicity with the particular matrices involved throughout experiments [93–95].

Experiment 1

To prepare our baseline results, we set $\varphi(\varepsilon), \sigma(x, y) \equiv 1$ in (4.28)-(4.31). Without the concerns of stochastic and degenerate impacts, we adopt a symmetric nonuniform spatial grid generated in a similar manner to that in [95]. A typical symmetric nonuniform grid can be seen in Figure 4.2. Adaption in the temporal direction is implemented via u_t based arc-length monitoring functions [21, 39, 95]. Quenching is observed precisely at the origin for $T_q \approx 0.51971548$ which agrees well with existing results [20, 21, 33, 37, 39, 93, 94]. While the peak value of u reaches unity peacefully, the temporal derivative function u_t grows at an explosive rate to reach $u_t^* \approx 4635.87012832$ as $t \to T_q$. Profiles of the numerical solution and its temporal derivative function are depicted in Figure 4.1.

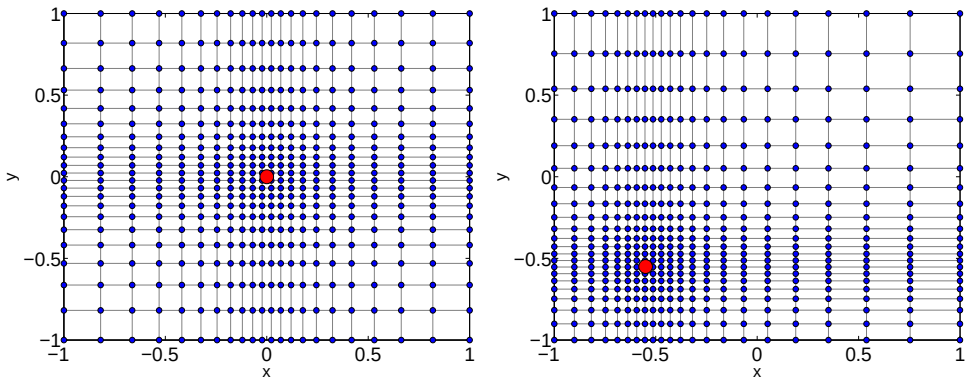

Figure 4.2: [LEFT] A typical symmetric nonuniform mesh used in computations for the non-degenerate case. [RIGHT] A symmetric nonuniform mesh which can be used in degenerate computations for a possible degeneracy that is concentrated at $(-1,-1)$. In both plots, the red point represents the quenching point.

To examine the convergence of the numerical solution numerically, we arbitrarily choose two temporal points close to the quenching time T_q :

$$T_1 = 0.51544143 \text{ and } T_2 = 0.51892238.$$

Let u_h^τ denote the numerical solution obtained by using the set of nonuniform spatial steps represented by size h and the particular adaptive temporal step τ. Suppose that $h/2$ represents the new set of nonuniform spatial steps obtained from dividing each nonuniform mesh step in set h by two. Likewise, $h/4$ is for the new set of nonuniform spatial steps obtained from dividing each nonuniform mesh step in set $h/2$ by two. By the same token, we may define sets of temporal steps $\tau/2$. $\tau/4$ based on set τ. Now, we define the following generalized Milne device for rates of point-wise convergence in space and time, respectively:

$$p_{\text{PW}}^h \approx \frac{1}{\ln 2} \ln \frac{|u_h^\tau - u_{h/2}^\tau|}{|u_{h/2}^\tau - u_{h/4}^\tau|}, \quad q_{\text{PW}}^\tau \approx \frac{1}{\ln 2} \ln \frac{|u_h^\tau - u_h^{\tau/2}|}{|u_h^{\tau/2} - u_h^{\tau/4}|}, \quad t \in \{T_1, T_2\},$$

where these differences are defined on mesh points corresponding to τ, h. The estimates can also be reformulated via any vector norm. As an example of such reformulations, we include estimates for convergence rates with respect the spectral norm, denoted by p_2^h and q_2^τ.

Table 4.1 presents the convergence data for space and time at sampling times T_1 and T_2. From Table 4.1 we may also notice that the mean, median, and maximal point-wise convergence rates and the spectral convergence rates agree well in both space and time with a slight reduction when considering spectral convergence. We note that the method used to generate the nonuniform mesh for this experiment meets the criteria of Lemma 2.2, hence, we observe second-order spatial convergence. Further, these results support the Courant-Friedrichs-Lewy condition remarkably.

Figure 4.3 depicts the dynamic profile of convergence rates between T_1 and T_2. The lines indicate movements of the maximal, median, and mean point-wise convergence rates as well as the spectral convergence rates in both space and time. When considering the spatial convergence, we observe that the curves are very close to two, and when considering the temporal convergence, we notice that the curves are grouped very close to one. Minimal spatial and temporal convergence rates are recorded in Table 4.1. The minimum spatial convergence rates most likely due to the smoothness of the solution about corners of the spatial domain [38]. The minimal temporal convergence rates are most likely due to the development of quenching singularity, which indicated by rate drops from T_1 to T_2. The quenching singularity also affects the spatial convergence, but less violently as the gradient of the solution is bounded. These expectations follow from a generalization of the results in [85].

Further, Figure 4.4 depicts the solution, its temporal derivative, and convergence rates at T_2. We note that the peaks of the solution and the derivative are concentrated at the origin, which is the quenching location in this particular problem [36,39,69,85,95]. In the bottom row of the figure, rates of point-wise spatial and temporal convergences are plotted as surfaces. It is easy to observe that both rates decrease near the origin. This, once again, is due to the reaction term becoming unbounded near quenching, or combustion. The singularity has an explosive impact to the overall convergence rates. It is also observed that that there are decreased

spatial convergence rates near corners of the domain, which has been predicted by several authors [34, 38, 107].

Despite drops in convergence rates near the quenching point, the mean convergence rate of the scheme is well-maintained near quenching at time T_2. At this time, the mean spatial rate is approximately 1.99801398 and the mean temporal rate is approximately 0.99139175. The spectral convergence rates in space and time are 1.99553923 and 0.95368736, respectively. We note that the spatial convergence matches the expectations of Lemma 2.2 but the temporal convergence rate is lower than the expected rate from Lemma 2.1. However, the temporal convergence rate is appropriately proportional to the spatial rate, hence, the reduced temporal convergence is a result of the Courant-Friedrichs-Lewy condition.

We would like to also note that implementing uniform grids or considerations of less exotic initial data will not drastically change the convergence rates nor the overall shape of the convergence surface plots. Furthermore, similar conclusions are confirmed in our experiments when nonsymmetric grids are utilized, though these results are admitted for brevity. The effects of nonuniform grids, that are not generated in a smooth manner, on convergence rates have yet to be explored in relation to quenching-combustion problems. On the other hand, to further raise the accuracy of schemes, say, to obtain a second-order temporal accuracy, we would need to implement spatial discretizations to the fourth order. This could be fulfilled via a nine-point scheme or a compact algorithm [64]. We also observe that, while the emergence of the quenching singularity reduces the spatial convergence rate significantly near the origin, the reduction is less severe than the reduction in temporal convergence. This is probably due to the fact that u and its spatial derivatives are well-behaved in our quenching computations [73, 85].

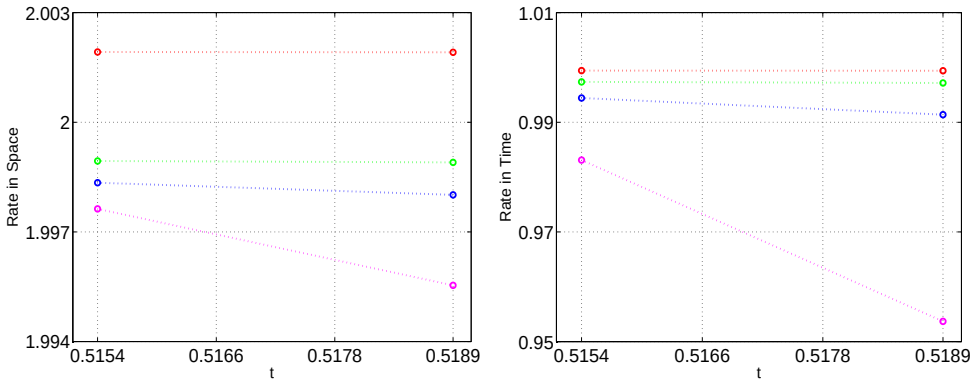

Figure 4.3: Spatial convergence rate p^h_{PW} and p^h_2 [LEFT] and temporal convergence rate q^τ_{PW} and p^h_2 [RIGHT] for the solution at times T_1, T_2 are given. The mean (blue), median (green), maximal (red), and spectral (magenta) convergence rates are included. Spatial and temporal rates are approximately two and one, respectively.

The temporal derivative of the solution of (4.28)-(4.31) becomes unbounded as $t \to T_q$ [73]. As a reference, in Figure 4.5 we explore the temporal convergence rate of u_t at times T_1 and T_2, respectively, in order to examine whether the explosive rate of change can significantly affect the convergence rate. The shapes of the surfaces in Figure 4.5 are no doubt similar to that in Figure 4.4. We find that the convergence rates drop significantly near the origin. However, the mean temporal convergence rate is still approximately first-order. We observe the average point-wise convergence rate is approximately 0.99167464 at T_1 and 0.98679266 at T_2. Further, the spectral convergence rates of u_t are 0.94815426 and 0.81981770 at times T_1 and T_2, respectively. This novel exploration of convergence issues provides profound insights into the full nature of singular nonlinear problems such as (4.1)-(4.3).

Table 4.1: Detailed spatial and temporal convergence rates. Spectral convergence rates in both space and time are also provided. The convergencerates in space match the expectations of Lemma 2.2. Temporal convergence rates agree well with the Courant-Friedrichs-Lewy condition.

Rate in Space		
p^h_{PW}	T_1	T_2
Maximum	2.0019227	2.0019154
Minimum	1.8354599	1.8354793
Median	1.9989409	1.9989027
Mean	1.9983457	1.9980140
p^h_2	1.9976312	1.9955392

Rate in Time		
q^τ_{PW}	T_1	T_2
Maximum	0.9994286	0.9993982
Minimum	0.9622788	0.8646401
Median	0.9973630	0.9971718
Mean	0.9944337	0.9913917
q^τ_2	0.9831086	0.9536874

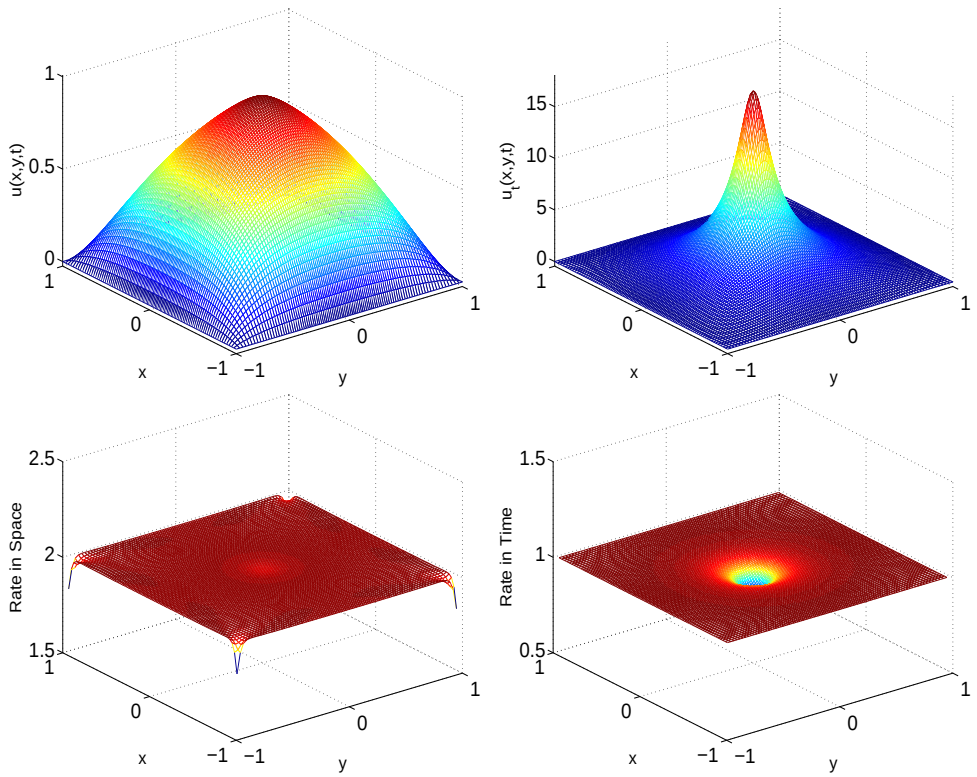

Figure 4.4: Three-dimensional profiles at T_2. The first row of surfaces are for the solution [LEFT] and its temporal derivative function [RIGHT], whereas the second row of surfaces represent the spatial convergence rate p^h_{PW} [LEFT] and temporal convergence rate q^τ_{PW} [RIGHT].

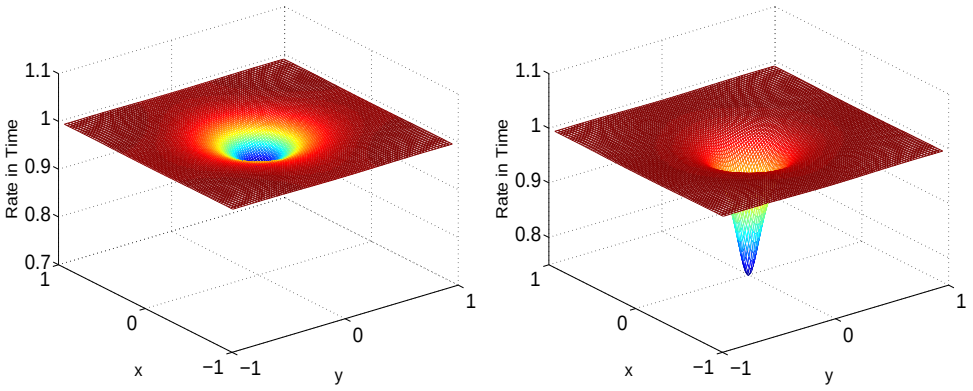

Figure 4.5: Surface profiles representing convergence rates, p^h_{PW}, q^τ_{PW}, of the temporal derivative of the solution, u_t, at T_1 [LEFT] and T_2 [RIGHT] . The minimum in the latter case is approximately 0.75147603.

Experiment 2

In this experiment we explore impacts of a degeneracy and a mild stochastic influence on both the solution and rates of convergence. In the following, we set $\varphi(\varepsilon) = \sqrt{\varepsilon}$ for $\varepsilon \in [0.98, 1.02]$, and $\sigma(x, y) = \sqrt{(x+1)^2 + (y+1)^2}$, $-1 \leq x, y \leq 1$. We note that this choice for $\sigma(x, y)$ forces the degeneracy to occur at $(-1, -1)$ [19, 75]. By choosing such a degeneracy function, we will be better able to observe its fast spreading effects on the solution. Our nonuniform grids are generated in the consideration that the quenching location will be shifted, but not too far away, from the origin [39]. See Figure 4.2 for a possible example of how to shift the grid appropriately. The convergence rates are computed in a manner similar similar to the previous experiment.

An elevated quenching time, $T_q \approx 0.83647379$, probably primarily due to the degeneracy [34], is observed. However, the vibrant stochastic feature of the reaction term may also increase quenching time [95]. Figure 4.6 depicts the solution and its derivative immediately prior to quenching. Just as we have anticipated, the quenching location is slightly shifted away from the origin to

$$(x_q, y_q) \approx (-0.15153317, -0.15153317).$$

The peak value of u_t, which is concentrated around the quenching location, reaches 279.53751378 immediately prior to quenching.

Due to our slightly delayed ignition-quenching time, T_q, we consider the following two arbitrary convergence testing times

$$T_1 = 0.82720376 \quad \text{and} \quad T_2 = 0.83420651.$$

A major change in spatial convergence is expected since the degeneracy $\sigma(x, y)$ is a spatial function creating strong singularities on the boundary of the spatial domain. In particular, a modification of the proof of Lemma 2.2 will show that the degeneracy limits the effects of generating a nonuniform grid via a smooth mapping due to its effects on solution smoothness [71, 85]. It seems that the stronger the singularity is, the more the order of spatial accuracy and convergence is reduced.

Table 4.2 is devoted to convergence information in space and time at sampling times T_1 and T_2. From Table 4.2 we may also notice that while the mean and median convergence rates strongly suggest a slightly higher than one rate of convergence in space and slightly lower than one rate of convergence in time, minimal and maximal rate estimates differ significantly. Again, the point-wise rates of convergence and temporal spectral rate of convergence decrease as $t \to T_q$, though reductions are less significant probably also due to a stronger restriction on temporal step sizes to maintain the solution positivity when $\sigma(x, y)$ is nontrivial [19–21, 39, 93–95]. The spatial spectral convergence rate actually increases in time, but this is due to the solution becoming more smooth near the corners of the domain as the solution is iterated. These phenomenon are well documented by Figure 4.7 where spatial and temporal convergence rates of the numerical solution under the influences of a nonconstant degenerate function $\sigma(x, y)$ and a nonlinear stochastic reaction term are exhibited.

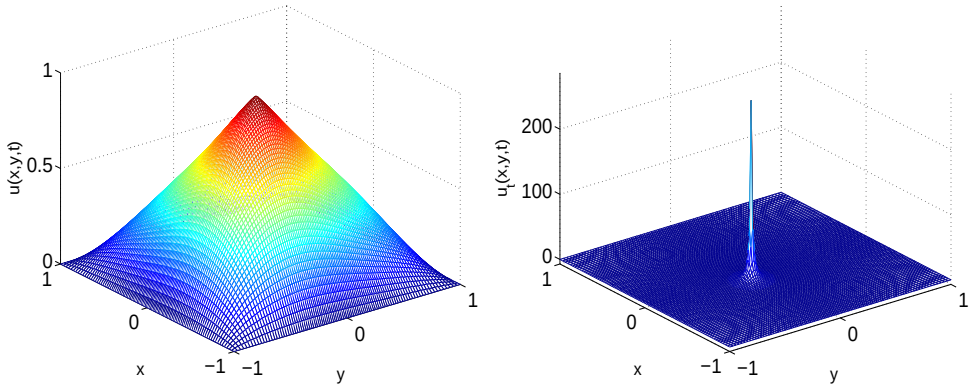

Figure 4.6: Solution u [LEFT] and its temporal derivative function u_t [RIGHT] as $t \to T_q$. We have the maximum $_{-1\leq x,y\leq 1} u_t(x, y, t) = u_t(x_q, y_q, t) \approx 279.53751378$ as $t \to T_q$.

Table 4.2: Detailed spatial and temporal convergence rates. The experimental results suggest clearly a slightly above one spatial convergence rate, and slightly below one temporal rate.

Rate in Space			Rate in Time		
p^h_{PW}	T_1	T_2	q^τ_{PW}	T_1	T_2
Maximum	3.8371304	3.7599219	Maximum	0.9999996	0.9999993
Minimum	-1.2521872	-1.2048243	Minimum	0.9989553	0.9956911
Median	1.1193987	1.1231935	Median	0.9999220	0.9999153
Mean	1.1156642	1.1258041	Mean	0.9998710	0.9998046
p^h_2	1.2147392	1.3080651	q^τ_2	0.9995514	0.9985600

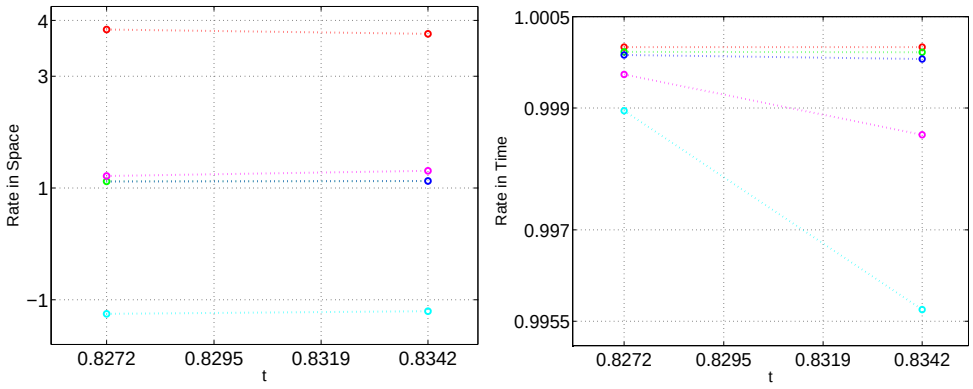

Figure 4.7: Spatial convergence rates p^h_{PW} and p^h_2 [LEFT] and temporal convergence rates q^h_{PW} and q^h_2 [RIGHT] for the solution at times T_1 and T_2. The mean (blue), median (green), maximal (red), minimal (cyan), and spectral (magenta) rates are included. The mean and median curves almost overlap in the first picture. The negative minimal rate of convergence in space is due to spurious artifacts of the degeneracy.

Figure 4.8 illustrates the solution of our stochastic degenerate problem, as well as its derivative, at time T_2. Surface plots of the spatial and temporal convergence are also presented. We note that there is a visible shift of the quenching location, as well as the position of the peaks of $u,\ u_t$, to (x_q, y_q). This shift agrees well with existing predictions [39]. Slight dips in convergence rates at the quenching point can also be observed in Figure 4.8. Needless to say, the point-wise convergence rate surfaces provide further insights into the maximal and minimal rates noted in Table 4.2 and Figure 4.7.

From the surface plots in Figure 4.8, we observe that spurious issues occur at the corner opposite of the degeneracy in the spatial domain. This phenomenon can be explained by the fact that the degeneracy simplifies the problem at $(-1, -1)$ by reducing the parabolic problem computationally to an elliptic problem. However, the degeneracy still creates disturbances, which are observed in the extreme convergence rates near the point $(1, 1)$.

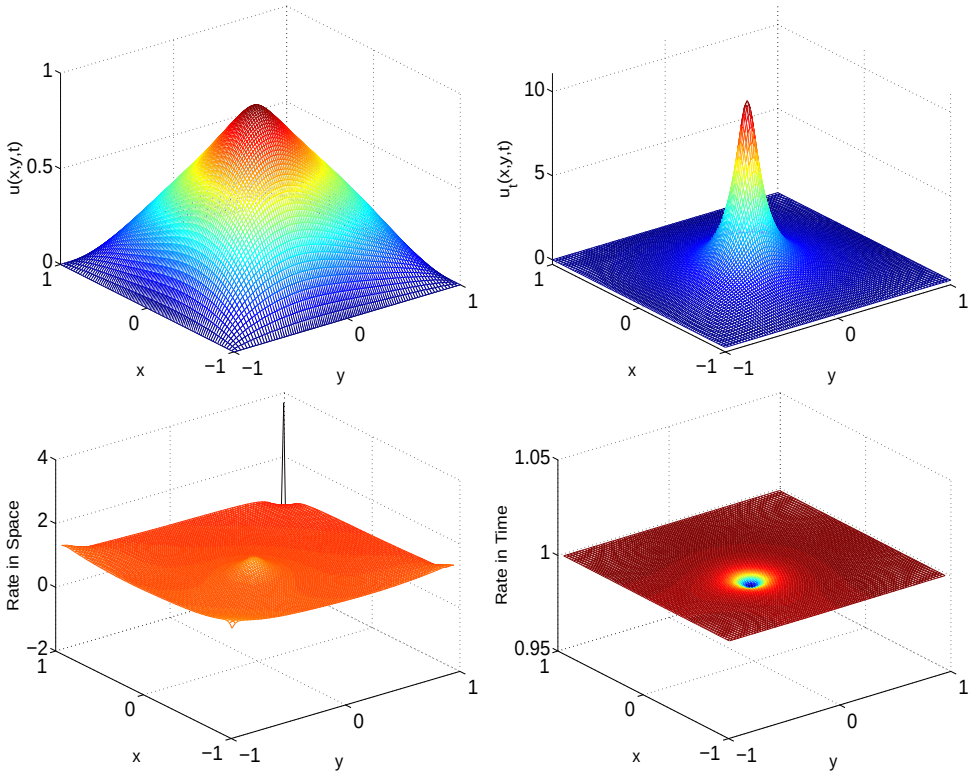

Figure 4.8: Surface profiles at time T_2. The first row is for the solution [LEFT] and its temporal derivative [RIGHT], whereas the second row is for the rates of convergences in space [LEFT] and in time [RIGHT].

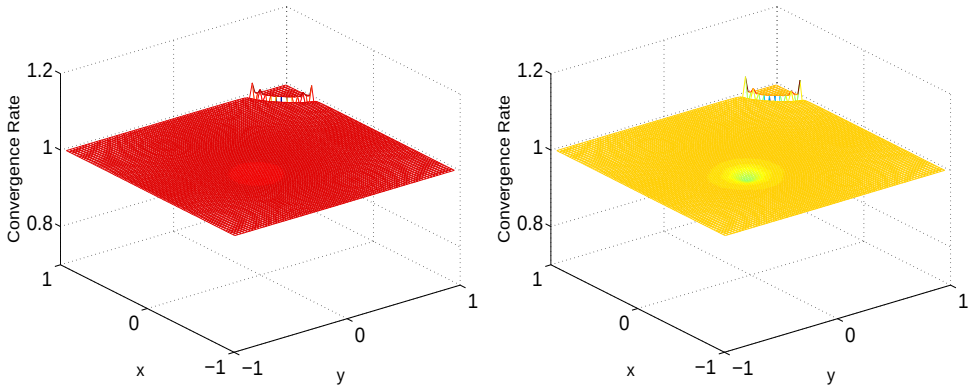

Figure 4.9: Surface plots of the point-wise rates of convergence rates in time for the temporal derivative function of the solution, u_t, at T_1 [LEFT] and T_2 [RIGHT] within the spatial domain. The mean convergence rates are approximately 0.991674641553278 and 0.986792663593675, respectively.

As we have seen, surface illustrations will reflect the fact that the convergence issues can be restricted to a small number of mesh points near a corner of the domain due to the impacts from degeneracy. This is further recorded in Figure 4.9 which shows that the degeneracy has a noticeable effect on the temporal convergence of u_t. There is an obvious ring of distinctive oscillatory waves near $(1, 1)$ in the figure. However, these oscillations have little impact on the mean or median convergence rates which evolve from 0.99167464 to 0.98679266 in Figure 4.11. Further, the spectral convergence rates of u_t evolve from 0.99633898 to 0.98532666. These rates of convergence for the temporal derivative function are ideal, as their magnitudes resemble those of the previous example.

CHAPTER FIVE

The Three-Dimensional Degenerate Stochastic Kawarada Equation

5.1 Introduction

Let $\Omega = (-a, a) \times (-b, b) \times (-c, c) \subset \mathbb{R}^3$, where $a, b, c > 0$, and $\partial\Omega$ be its boundary. Denote $\mathcal{D} = \Omega \times (t_0, T_q)$, $\mathcal{S} = \partial\Omega \times (t_0,\ T_q)$ for given $0 \leq t_0 < T_q < \infty$. We consider the following degenerate Kawarada problem with vibrant stochastic influence,

$$\sigma(x, y, z)u_t = u_{xx} + u_{yy} + u_{zz} + \varphi(\varepsilon)f(u), \quad (x, y, z, t) \in \mathcal{D}, \tag{5.1}$$

$$u(x, y, z, t) = 0, \quad (x, y, z, t) \in \mathcal{S}, \tag{5.2}$$

$$u(x, y, z, t_0) = u_0(x, y, z), \quad (x, y, z) \in \Omega, \tag{5.3}$$

where $\sigma(x, y, z) = ((-1 + x)^2 + (-1 + y)^2 + (-1 + z)^2)^{p/2}$, $p \in [0, 2]$. The nonlinear source function, $f(u)$, is strictly increasing for $0 \leq u < 1$ with

$$f(0) = f_0 > 0, \quad \lim_{u \to 1^-} f(u) = \infty$$

and $\varphi(\varepsilon) : 0 < \varphi_{\min} \leq \varphi \leq \varphi_{\max}$, is a stochastic inference function of the random variable $\varepsilon(x, y, z)$. In idealized thermal combustion applications [4, 22, 105], u represents the temperature in the combustion chamber, and the x-, y-, and z-coordinates coincide with the chamber walls. The initial temperature $0 \leq u_0 \ll 1$ is typically chosen to be small. The function $\sigma(x, y, z)$ represents certain singularities in the temperature transportation speed within the channel, which causes the degeneracy in the differential equation (5.1) [20, 75, 92, 108].

Numerous computational procedures, including moving mesh adaptive methods, have been constructed for solving blow-up and Kawarada problems in the past decades (interested readers are referred to [5, 39, 48, 75, 108] and references therein). Though in the former case, adaptations are frequently achieved via monitoring func-

tions on the arc-length of the function u; in the latter situation, adaptations are more likely to be built upon the arc-length of u_t, since it is directly proportional to $f(u)$, which blows up as u quenches [36, 84, 109].

As reported in several recent investigations, when quenching locations can be predetermined, it is preferable to use nonuniform spatial grids throughout the computations [20, 75, 79]. In this case, key quenching characteristics such as the quenching time and critical domain, are more easily observed; also important numerical properties of underlying algorithms, including the monotonicity, stability and convergence, can be more precisely studied. To that end, this chapter develops a temporally adaptive splitting scheme utilizing predetermined nonuniform spatial grids. The positivity, monotonicity, and stability of the method will be investigated. It is also observed that the impact of the degeneracy is limited for our implicit scheme. Our discussions will be organized as follows. In the next section, the semi-adaptive LOD scheme for solving (5.1)-(5.3) will be constructed and discussed. Then, in Section 5.3, criteria to guarantee the positivity of the numerical scheme will be determined. In Section 5.4, appropriate criteria for guaranteeing the monotonicity will be obtained. These two sections together serve as the platform for carrying out investigations of stability. Section 5.5 is devoted to the stability analysis of the semi-adaptive LOD scheme. The analysis will first be carried out for a fully linearized scheme, and then a more realistic stability analysis is proposed without freezing the nonlinear stochastic source term. For now, no numerical studies of the three-dimensional degenerate Karawada problem will be given.

5.2 Semi-Adaptive LOD Scheme

Utilizing the transformations $\tilde{x} = x/a,\ \tilde{y} = y/b,\ \tilde{z} = z/c$, and reusing the original variables for simplicity, we may reformulate (5.1)-(5.3) as

$$u_t = \frac{1}{a^2\sigma}u_{xx} + \frac{1}{b^2\sigma}u_{yy} + \frac{1}{c^2\sigma}u_{zz} + g(\varepsilon, u), \quad (x, y, z, t) \in \mathcal{D}, \tag{5.4}$$

$$u(x,y,z,t) = 0, \quad (x,y,z) \in \mathcal{S}, \tag{5.5}$$

$$u(x,y,z,t_0) = u_0, \quad (x,y,z) \in \Omega, \tag{5.6}$$

where $g(\varepsilon,u) = \varphi(\varepsilon)f(u)/\sigma,\ \sigma(x,y,z) = (a^2x^2 + b^2y^2 + c^2z^2)^{p/2}$, and $\Omega = (-1,1) \times (-1,1) \times (-1,1) \subset \mathbb{R}^3$.

Let $N_x, N_y, N_z \gg 1$ be fixed integers. We inscribe over $\bar{\Omega}$ the following variable grid:

$$\Omega_h = \{(x_i, y_j, z_k)\ :\ 0 \le i \le N_x + 1;\ 0 \le j \le N_y + 1; 0 \le k \le N_z + 1;\}$$

where $x_0 = y_0 = z_0 = -1,\ x_{N_x+1} = y_{N_y+1} = z_{N_z+1} = 1$. Denote $h_{x,i} = x_{i+1} - x_i > 0,\ h_{y,j} = y_{j+1} - y_j > 0$, and $h_{z,k} = z_{k+1} - z_k > 0$ for $1 \le i \le N_x,\ 1 \le j \le N_y,\ 1 \le k \le N_z$. See Figure 5.1 for possible nonuniform grids to be used for solving (5.4)-(5.6). Let $u_{i,j,k}(t)$ be an approximation of the solution of (5.4)-(5.6) at the point (x_i, y_j, z_k, t) and consider the following first-order finite differences [75],

$$\begin{aligned}
\partial_x^2 u(x_i,y_j,z_k,t) &\approx \frac{2u_{i-1,j,k}(t)}{h_{x,i-1}(h_{x,i-1}+h_{x,i})} - \frac{2u_{i,j,k}(t)}{h_{x,i-1}h_{x,i}} + \frac{2u_{i+1,j,k}(t)}{h_{x,i}(h_{x,i-1}+h_{x,i})},\\
\partial_y^2 u(x_i,y_j,z_k,t) &\approx \frac{2u_{i,j-1,k}(t)}{h_{y,j-1}(h_{y,j-1}+h_{y,j})} - \frac{2u_{i,j,k}(t)}{h_{y,j-1}h_{y,j}} + \frac{2u_{i,j+1,k}(t)}{h_{y,j}(h_{y,j-1}+h_{y,j})},\\
\partial_z^2 u(x_i,y_j,z_k,t) &\approx \frac{2u_{i,j,k-1}(t)}{h_{z,k-1}(h_{z,k-1}+h_{z,k})} - \frac{2u_{i,j,k}(t)}{h_{z,k-1}h_{z,k}} + \frac{2u_{i,j,k+1}(t)}{h_{z,k}(h_{z,k-1}+h_{z,k})},
\end{aligned}$$

for $(x_i, y_j, z_k) \in \Omega_h^\circ$. Further, denote

$$\begin{aligned}
v(t) &= (u_{1,1,1}, u_{2,1,1}, \ldots, u_{N_x,1,1}, u_{1,2,1}, u_{2,2,1}, \ldots, u_{N_x,2,1}, \ldots, u_{1,N_y,1}, u_{2,N_y,1},\\
&\qquad \ldots, u_{N_x,N_y,1}, \ldots, u_{1,N_y,N_z}, u_{2,N_y,N_z}, \ldots, u_{N_x,N_y,N_z})^\intercal \in \mathbb{R}^{N_xN_yN_z}
\end{aligned}$$

and let $g(\varepsilon, v)$ be an appropriate discretization of the nonhomogeneous term of (5.4). We obtain readily from (5.4)-(5.6) the following semi-discretized system

$$v'(t) = \sum_{\sigma=1}^{3} M_\sigma v(t) + g(\varepsilon, v(t)), \quad t_0 < t < T_q, \tag{5.7}$$

$$v(t_0) = v_0, \tag{5.8}$$

where

$$M_1 = \frac{1}{a^2} B(I_{N_z} \otimes I_{N_y} \otimes P_x),\ M_2 = \frac{1}{b^2} B(I_{N_z} \otimes P_y \otimes I_{N_x}),\ M_3 = \frac{1}{c^2} B(P_z \otimes I_{N_y} \otimes I_{N_x}),$$

$\otimes$ stands for the Kronecker product, $I_{N_\sigma} \in \mathbb{R}^{N_\sigma \times N_\sigma}$, $\sigma = 1, 2, 3$, are identity matrices, and

$$\begin{aligned}
B &= \operatorname{diag}\left(\phi_{1,1,1}^{-1}, \phi_{2,1,1}^{-1}, ..., \phi_{N_x,1,1}^{-1}, \phi_{1,2,1}^{-1}, ..., \phi_{N_x,N_y,N_z}^{-1}\right) \in \mathbb{R}^{N_x N_y N_z \times N_x N_y N_z}, \\
\phi_{i,j,k} &= \left[a^2 \left(-1 + \sum_{\ell=0}^{i-1} h_{x,\ell} \right)^2 + b^2 \left(-1 + \sum_{\ell=0}^{j-1} h_{y,\ell} \right)^2 + c^2 \left(-1 + \sum_{\ell=0}^{k-1} h_{z,\ell} \right)^2 \right]^{q/2}, \\
P_\sigma &= \begin{pmatrix}
m_{\sigma,1} & n_{\sigma,1} & & & \\
l_{\sigma,1} & m_{\sigma,2} & n_{\sigma,2} & & \\
 & \cdots & \cdots & \cdots & \\
 & & l_{\sigma,N_\sigma-2} & m_{\sigma,N_\sigma-1} & n_{\sigma,N_\sigma-1} \\
 & & & l_{\sigma,N_\sigma-1} & m_{\sigma,N_\sigma}
\end{pmatrix} \in \mathbb{R}^{N_\sigma \times N_\sigma}, \quad \sigma = 1, 2, 3,
\end{aligned}$$

and for the above

$$\begin{aligned}
l_{\sigma,j} &= \frac{2}{h_{\sigma,j}(h_{\sigma,j} + h_{\sigma,j+1})},\ n_{\sigma,j} = \frac{2}{h_{\sigma,j}(h_{\sigma,j-1} + h_{\sigma,j})}, \quad j = 1, \ldots, N_\sigma - 1, \\
m_{\sigma,j} &= -\frac{2}{h_{\sigma,j-1} h_{\sigma,j}}, \quad j = 1, \ldots, N_\sigma;\ \sigma = x, y, z.
\end{aligned}$$

The formal solution of (5.7), (5.8) can thus be written as

$$v(t) = E(tC)v_0 + \int_{t_0}^{t} E((t-s)C) g(\varepsilon, v(s))\, ds, \quad t_0 < t < T_q, \tag{5.9}$$

where $E(\cdot) = \exp(\cdot)$ is the matrix exponential and $C = \sum_{\sigma=1}^{3} M_\sigma$ [105].

In principle, different approximation techniques can be used to yield different splitting methods based on (5.9) [53, 105, 109]. Yet, we are particularly interested in approximating (5.9) via a trapezoidal rule and a [1/1] Padé approximations, $E(tC) = p(t) + \mathcal{O}(t^2)$, $t \to 0$, where

$$p(t) = \prod_{\sigma=1}^{3} \left(I - \frac{t}{2} M_\sigma \right)^{-1} \left(I + \frac{t}{2} M_\sigma \right), \quad t_0 < t < T_q.$$

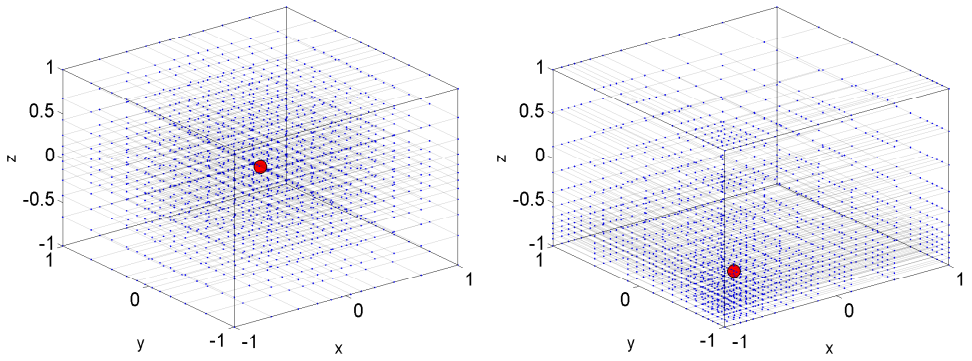

Figure 5.1: An illustration of three-dimensional nonuniform grids to be used for solving (5.4)-(5.6). A standard symmetric nonuniform grid to be used when $\sigma(x, y, z) \equiv 1$ [LEFT] and a possible nonuniform grid to be used when $\sigma(x, y, z)$ is defined as above [RIGHT].

The above leads to

$$v(t) = p(t)\left[v_0 + \frac{t}{2}g(v_0)\right] + \frac{t}{2}g(\varepsilon, v(t)) + \mathcal{O}\left((t - t_0)^2\right), \quad t \to t_0. \tag{5.10}$$

The above LOD algorithm provides a highly efficient way to compute numerical solutions of multidimensional problems such as (5.4)-(5.6) [53, 75, 104, 108]. Based on (5.10), we obtain the following first-order in space and time semi-adaptive LOD scheme:

$$v_{\ell+1} = \left[\prod_{\sigma=1}^{3}\left(I - \frac{\tau_\ell}{2}M_\sigma\right)^{-1}\left(I + \frac{\tau_\ell}{2}M_\sigma\right)\right]\left(v_\ell + \frac{\tau_\ell}{2}g(\varepsilon, v_\ell)\right) + \frac{\tau_\ell}{2}g(\varepsilon, v_{\ell+1}), \tag{5.11}$$

where v_ℓ and $v_{\ell+1}$ are approximations of $v(t_\ell)$ and $v(t_{\ell+1})$, respectively, v_0 is the initial vector, $t_\ell = t_0 + \sum_{k=0}^{\ell-1}\tau_k$, $\ell = 0, 1, 2, \ldots$, and $\{\tau_\ell\}_{\ell\geq 0}$ is a set of variable temporal steps determined by an adaptive procedure.

Again, we interpret all inequalities to be componentwise in the following analysis.

Since positive computational solutions preserve the correct physical features of quenching phenomena, it is crucial that our numerical solution also possesses this feature. Once again, we determine criteria to guarantee this property.

Lemma 5.1. $\|P_\sigma\|_2 \leq \max_{j=1,\ldots,N_\sigma} \left\{4/h_{\sigma,j}^2\right\},\ \sigma = 1,2,3.$

Proof. Due to the similarity in structure, we only consider P_1 since the other two cases follow by similar arguments. Note that, in general, P_1 is not symmetric. However, $\|P_1\|_2^2 = \rho(P_1^\intercal P_1)$ and $P_1^\intercal P_1$ is symmetric with a bandwidth of five. Thus,

$$P_1^\intercal P_1 = \begin{pmatrix} \tilde{m}_{1,1} & \tilde{n}_{1,1} & \tilde{N}_{1,1} & & & & \\ \tilde{l}_{1,1} & \tilde{m}_{1,2} & \tilde{n}_{1,2} & \tilde{N}_{1,2} & & & \\ \tilde{L}_{1,1} & \tilde{l}_{1,2} & \tilde{m}_{1,3} & \tilde{n}_{1,3} & \tilde{N}_{1,3} & & \\ & & \cdots & \cdots & \cdots & \cdots & \\ & & \tilde{L}_{1,N_1-4} & \tilde{l}_{1,N_1-3} & \tilde{m}_{1,N_1-2} & \tilde{n}_{1,N_1-2} & \tilde{N}_{1,N_1-2} \\ & & & \tilde{L}_{1,N_1-3} & \tilde{l}_{1,N_1-2} & \tilde{m}_{1,N_1-1} & \tilde{n}_{1,N_1-1} \\ & & & & \tilde{L}_{1,N_1-2} & \tilde{l}_{1,N_1-1} & \tilde{m}_{1,N_1} \end{pmatrix} \in \mathbb{R}^{N_1 \times N_1},$$

where

$$\begin{aligned} \tilde{N}_{1,j} &= \tilde{L}_{1,j} = l_{1,j} n_{1,j+1}, \quad j = 1,\ldots,N_1-2, \\ \tilde{n}_{1,j} &= \tilde{l}_{1,j} = m_{1,j} n_{1,j} + m_{1,j+1} l_{1,j}, \quad j = 1,\ldots,N_1-1, \\ \tilde{m}_{1,j} &= \begin{cases} m_{1,1}^2 + l_{1,1}^2, & j = 1, \\ n_{1,j-1}^2 + m_{1,j}^2 + l_{1,j}^2, & j = 2,\ldots,N_1-1, \\ n_{1,N_1-1}^2 + m_{1,N_1}^2, & j = N_1. \end{cases} \end{aligned}$$

We may determine a bound on the spectral radius of $P_1^\intercal P_1$ by using Geršchgorin's circle theorem. In fact, only rows containing five nontrivial elements, *i.e.,* $j = 3,\ldots,N_1-2$, need to be considered. To this end,

$$|\lambda_{1,j} - \tilde{m}_{1,j}| \leq |\tilde{L}_{1,j-2}| + |\tilde{l}_{1,j-1}| + |\tilde{n}_{1,j}| + |\tilde{N}_{1,j}|, \quad j = 3,\ldots,N_1-2,$$

which gives

$$\begin{aligned} -|m_{1,j-1}n_{1,j-1} + m_{1,j}l_{1,j-1}| - |m_{1,j}n_{1,j} + m_{1,j+1}l_{1,j}| \\ -|l_{1,j-2}n_{1,j-1}| - |l_{1,j}n_{1,j+1}| + n_{1,j-1}^2 + m_{1,j}^2 + l_{1,j}^2 \;\leq\; \lambda_{1,j} \end{aligned} \tag{5.12}$$

and

$$\begin{aligned} \lambda_{1,j} \;\leq\; & |m_{1,j-1}n_{1,j-1} + m_{1,j}l_{1,j-1}| + |m_{1,j}n_{1,j} + m_{1,j+1}l_{1,j}| \\ & +|l_{1,j-2}n_{1,j-1}| + |l_{1,j}n_{1,j+1}| + n_{1,j-1}^2 + m_{1,j}^2 + l_{1,j}^2. \end{aligned} \tag{5.13}$$

Let $h_1 \equiv \min_{j=1,\ldots,N_1}\{h_{1,j}\}$. From (5.13) we acquire that

$$\begin{aligned} \lambda_{1,j} \;\leq\; & \frac{2}{h_1^2}\cdot\frac{2}{2h_1^2} + \frac{2}{h_1^2}\cdot\frac{2}{2h_1^2} + \frac{2}{h_1^2}\cdot\frac{2}{2h_1^2} + \frac{2}{h_1^2}\cdot\frac{2}{2h_1^4} + \frac{4}{4h_1^4} + \frac{4}{4h_1^2} \\ & + \left(\frac{2}{2h_1^2}\right)^2 + \left(\frac{2}{h_1^2}\right)^2 + \left(\frac{2}{2h_1^2}\right)^2 \;=\; \frac{16}{h_1^4}. \end{aligned}$$

Now, reverse (5.12) and by the same token,

$$\begin{aligned} -\lambda_{1,j} \;\leq\; & |m_{1,j-1}n_{1,j-1} + m_{1,j}l_{1,j-1}| + |m_{1,j}n_{1,j} + m_{1,j+1}l_{1,j}| + |l_{1,j-2}n_{1,j-1}| \\ & +|l_{1,j}n_{1,j+1}| - n_{1,j-1}^2 - m_{1,j}^2 - l_{1,j}^2 \\ \leq\; & |m_{1,j-1}n_{1,j-1} + m_{1,j}l_{1,j-1}| + |m_{1,j}n_{1,j} + m_{1,j+1}l_{1,j}| + |l_{1,j-2}n_{1,j-1}| \\ & +|l_{1,j}n_{1,j+1}| + n_{1,j-1}^2 + m_{1,j}^2 + l_{1,j}^2 \;\leq\; \frac{16}{h_1^4}\,, \end{aligned}$$

where, once again, $h_1 \equiv \min_{j=1,\ldots,N_1}\{h_{1,j}\}$. Thus, combining the bounds we have $\|P_1\|_2 \leq \max_{i=1,\ldots,N_1}\left\{4/h_{1,j}^2\right\}$. The other bounds follow similarly. ∎

Lemma 5.2. *Let*

$$\beta_{\min} = \frac{h^2}{2\|B\|_2} = \frac{h^2\min_{i,j,k}\phi_{i,j,k}}{2}, \quad h = \min_{j=1,\ldots,N_\sigma;\,\sigma=1,2,3}\{h_{\sigma,j}\},$$

If

$$\frac{\tau_\ell}{\beta_{\min}} < \min\left\{a^2, b^2, c^2\right\}, \tag{5.14}$$

then the matrices

$$I - \frac{\tau_\ell}{2}M_\sigma,\; I + \frac{\tau_\ell}{2}M_\sigma, \quad \sigma = 1,2,3,$$

are nonsingular. Further, $I - \frac{\tau_\ell}{2} M_\sigma,\ \sigma = 1, 2, 3,$ *are monotone and inverse-positive, and* $I + \frac{\tau_\ell}{2} M_\sigma,\ \sigma = 1, 2, 3,$ *are nonnegative.*

Proof. First, note that

$$\begin{aligned} \left\| \frac{\tau_\ell}{2} M_1 \right\|_2 &= \frac{\tau_\ell}{2a^2} \|B(I_{N_3} \otimes I_{N_2} \otimes P_1)\|_2 \\ &\leq \frac{\tau_\ell}{2a^2} \|B\|_2 \|I_{N_3} \otimes I_{N_2} \otimes P_1\|_2 \\ &= \frac{\tau_\ell}{2a^2} \|B\|_2 \|P_1\|_2 \\ &\leq \frac{\tau_\ell}{a^2} \|B\|_2 \max_{j=1,\ldots,N_1} \left\{ \frac{2}{h_{1,j}^2} \right\} \\ &< 1. \end{aligned}$$

Hence, $I + \frac{\tau_\ell}{2} M_1$ is nonsingular, and also nonnegative. Similar arguments give that $I + \frac{\tau_\ell}{2} M_2$ and $I + \frac{\tau_\ell}{2} M_3$ are nonsingular and nonnegative.

Now, consider $A = I - \frac{\tau_\ell}{2} M_1$. As $A_{ij} \leq 0$ for $i \neq j$ and the weak row sum criterion is satisfied, A is monotone, and hence an inverse exists and is nonnegative. So, A must be inverse-positive [54]. Similar arguments can be given for $I - \frac{\tau_\ell}{2} M_2$ and $I - \frac{\tau_\ell}{2} M_3$. This ensures the proof. ∎

5.4 Monotonicity

Another key characteristic which distinguishes a solution to a quenching problem from a solution to most blow-up problems is its monotonicity with respect to time $t \geq t_0$ [4, 5, 36, 84, 108]. Thus, it is once again necessary to guarantee that our numerical solution preserves this property throughout computations when solving the Kawarada equation (5.1)-(5.3) or (5.4)-(5.6).

In the following, we denote

$$\Phi_\ell = \prod_{\sigma=1}^{3} \left(I - \frac{\tau_\ell}{2} M_\sigma \right)^{-1} \left(I + \frac{\tau_\ell}{2} M_\sigma \right).$$

Further, due to (5.14), if $\tau_\ell > 0$ is sufficiently small, then we have

$$\Phi_\ell = \Psi_\ell + \mathcal{O}\left(\tau_\ell^2\right), \quad \tau_\ell \to 0^+,$$

where

$$\Psi_\ell = \left(I - \frac{\tau_\ell}{2}C\right)^{-1}\left(I + \frac{\tau_\ell}{2}C\right).$$

Lemma 5.3. *If $Cv_0 + g(\varepsilon, v_0) > 0$ and $\tau_k \geq 0$ are sufficiently small for $0 \leq k \leq \ell$, then it follows that $Cv_\ell + g(\varepsilon, v_\ell) > 0$ for all $\ell \geq 0$.*

Proof. First, we proceed be computing the following:

$$\begin{aligned}
Cv_{k+1} + g(\varepsilon, v_{k+1}) &= C\left[\Phi_k\left(v_k + \frac{\tau_k}{2}g(\varepsilon, v_k)\right) + \frac{\tau_k}{2}g(\varepsilon, v_{k+1})\right] + g(\varepsilon, v_{k+1}) \\
&= C\left[\Psi_k\left(v_k + \frac{\tau_k}{2}g(\varepsilon, v_k)\right) + \frac{\tau_k}{2}g(\varepsilon, v_{k+1})\right] \\
&\qquad + g(\varepsilon, v_{k+1}) + \mathcal{O}\left(\tau_k^2\right), \quad \tau_k \to 0^+ \\
&= C\left(I - \frac{\tau_k}{2}C\right)^{-1}\left[\left(I + \frac{\tau_k}{2}C\right)\left(v_k + \frac{\tau_k}{2}g(\varepsilon, v_k)\right)\right] \\
&\qquad + \left(I + \frac{\tau_k}{2}C\right)g(\varepsilon, v_{k+1}) + \mathcal{O}\left(\tau_k^2\right), \quad \tau_k \to 0^+ \\
&> C\left(I - \frac{\tau_k}{2}C\right)^{-1}\left[\left(I + \frac{\tau_k}{2}C\right)\left(v_k + \frac{\tau_k}{2}g(\varepsilon, v_k)\right)\right] \\
&\qquad + \left(I + \frac{\tau_k}{2}C\right)g(\varepsilon, v_k) + \mathcal{O}\left(\tau_k^2\right), \quad \tau_k \to 0^+ \\
&= \left(I - \frac{\tau_k}{2}C\right)^{-1}\left(I + \frac{\tau_k}{2}C\right)\left[Cv_k + \frac{\tau_k}{2}Cg(\varepsilon, v_k)\right. \\
&\qquad \left. + \left(I - \frac{\tau_k}{2}C\right)g(\varepsilon, v_k)\right] + \mathcal{O}\left(\tau_k^2\right) \\
&= \left(I - \frac{\tau_k}{2}C\right)^{-1}\left(I + \frac{\tau_k}{2}C\right)\left[Cv_k + g(\varepsilon, v_k)\right] \\
&\qquad + \mathcal{O}\left(\tau_k^2\right), \quad \tau_k \to 0^+,
\end{aligned}$$

where the inequality follows from the fact that $f(u)$ is strictly increasing and Lemma 3.4. Second, we proceed by induction. Letting $k = 0$ we have

$$Cv_1 + g(\varepsilon, v_1) > \left(I - \frac{\tau_0}{2}C\right)^{-1}\left(I + \frac{\tau_0}{2}C\right)\left[Cv_0 + g(\varepsilon, v_0)\right] + \mathcal{O}\left(\tau_0^2\right) > 0$$

for τ_0 sufficiently small by the assumption and Lemmas 5.2 and 3.4. Third, we assume that the inequality holds for $k = \ell - 1$. It follows that

$$Cv_\ell + g(\varepsilon, v_\ell) > \left(I - \frac{\tau_{\ell-1}}{2}C\right)^{-1}\left(I + \frac{\tau_{\ell-1}}{2}C\right)\left[Cv_{\ell-1} + g(\varepsilon, v_{\ell-1})\right] + \mathcal{O}\left(\tau_\ell^2\right) > 0,$$

for τ_ℓ sufficiently small by the inductive assumption and Lemmas 5.2 and 3.4, which completes the induction. ∎

Lemma 5.4. *If* (5.14) *holds,* $\tau_k \geq 0$ *are sufficiently small for all* $0 \leq k \leq \ell$, *and* $Cv_0 + g(\varepsilon, v_0) > 0$, *then* $v_{\ell+1} \geq v_\ell$ *for all* $\ell \geq 0$. *That is, the sequence* $\{v_\ell\}_{\ell=0}^{\infty}$ *is monotonically increasing.*

Proof. From (5.11) we observe that

$$\begin{aligned}
v_{k+1} - v_k &= \Phi_k\left(v_k + \frac{\tau_k}{2} g(\varepsilon, v_k)\right) + \frac{\tau_k}{2} g(\varepsilon, v_{k+1}) - v_k \\
&> \Phi_k\left(v_k + \frac{\tau_k}{2} g(\varepsilon, v_k)\right) + \frac{\tau_k}{2} g(\varepsilon, v_k) - v_k \\
&= \Psi_k\left(v_k + \frac{\tau_k}{2} g(\varepsilon, v_k)\right) + \frac{\tau_k}{2} g(\varepsilon, v_k) - v_k + \mathcal{O}\left(\tau_k^2\right), \quad \tau_k \to 0^+ \\
&= \left(I - \frac{\tau_k}{2} C\right)^{-1} \left\{\left(I + \frac{\tau_k}{2} C\right)\left[v_k + \frac{\tau_k}{2} g(\varepsilon, v_k)\right]\right. \\
&\qquad \left. - \left(I - \frac{\tau_k}{2} C\right)\left[v_k - \frac{\tau_k}{2} g(\varepsilon, v_k)\right]\right\} + \mathcal{O}\left(\tau_k^2\right), \quad \tau_k \to 0^+ \\
&= \left(I - \frac{\tau_k}{2} C\right)^{-1} \left(I + \frac{\tau_k}{2} C\right)\left[\tau_k \left(C v_k + g(\varepsilon, v_k)\right)\right] + \mathcal{O}\left(\tau_k^2\right), \quad \tau_k \to 0^+ \\
&> 0,
\end{aligned}$$

by the assumptions and Lemmas 5.2 and 3.4. Since the result holds for all $k \geq 0$, we have that the sequence $\{v_\ell\}_{\ell \geq 0}$ is monotonically increasing as desired. ∎

It is not uncommon to set $v_0 \equiv 0$ in practical combustion simulations. The following corollary shows that in this case the conditions in Lemma 4.1 are satisfied for $\ell = 0$.

Corollary 5.5. *If* $v_0 \equiv 0$ *then* $Cv_0 + g(\varepsilon, v_0) > 0$.

Proof. For $v_0 \equiv 0$ we have

$$Cv_0 + g(\varepsilon, v_0) = g(\varepsilon, v_0).$$

Since $\varphi(\varepsilon) \geq \varphi_{\min} > 0$ and $f(0) = f_0 > 0$, the result follows. ∎

Lemma 5.6. *For any* $\tau_\ell > 0$ *we have*

$$\left(I - \frac{\tau_\ell}{2} M_\sigma\right) x \geq x, \quad \sigma = 1, 2, 3,$$

where $x = (1, 1, \ldots, 1)^\intercal$.

Proof. We only need to show the case with

$$w = \left(I - \frac{\tau_\ell}{2} M_1\right) x = (w_{1,1,1}, \ldots, w_{i,j,k}, \ldots, w_{N_1,N_2,N_3})^\intercal.$$

First, we observe that

$$\begin{aligned} w_{1,1,1} &= \left(1 - \frac{\tau_\ell}{2} \cdot \frac{-2}{a^2 \phi_{1,1,1} h_{1,0} h_{1,1}}\right) - \frac{\tau_\ell}{2} \cdot \frac{2}{a^2 \phi_{1,1,1} h_{1,1} (h_{1,0} + h_{1,1})} \\ &= 1 + \frac{\tau_\ell}{a^2 \phi_{1,1,1}} \left(\frac{1}{h_{1,0} h_{1,1}} - \frac{1}{h_{1,1}(h_{1,0} + h_{1,1})}\right) \;>\; 1. \end{aligned}$$

Second, for $i = 2, \ldots, N_1 - 1$ we have

$$\begin{aligned} w_{i,1,1} &= -\frac{\tau_\ell}{2} \cdot \frac{2}{a^2 \phi_{i,1,1} h_{1,i-1}(h_{1,i-1} + h_{1,i})} + \left(1 - \frac{\tau_\ell}{2} \cdot \frac{-2}{a^2 \phi_{i,1,1} h_{1,i-1} h_{1,i}}\right) \\ &\quad -\frac{\tau_\ell}{2} \cdot \frac{2}{a^2 \phi_{i,1,1} h_{1,i}(h_{1,i-1} + h_{1,i})} \\ &= 1 + \frac{\tau_\ell}{a^2 \phi_{i,1,1}} \left[\frac{-h_{1,i} + (h_{1,i-1} + h_{1,i}) - h_{1,i-1}}{h_{1,i-1} h_{1,i}(h_{1,i-1} + h_{1,i})}\right] \;=\; 1. \end{aligned}$$

Third, we have

$$\begin{aligned} w_{N_1,1,1} &= -\frac{\tau_\ell}{2} \cdot \frac{2}{a^2 \phi_{N_1,1,1} h_{1,N_1-1}(h_{1,N_1-1} + h_{1,N_1})} \\ &\qquad + \left(1 - \frac{\tau_\ell}{2} \cdot \frac{-2}{a^2 \phi_{N_1,1,1} h_{1,N_1-1} h_{1,N_1}}\right) \\ &= 1 + \frac{\tau_\ell}{a^2 \phi_{N_1,1,1}} \left[\frac{1}{h_{1,N_1}(h_{1,N_1-1} + h_{1,N_1})}\right] \;>\; 1. \end{aligned}$$

Hence, we conclude that $w_{i,1,1} \geq 1,\ i = 1, \ldots, N_1$. Similar arguments may show that all remaining elements of w are also bounded below by 1. Therefore we have $w \geq x$. Similar discussions may be utilized to reach the same conclusion for the cases involving M_2 or M_3. ∎

In the next lemma we show that numerical quenching, *i.e.,* one or more components of v_ℓ reaching or exceeding unity, cannot occur immediately after the first time step under appropriate constraints. To this end, we denote

$$h \equiv \max_{j=1,\ldots,N_\sigma,\ \sigma=1,2,3} \{h_{\sigma,j}\}.$$

Lemma 5.7. *If* (5.14) *holds and*

$$h^2 < \frac{1}{2\varphi_{\max}\min\{a^2,b^2,c^2\}}\min\left\{\frac{1}{f_0},\frac{4}{f(\tau_0\varphi_{\max}f_0/\phi_{\min})}\right\},$$

then for given $v_0 \equiv 0$*, we have that all components of* $v_1 < 1$.

Proof. If $v_0 \equiv 0$, then from (5.11) we have

$$v_1 = \left[\prod_{\sigma=1}^{3}\left(I-\frac{\tau_0}{2}M_\sigma\right)^{-1}\left(I+\frac{\tau_0}{2}M_\sigma\right)\right]\frac{\tau_0}{2}g(\varepsilon,0)+\frac{\tau_0}{2}g(\varepsilon,v_1).$$

Using

$$g(\varepsilon,v_1)\approx g(\varepsilon,w_0)=g(\varepsilon,v_0+\tau_0(Cv_0+g(\varepsilon,v_0)))=g(\varepsilon,\tau_0f_0\xi),$$

where $\xi = \left(\varphi_{1,1,1}\phi_{1,1,1}^{-1},\ldots,\varphi_{N_1,N_2,N_3}\phi_{N_1,N_2,N_3}^{-1}\right)^\intercal \in \mathbb{R}^{N_1N_2N_3}$, we have following decomposed connections

$$\left(I-\frac{\tau_0}{2}M_1\right)\tilde{v}_0 = \left(I+\frac{\tau_0}{2}M_1\right)\frac{\tau_0}{2}f_0\xi, \tag{5.15}$$

$$\left(I-\frac{\tau_0}{2}M_2\right)\bar{v}_0 = \left(I+\frac{\tau_0}{2}M_2\right)\tilde{v}_0, \tag{5.16}$$

$$\left(I-\frac{\tau_0}{2}M_3\right)\left(v_1-\frac{\tau_0}{2}g(\varepsilon,\tau_0f_0\xi)\right) = \left(I+\frac{\tau_0}{2}M_3\right)\bar{v}_0. \tag{5.17}$$

From (5.15) we observe that

$$\begin{aligned}\tilde{v}_0-\frac{1}{4}x &= \left(I-\frac{\tau_0}{2}M_1\right)^{-1}\left[\left(I+\frac{\tau_0}{2}M_1\right)\frac{\tau_0}{2}f_0\xi-\frac{1}{4}\left(I-\frac{\tau_0}{2}M_1\right)x\right]\\ &= \left(I-\frac{\tau_0}{2}M_1\right)^{-1}\left(s_1^+ + s_1^-\right)\end{aligned}$$

for which

$$\begin{aligned}|s_1^+| &= \left|\left(I+\frac{\tau_0}{2}M_1\right)\frac{\tau_0f_0}{2}\xi\right|\\ &\le \frac{\tau_0f_0}{2}\varphi_{\max}\phi_{\min}^{-1}\left\|I+\frac{\tau_0}{2}M_1\right\|_2\\ &< \tau_0f_0\varphi_{\max}\phi_{\min}^{-1}\\ &< \frac{h^2f_0}{2\|B\|_2}\min\left\{a^2,b^2,c^2\right\}\varphi_{\max}\phi_{\min}^{-1}\\ &\le \frac{h^2f_0\varphi_{\max}}{2}\min\left\{a^2,b^2,c^2\right\}.\end{aligned}$$

The above indicates that

$$s_1^+ \leq \frac{h^2 f_0 \varphi_{\max}}{2} \min\left\{a^2, b^2, c^2\right\} x.$$

On the other hand, according to Lemma 5.6 we have

$$s_1^- \leq -\frac{1}{4} x,$$

and thus,

$$s_1^+ + s_1^- \leq \left(\frac{h^2 f_0 \varphi_{\max}}{2} \min\left\{a^2, b^2, c^2\right\} - \frac{1}{4}\right) x.$$

Since we wish each component of $s_1^+ + s_1^-$ to be negative, we require

$$\frac{h^2 f_0 \varphi_{\max}}{2} \min\left\{a^2, b^2, c^2\right\} - \frac{1}{4} < 0, \quad \text{or} \quad h < \frac{1}{\sqrt{2 f_0 \varphi_{\max} \min\left\{a^2, b^2, c^2\right\}}}. \tag{5.18}$$

Now, recall (5.16). It follows that

$$\begin{aligned} \bar{v}_0 - \frac{1}{2} x &= \left(I - \frac{\tau_0}{2} M_2\right)^{-1} \left[\left(I + \frac{\tau_0}{2} M_2\right) \tilde{v}_0 - \frac{1}{2} x\right] \\ &= \left(I - \frac{\tau_0}{2} M_2\right)^{-1} \left(s_2^+ + s_2^-\right). \end{aligned}$$

Note that

$$\left|s_2^+\right| = \left|\left(I + \frac{\tau_0}{2} M_2\right) \tilde{v}_0\right| < \frac{1}{4} \left\|I + \frac{\tau_0}{2} M_2\right\|_2 \leq \frac{1}{2},$$

which implies that $s_2^+ < \frac{1}{2} x$. Therefore we arrive at

$$s_2^+ + s_2^- < \frac{1}{2} x - \frac{1}{2} x = 0.$$

By the same token, based on (5.17) we observe that

$$\begin{aligned} v_1 - x &= \left(I - \frac{\tau_0}{2} M_3\right)^{-1} \left[\left(I + \frac{\tau_0}{2} M_3\right) \bar{v}_0 + \left(I - \frac{\tau_0}{2} M_3\right) \left(\frac{\tau_0}{2} g(\varepsilon, \tau_0 f_0 \xi) - x\right)\right] \\ &= \left(I - \frac{\tau_0}{2} M_3\right)^{-1} \left(s_3^+ + s_3^-\right). \end{aligned}$$

It can be seen that

$$\left|s_3^+\right| = \left|\left(I + \frac{\tau_0}{2} M_3\right) \bar{v}_0 + \left(I - \frac{\tau_0}{2} M_3\right) \frac{\tau_0}{2} g(\varepsilon, \tau_0 f_0 \xi)\right|$$

$$
\begin{aligned}
&\leq \max\left\{|\bar{v}_0|, \left|\frac{\tau_0}{2} g(\varepsilon, \tau_0 f_0 \xi)\right|\right\} \left\| \left(I + \frac{\tau_0}{2} M_3\right) + \left(I - \frac{\tau_0}{2} M_3\right) \right\|_2 \\
&< \max\left\{2|\bar{v}_0|, \tau_0 |f(\tau_0 \varphi_{\max} f_0 \phi_{\min}^{-1}) \xi|\right\} \\
&< \max\left\{1, \frac{h^2}{2} \|B\|_2^{-1} \min\left\{a^2, b^2, c^2\right\} f(\tau_0 \varphi_{\max} f_0 \phi_{\min}^{-1}) \varphi_{\max} \phi_{\min}^{-1}\right\} \\
&= \max\left\{1, \frac{h^2 \varphi_{\max} f(\tau_0 \varphi_{\max} f_0 \phi_{\min}^{-1})}{2} \min\left\{a^2, b^2, c^2\right\}\right\},
\end{aligned}
$$

and the above indicates that

$$
s_3^+ \leq \max\left\{1, \frac{h^2 \varphi_{\max} f(\tau_0 \varphi_{\max} f_0 \phi_{\min}^{-1})}{2} \min\left\{a^2, b^2, c^2\right\}\right\} x.
$$

By Lemma 5.6 we conclude that $s_3^- \leq -x$, and therefore,

$$
\begin{aligned}
s_3^+ + s_3^- &\leq \max\left\{1, \frac{h^2 \varphi_{\max} f(\tau_0 \varphi_{\max} f_0 \phi_{\min}^{-1})}{2} \min\left\{a^2, b^2, c^2\right\}\right\} x - x \\
&= \max\left\{0, \frac{h^2 \varphi_{\max} f(\tau_0 \varphi_{\max} f_0 \phi_{\min}^{-1})}{2} \min\left\{a^2, b^2, c^2\right\} - 1\right\} x.
\end{aligned}
$$

Since we again wish each component of the above vector to be negative, we need

$$
\frac{h^2 \varphi_{\max} f(\tau_0 \varphi_{\max} f_0 \phi_{\min}^{-1})}{2} \min\left\{a^2, b^2, c^2\right\} - 1 < 0,
$$

or

$$
h^2 < \frac{2}{\varphi_{\max} f(\tau_0 \varphi_{\max} f_0 / \phi_{\min}) \min\left\{a^2, b^2, c^2\right\}}.
$$

Hence $v_1 - x \leq 0$ follows immediately from (5.18) and the above. ∎

Remark 5.8. We could generalize the above lemma to include nonzero initial vectors, if desired. Let $0 \leq v_0 < 1/8$ be given. If (5.14) holds and

$$
h^2 < (1 - 8 \max\{v_0\}) \,/\, \left(2F \min\{a^2, b^2, c^2\}\right),
$$

where

$$
F = \varphi_{\max} f\left(\|v_0\|_2 + \tau_0 (C\|v_0\|_2 + \varphi_{\max} f(\|v_0\|_2 \varphi_{\max} \phi_{\min}^{-1}))\right),
$$

then all components of v_1 generated by (5.11) are bounded above by unity. This follows by modifying the proof of Lemma 5.7.

Combining above results we obtain the following theorem.

Theorem 5.9. *For any beginning step $\ell_0 \geq 0$ if τ_ℓ is sufficiently small for $\ell \geq \ell_0$ and*

(i) (5.14) *holds for all $\ell \geq \ell_0$,*

(ii) $$\max_{j=1,\ldots,N_\sigma,\ \sigma=1,2,3}\{h_{\sigma,j}^2\} < \frac{1}{2\varphi_{\max}\min\{a^2,b^2,c^2\}}\min\left\{\frac{1}{f_0},\frac{4}{f(\tau_0\varphi_{\max}f_0/\phi_{\min})}\right\},$$

(iii) $$Cv_{\ell_0} + g(\varepsilon, v_{\ell_0}) > 0,$$

then the sequence $\{v_\ell\}_{\ell\geq\ell_0}$ produced by the semi-adaptive LOD scheme (5.11) *increases monotonically until unity is reached or exceeded by one or more components of the solution vector, i.e., until quenching occurs.*

5.5 Stability

We again consider the stability issues for a numerical scheme that solves a degenerate stochastic Kawarada equations. Nonlinear stability has been an extremely difficult issue when considering nonlinear Kawarada equations [4,20,30,75,108,109]. However, when the numerical solution varies relatively slowly, that is, before reaching a certain neighborhood of quenching, instability may be detected through a linear stability analysis of the nonlinear scheme utilized [39,79,100]. In the following section, we will first carry out a linearized stability analysis in the von Neumann sense for (5.11) with its nonlinear stochastic source term frozen. This is equivalent to assuming that the source term is effectively accurate throughout computations. The analysis will then be extended to circumstances where the nonlinear stochastic reaction term is not frozen. In the latter case, the boundedness of the Jacobian of the reaction term, $\|g_v(\varepsilon, v)\|_2$, which is equivalent to assuming that we are some neighborhood away from quenching, is assumed.

For the semi-adaptive LOD method (5.11) with its nonlinear stochastic reaction term frozen, n we impose regularity conditions upon the nonuniform spatial

grids in order to carry out a linear stability analysis. For this purpose, let us denote

$$h_\sigma = \min_{j=1,\ldots,N_\sigma} \{h_{\sigma,j}\},\ \sigma = 1,2,3.$$

Lemma 5.10. *If*

$$\frac{1}{h_1^2\phi_{i-1,j,k}} - \frac{1}{h_{1,i-1}h_{1,i}\phi_{i,j,k}} \leq \frac{K}{2}, \tag{5.19}$$

$$\frac{1}{h_2^2\phi_{i,j-1,k}} - \frac{1}{h_{2,j-1}h_{2,j}\phi_{i,j,k}} \leq \frac{K}{2}, \tag{5.20}$$

$$\frac{1}{h_3^2\phi_{i,j,k-1}} - \frac{1}{h_{3,k-1}h_{3,k}\phi_{i,j,k}} \leq \frac{K}{2}, \tag{5.21}$$

where the constant $K > 0$ is independent of $h_{\sigma,j},\ j = 1,\ldots,N_\sigma,\ \sigma = 1,2,3$. then

$$\mu(M_\sigma) \leq K,\ \sigma = 1,2,3.$$

Proof. We only need to consider the case involving M_1 since the other cases are similar. Note that $\mu(M_1) = \frac{1}{2}\lambda_{\max}\left(M_1 + M_1^\intercal\right)$ and

$$\frac{1}{2}\left(M_1 + M_1^\intercal\right) = \operatorname{diag}(X_{1,1},\ldots,X_{N_2,1},X_{1,2},\ldots,X_{N_2,N_3}) \in \mathbb{R}^{N_1N_2N_3\times N_1N_2N_3},$$

where

$$(X_{j,k})_{n,p} = \begin{cases} \frac{m_{1,n}}{\phi_{n,j,k}}, & \text{if } n = p, \\ \frac{n_{1,n-1}}{2\phi_{n-1,j,k}} + \frac{l_{1,n-1}}{2\phi_{n,j,k}}, & \text{if } n - p = 1, \\ \frac{n_{1,n}}{2\phi_{n,j,k}} + \frac{l_{1,n}}{2\phi_{n+1,j,k}}, & \text{if } p - n = 1, \\ 0, & \text{otherwise.} \end{cases}$$

We apply Geršchgorin's circle theorem to an arbitrary $X_{j,k}$ and note that a similar argument works for each $X_{j,k},\ j = 1,\ldots,N_2,\ k = 1,\ldots,N_3$. Further, notice that we only need to consider circumstances where the bandwidth of $M_1 + M_1^\intercal$ is three. Thus,

$$\begin{aligned} \left|\lambda_{1,i} - \frac{m_{1,i}}{\phi_{i,j,k}}\right| &\leq \left|\frac{n_{1,i-1}}{2\phi_{i-1,j,k}} + \frac{l_{1,i-1}}{2\phi_{i,j,k}}\right| + \left|\frac{n_{1,i}}{2\phi_{i,j,k}} + \frac{l_{1,i}}{2\phi_{i+1,j,k}}\right| \\ &\leq \frac{2}{h_1^2\phi_{i-1,j,k}}, \end{aligned}$$

for $i = 2, \ldots, N_1 - 1,\ j = 1, \ldots, N_2,\ k = 1, \ldots, N_3$. We then see that (5.19) follows immediately from the above and the fact that

$$\frac{2}{h_1^2 \phi_{i-1,j,k}} - \frac{2}{h_{1,i-1} h_{1,i} \phi_{i,j,k}} \leq K,$$

for $i = 2, \ldots, N_1 - 1,\ j = 1, \ldots, N_2,\ k = 1, \ldots, N_3$. ∎

Remark 5.11. We note that the regularity conditions (5.19)-(5.21) are not restrictive, as they may be reformulated to be

$$\phi_{\max} h_{\max}^2 - \phi_{\min} h_\sigma^2 \leq \tilde{K}, \quad \sigma = 1, 2, 3.$$

The constant $\tilde{K}$ depends on $\phi_{\max}$ and $\phi_{\min}$, but not the nonuniform grid, and serves a similar purpose to the condition number $\kappa(B)$ from Chapters 3 and 4 in the following stability analysis. This consideration leads us to conclude that realistic computational grids will satisfy (5.19)-(5.21). However, in computations, $\tilde{K}$ could become quite large.

Lemma 5.12. *If* (5.19)-(5.21) *hold then*

$$\left\| \left(I - \frac{\tau_\ell}{2} M_\sigma \right)^{-1} \left(I + \frac{\tau_\ell}{2} M_\sigma \right) \right\|_2 \leq 1 + \tau_\ell K + \mathcal{O}\left(\tau_\ell^2\right), \quad \ell \geq 0,\ \sigma = 1, 2, 3, \quad (5.22)$$

for sufficiently small $\tau_\ell > 0$.

Proof. Recalling the [1/1] Padé approximation, we have

$$\left(I - \frac{\tau_\ell}{2} M_\sigma \right)^{-1} \left(I + \frac{\tau_\ell}{2} M_\sigma \right) = E(\tau_\ell M_\sigma) + \mathcal{O}\left(\tau_\ell^3\right), \quad \tau_\ell \to 0^+,\ \sigma = 1, 2, 3.$$

Now, based on Lemmas 2.5 and 5.10,

$$\begin{aligned}
\left\| \left(I - \frac{\tau_\ell}{2} M_\sigma \right)^{-1} \left(I + \frac{\tau_\ell}{2} M_\sigma \right) \right\|_2 &= \|E(\tau_\ell M_\sigma)\|_2 + \mathcal{O}(\tau_\ell^3), \quad \tau_\ell \to 0^+ \\
&\leq E(\tau_\ell \mu(M_\sigma)) + \mathcal{O}\left(\tau_\ell^3\right), \quad \tau_\ell \to 0^+ \\
&\leq E(\tau_\ell K) + \mathcal{O}\left(\tau_\ell^3\right), \quad \tau_\ell \to 0^+ \\
&= \left[1 + \tau_\ell K + \mathcal{O}\left(\tau_\ell^2\right)\right] + \mathcal{O}\left(\tau_\ell^3\right), \quad \tau_\ell \to 0^+
\end{aligned}$$

$$= \quad 1 + \tau_\ell K + \mathcal{O}\left(\tau_\ell^2\right), \quad \tau_\ell \to 0^+,$$

which is the desired bound. ∎

Combining the above results gives the following theorem.

Theorem 5.13. *If* (5.14) *and* (5.19)-(5.21) *hold and* τ_ℓ *are sufficiently small, then the semi-adaptive LOD method* (5.11) *with the nonlinear stochastic source term frozen is unconditionally stable in the von Neumann sense under the spectral norm, that is,*

$$\|z_{\ell+1}\|_2 \leq c\|z_0\|_2, \quad \ell \geq 0,$$

where $z_0 = v_0 - \tilde{v}_0$ *is an initial error,* $z_{\ell+1} = v_{\ell+1} - \tilde{v}_{\ell+1}$ *is the* $(\ell+1)$*th perturbed error vector, and* $c > 0$ *is a constant independent of* ℓ *and* τ_ℓ.

Proof. When the nonlinear stochastic source term is frozen, $z_{\ell+1}$ takes the form of

$$z_{\ell+1} \quad = \quad \prod_{\sigma=1}^{3} \left(I - \frac{\tau_\ell}{2} M_\sigma\right)^{-1} \left(I + \frac{\tau_\ell}{2} M_\sigma\right) z_\ell, \quad \ell \geq 0. \tag{5.23}$$

Recall that $\sum_{k=0}^{\ell} \tau_k \leq T_q,\ \ell > 0$. It follows by taking the norm on both sides of (5.23) that

$$\begin{aligned}
\|z_{\ell+1}\|_2 &\leq \prod_{\sigma=1}^{3} \left\| \left(I - \frac{\tau_\ell}{2} M_\sigma\right)^{-1} \left(I + \frac{\tau_\ell}{2} M_\sigma\right) \right\|_2 \|z_\ell\|_2 \\
&\leq \left(1 + \tau_\ell K + c_1 \tau_\ell^2\right)^3 \|z_\ell\|_2 \\
&\leq \left(1 + 3\tau_\ell K + c_2 \tau_\ell^2\right) \|z_\ell\|_2 \\
&\leq \prod_{k=0}^{\ell} \left(1 + 3\tau_k K + c_3 \tau_k^2\right) \|z_0\|_2 \\
&\leq \left(1 + 3KT_q + c_4 \sum_{k=0}^{\ell} \tau_k^2\right) \|z_0\|_2 \\
&\leq c\|z_0\|_2,
\end{aligned}$$

for sufficiently small $\tau_k,\ k = 0, 1, \ldots, \ell$, and where c_1, c_2, c_3, c_4 and c are positive constants independent of $\ell,\ \tau_k,\ k = 0, 1, \ldots, \ell$. Therefore the theorem is clear. ∎

We now consider the case without freezing the nonlinear stochastic source term in (5.11). In this situation, restrictions upon the Jacobian matrix $g_v(\varepsilon, v)$ become necessary.

Theorem 5.14. *Let $\tau_k \geq 0,\ 0 \leq k \leq \ell$, be sufficiently small and* (5.14), (5.19)-(5.21) *hold. If there exists a constant $G < \infty$ such that*

$$\|g_v(\varepsilon, \xi)\|_2 \leq G, \quad \forall \xi_j \in [0, 1),\ j = 1, \ldots, N_1 N_2 N_3, \tag{5.24}$$

then the semi-adaptive LOD method (5.11) *is unconditionally stable in the von Neumann sense, that is,*

$$\|z_{\ell+1}\|_2 \leq \tilde{c}\, \|z_0\|_2, \quad \ell > 0,$$

where $z_0 = v_0 - \tilde{v}_0$ is an initial error, $z_{\ell+1} = v_{\ell+1} - \tilde{v}_{\ell+1}$ is the $(\ell+1)$th perturbed error vector, and $\tilde{c} > 0$ is a constant independent of ℓ and τ_ℓ.

Proof. By definition we have

$$\begin{aligned} v_{\ell+1} &= \prod_{\sigma=1}^{3} \left(I - \frac{\tau_\ell}{2} M_\sigma\right)^{-1} \left(I + \frac{\tau_\ell}{2} M_\sigma\right) \left(v_\ell + \frac{\tau_\ell}{2} g(\varepsilon, v_\ell)\right) + \frac{\tau_\ell}{2} g(\varepsilon, v_{\ell+1}) \\ &= \Phi_\ell \left(v_\ell + \frac{\tau_\ell}{2} g(v_\ell)\right) + \frac{\tau_\ell}{2} g(v_{\ell+1}). \end{aligned}$$

It follows that

$$\begin{aligned} z_{\ell+1} &= \Phi_\ell z_\ell + \frac{\tau_\ell}{2} \Phi_\ell (g(\varepsilon, v_\ell) - g(\varepsilon, \tilde{v}_\ell)) + \frac{\tau_\ell}{2} (g(\varepsilon, v_{\ell+1}) - g(\varepsilon, \tilde{v}_{\ell+1})) \\ &= \Phi_\ell z_\ell + \frac{\tau_\ell}{2} \Phi_\ell g_v(\varepsilon, \xi_\ell) z_\ell + \frac{\tau_\ell}{2} g_v(\varepsilon, \xi_{\ell+1}) z_{\ell+1}, \end{aligned}$$

where $\xi_k \in \mathcal{L}(v_k, \tilde{v}_k),\ k = \ell, \ell+1$. Rearranging the above equality, we have

$$\left(I - \frac{\tau_\ell}{2} g_v(\varepsilon, \xi_{\ell+1})\right) z_{\ell+1} = \Phi_\ell \left(I + \frac{\tau_\ell}{2} g_v(\varepsilon, \xi_\ell)\right) z_\ell.$$

Further, recall (5.24). When τ_k is sufficiently small we may claim that

$$\left(I - \frac{\tau_k}{2} g_v(\varepsilon, \xi)\right)^{-1},\ I + \frac{\tau_k}{2} g_v(\varepsilon, \xi) = E\left(\frac{\tau_k}{2} g_v(\varepsilon, \xi)\right) + \mathcal{O}\left(\tau_k^2\right), \quad \tau_k \to 0^+.$$

Thus,

$$\begin{aligned} z_{\ell+1} &= \left(I - \frac{\tau_\ell}{2} g_v(\varepsilon, \xi_{\ell+1})\right)^{-1} \Phi_\ell \left(I + \frac{\tau_\ell}{2} g_v(\varepsilon, \xi_\ell)\right) z_\ell \\ &= \prod_{k=0}^{\ell} \left(I - \frac{\tau_k}{2} g_v(\varepsilon, \xi_{k+1})\right)^{-1} \Phi_k \left(I + \frac{\tau_k}{2} g_v(\varepsilon, \xi_k)\right) z_0 \\ &= \left\{ \prod_{k=0}^{\ell} \left[E\left(\frac{\tau_k}{2} g_v(\varepsilon, \xi_{k+1})\right) + \mathcal{O}\left(\tau_k^2\right)\right] \Phi_k \right. \\ &\qquad \left. \left[E\left(\frac{\tau_k}{2} g_v(\varepsilon, \xi_k)\right) + \mathcal{O}\left(\tau_k^2\right)\right] \right\} z_0, \quad \tau_k \to 0^+. \end{aligned}$$

It follows therefore

$$\begin{aligned} \|z_{\ell+1}\|_2 &\leq \left\{ \prod_{k=0}^{\ell} \left\| E\left(\frac{\tau_k}{2} g_v(\varepsilon, \xi_{k+1})\right) \right\|_2 \|\Phi_k\|_2 \left\| E\left(\frac{\tau_k}{2} g_v(\varepsilon, \xi_k)\right) \right\|_2 + c_{1,k}\tau_k^2 \right\} \|z_0\|_2 \\ &\leq \left(1 + 3KT_q + c\sum_{k=0}^{\ell} \tau_k^2\right) \prod_{k=0}^{\ell} \left\{ \left[\left\| E\left(\frac{\tau_k}{2} g_v(\varepsilon, \xi_{k+1})\right) \right\|_2 + c_{1,k}\tau_k^2 \right] \right. \\ &\quad \left. \times \left[\left\| E\left(\frac{\tau_k}{2} g_v(\varepsilon, \xi_k)\right) \right\|_2 + c_{2,k}\tau_k^2 \right] \right\} \|z_0\|_2 \\ &\leq \left(1 + 3KT_q + c\sum_{k=0}^{\ell} \tau_k^2\right) \prod_{k=0}^{\ell} \left(e^{\tau_k G/2} e^{\tau_k G/2} + c_{3,k}\tau_k^2\right) \|z_0\|_2 \\ &\leq \left(1 + 3KT_q + c\sum_{k=0}^{\ell} \tau_k^2\right) \left(e^{GT_q} + c_1 \sum_{k=0}^{\ell} \tau_k^2\right) \|z_0\|_2 \\ &\leq \tilde{c}\, \|z_0\|_2, \end{aligned}$$

where $c_{1,k},\ k = 1, 2, \ldots, \ell$, are positive constants and $c, c_1, \tilde{c}$ are positive constants independent of ℓ and $\tau_\ell,\ \ell > 0$. Thus giving the desired stability. ∎

The above theorem provides further insight as to why the standard linear analysis can be useful in estimating the nonlinear stability. The extra cost paid, however, is assuming the boundedness of $\|g_v(\varepsilon, \xi)\|_2$. Nevertheless, this is an improvement upon the traditional methodology of having the nonlinear source term frozen. In fact, the aforementioned bound is well-maintained in numerical experiments until certain neighborhoods of quenching are reached. In these neighborhoods, accuracy and round-off errors may be of more concern that stability issues [17, 95]. This serves as an indication that the new analysis is valid and effective.

CHAPTER SIX

Summary

6.1 Thesis Contributions

In this dissertation we proposed and examined three different adaptive splitting methods for solving degenerate stochastic Kawarada equations on arbitrary grids. In Chapter Two, we outlined the mathematical preliminaries necessary for this study including basic theory regarding finite difference approximations on arbitrary grids, approximating exponential matrices, and exponential splitting methods. We also developed a new result that characterizes the global error incurred by splitting the exponential matrix $E(t(\sum_{i=1}^{n} A_i))$ for $A_i \in \mathbb{C}^{N\times N}$, $i = 1, \ldots, n$, via a parallel splitting method. This chapter served as a base for the derivation and analysis of the numerical procedures considered in Chapters Three, Four, and Five.

In Chapter Three, we considered a temporally adaptive Crank-Nicolson scheme for solving the one-dimensional degenerate stochastic Kawarada equation on arbitrary spatial grids. The scheme was shown to be positive, monotone, and stable. The analysis improved upon previous results by weakening the assumptions for monotonicity and carrying out the analysis using the spectral norm on nonsymmetric arbitrary grids. The stability analysis for the scheme was also carried out in a novel extended sense that fully considers the impacts of the nonlinear stochastic reaction term. The numerical experiments explored standard features of the quenching-combustion phenomenon and also provided insights into the impacts of stochastic influences on quenching time, location, and behavior.

In Chapter Four, we considered the degenerate stochastic Kawarada equation in two-dimensions. We developed a temporally adaptive semi-discretized numerical procedure via novel splitting strategies and implemented the procedure on fully

arbitrary spatial grids. The intermediate system of differential equations and numerical method are both shown to be positive and monotone prior to quenching. The stability of the numerical method is verified via the novel extended stability analysis.

Also in Chapter Four, we showed that the nonuniform finite difference approximation implemented may be second-order accurate, rather than first-order, when considering many realistic spatial grids. Numerical experiments are also conducted to verify that the novel semi-discretized scheme recovered previously accepted results while exploring the nature of the quenching-combustion phenomenon in two-dimensions. The numerical experiments provided new insights into the nature of numerical convergence for nonlinear and singular equations. These new convergence surfaces verified the claimed rates of convergence and highlighted the effects of the quenching singularity and degeneracy on these rates. These surfaces may motivate deeper understandings of convergence and stability issues when considering nonlinear problems.

In Chapter Five, we considered the three-dimensional degenerate stochastic Kawarada equation. A temporally adaptive LOD scheme is developed through splitting procedures and studied on nonsymmetric arbitrary grids. The numerical procedure is shown to preserve the desired positivity, monotonicity, and stability under reasonable restrictions. Once again, the stability is carried out in an extended sense. It is shown that the procedure is stable in all compact neighborhoods prior to quenching, which agrees well with existing local well-posedness results for Kawarada equations. The results improve upon existing multidimensional efforts by establishing results via the spectral norm and less restriction. The development of the numerical procedure and the analysis may be generalized to consider more exotic splitting procedures and higher dimensional problems.

Throughout Chapters Three, Four, and Five there are several major contributions developed. First, each algorithm considered incorporates fully arbitrary grids in both space and time, allowing for the developed algorithms to be applied to a wide range of problems. Second, we utilize the spectral norm throughout the numerical analysis, which improves upon existing results that utilize only the L_∞ norm when considering nonuniform grids. Finally, we develop an extended stability analysis for considering singular differential equations. This extended analysis provides a deeper understanding of singular differential equations and may also be used when considering other nonlinear differential equations. This extended stability analysis is an improvement upon the previous attempts to consider stability of Kawarada equations as it considers the impacts of the nonlinear singularity.

6.2 Future Research

6.2.1 Fractional Quenching-Combustion Problems

Numerous research fields, including anomalous diffusion, viscoelasticity, control theory, biology, and finance, have adopted fractional calculus as a valid modeling approach [9, 60, 76, 96, 98, 116]. It has also been determined that fractional operators naturally emerge in the physical modeling of phenomenon in combustion science [27, 28, 45, 55, 66, 96]. This natural emergence means that considerations of fractional derivatives in such models are physically relevant, and not simply interesting mathematical extensions. Since Kawarada equations may be used to model solid-fuel combustion we hope to explore the quenching-combustion phenomenon in nonlinear fractional partial differential equations.

In order to introduce the fractional Kawarada equation that we propose for future study, we need to introduce some basic definitions. For simplicity, we will only consider the one-dimensional problem. In the following, let $\Gamma(\cdot)$ be the Euler

gamma function [49, 76], $\Omega = (a, b) \subset \mathbb{R}$, and $u(x, t)$ be a sufficiently smooth real-valued function function defined on $\Omega \times [t_0, T_q)$ with $0 \leq u < 1$.

Definition 6.1 [76]. Let $\alpha \in \mathbb{R}^+$. The αth-order left-sided and right-sided Riemann-Liouville fractional integrals of u with respect to x are defined as

$$\left({}_aI_x^{\alpha}u\right)(x,t) = \frac{1}{\Gamma(\alpha)}\int_a^x (x-s)^{\alpha-1}u(s,t)\,ds, \tag{6.1}$$

and

$$\left({}_xI_b^{\alpha}u\right)(x,t) = \frac{1}{\Gamma(\alpha)}\int_x^b (x-s)^{\alpha-1}u(s,t)\,ds, \tag{6.2}$$

respectively, provided that the integrals converge.

Definition 6.2 [76]. Let $n \in \mathbb{N}$, $n-1 < \alpha < n$, and assume that ${}_aI_x^{n-\alpha}u$ and ${}_xI_b^{n-\alpha}u$ have partial derivatives with respect to x up to order n. Then the left-sided and right-sided Riemann-Liouville fractional derivatives of u with respect to x are defined as

$$\left({}^R\partial_{x^+}^{\alpha}u\right)(x,t) = \partial_x^n\left({}_aI_x^{n-\alpha}u\right)(x,t), \tag{6.3}$$

and

$$\left({}^R\partial_{x^-}^{\alpha}u\right)(x,t) = (-1)^n\partial_x^n\left({}_xI_b^{n-\alpha}u\right)(x,t), \tag{6.4}$$

respectively. In particular, when $n = \alpha$, we have ${}^R\partial_{x^+}^{\alpha}u = \partial_x^n u$ and ${}^R\partial_{x^-}^{\alpha}u = (-1)^n\partial_x^n u$.

Definition 6.3 [76]. Let $n \in \mathbb{N}$, $n-1 < \alpha < n$, and assume that ${}_aI_x^{n-\alpha}u$ and ${}_xI_b^{n-\alpha}u$ have partial derivatives with respect to x up to order n. Then the left-sided and right-sided Caputo fractional derivatives of u with respect to x are defined as

$$\left(\partial_{x^+}^{\alpha}u\right)(x,t) = \left({}_aI_x^{n-\alpha}\partial_x^n u\right)(x,t), \tag{6.5}$$

and

$$\left(\partial_{x^-}^{\alpha}u\right)(x,t) = (-1)^n\left({}_xI_b^{n-\alpha}\partial_x^n u\right)(x,t), \tag{6.6}$$

respectively. In particular, when $n = \alpha$, we have $\partial_{x^+}^{\alpha}u = \partial_x^n u$ and $\partial_{x^-}^{\alpha}u = (-1)^n\partial_x^n u$.

Based on Definitions 6.1-6.3, we have the following useful lemma to help simplify the quenching-combustion model.

Lemma 6.4 [122]. *Let* $0 < \alpha \leq 1$ *and assume that* (6.1)-(6.6) *are well-defined on* Ω. *If* $u(a,t) = u(b,t) = 0$ *for all* $t \in [t_0, T_q)$, *then*

$$ {}^{R}\partial^{\alpha}_{x^+} u = \partial^{\alpha}_{x^+} u \quad \textit{and} \quad {}^{R}\partial^{\alpha}_{x^-} u = \partial^{\alpha}_{x^-} u. $$

Analogously, we may define the Caputo fractional partial derivative of $u(x,t)$ with respect to t to be

$$ \left(\partial^{\alpha}_{t} u\right)(x,t) = \frac{1}{\Gamma(n-\alpha)} \int_{t_0}^{t} (t-s)^{n-\alpha-1} \partial_s u(x,s)\, ds, \tag{6.7} $$

provided that the integral converges, where $n \in \mathbb{N}$ and $n-1 < \alpha < n$.

Let $\mathcal{D} = \Omega \times (t_0, T_q)$ and $\mathcal{S} = \{a, b\} \times (t_0, T_q)$. We consider the following generalized fractional degenerate Kawarada quenching-combustion model

$$ \mathscr{L} u = f(u), \quad (x,t) \in \mathcal{D}, \tag{6.8} $$

$$ u(x,t) = 0, \quad (x,t) \in \mathcal{S}, \tag{6.9} $$

$$ u(x,t_0) = u_0(x), \quad x \in \Omega, \tag{6.10} $$

where

$$ \mathscr{L} := \sigma(x)\partial^{\alpha}_{t} + \partial^{\beta}_{x^-}\partial^{\beta}_{x^+}, \quad 0 < \alpha, \beta \leq 1, $$

is based on (6.1)-(6.7). There are numerous reasons for choosing $\mathscr{L}$ to be defined as such, but for brevity we refer interested readers to [1, 7, 8, 32, 122] and references therein. The degeneracy $\sigma(x)$ is nonnegative and vanishes only on some subset of $\partial\Omega$. The nonlinear reaction term, $f(u)$, is strictly increasing for $0 \leq u < 1$ with

$$ f(0) = f_0 > 0 \quad \text{and} \quad \lim_{u \to 1^-} f(u) = +\infty. $$

As an example, Figure 6.1 depicts a solution to the time-fractional Kawarada equation for $\alpha = 0.85$, $\beta = 1$, $\Omega = (-2, 2)$, $\sigma(x) = 1$, and $f(u) = (1-u)^{-1}$. We note

that in this case, the solution is still positive, monotonically increasing, and symmetric about the origin. Further, we note that quenching occurs and is accompanied by the blow-up of the left-sided Caputo fractional derivative of the solution. However, a reduced quenching time is observed when compared to our previous results from Chapter Three, with $T_q \approx 0.38458975$. We leave further discussions of these properties to our future endeavors.

Due to the recent emergence of the field, numerical methods for solving fractional differential equations are still in their infancy. Thus far, numerical methods for solving fractional differential equations have implemented primarily uniform grids, with only a few endeavors considering nonuniform temporal grids or nonuniform spatial grids with restrictive structures [10, 68, 91, 111, 125]. Fractional Kawarada equations have only been considered very recently and there are still numerous open questions regarding these problems, both theoretically and numerically [122, 123].

Future endeavors will initially develop in two different directions. For the fractional Kawarada problem (6.8)-(6.10) there is a need for more robust numerical procedures in order to better capture and explore the unique quenching-combustion phenomenon. To that end, we intend to develop adaptive numerical procedures for solving (6.8)-(6.10) and also extend (6.8)-(6.10) to higher dimensions in order to utilize exponential splitting strategies. There is also the need to utilized moving spatial grid strategies when considering fractional Kawarada problems in order to accurately predict quenching time and quenching locations [43,50,62,63]. In order to use such methods, a convergent nonuniform finite difference spatial discretization on nonuniform grids must be developed. Thus far, these efforts have been hindered by smoothness and convergence issues [125]. Development of such discretizations will also allow for more accurate and effective procedures to be developed in numerous other space fractional problems.

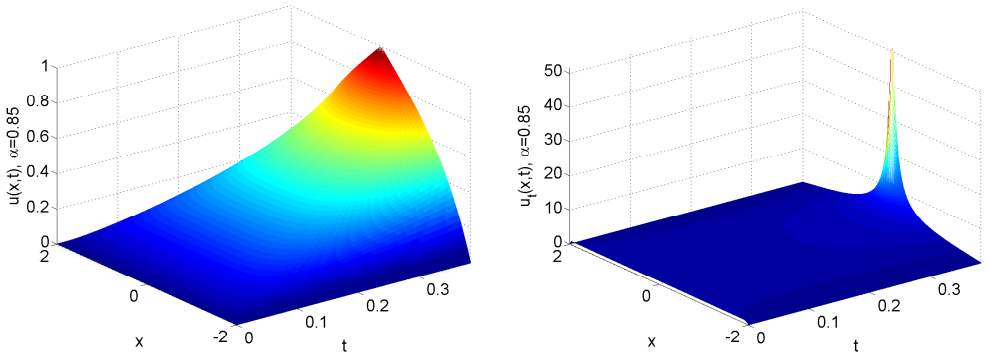

Figure 6.1: Solution [LEFT] and its left-sided Caputo fractional derivative [RIGHT] to (6.8)-(6.10) for $\Omega = (-2, 2)$. We note the decreased quenching time when compared to its non-fractional counterparts.

6.2.2 Nonlinear Biological Models

The methods considered in this dissertation can be applied to numerous nonlinear and singular problems, not just quenching-combustion problems. Of particular interest are three-species predator-prey models. Predator-prey interactions are commonly modeled by systems of nonlinear reaction-diffusion equations [2, 3, 13, 14, 16, 51, 80, 97, 120]. The populations and their complicated interactions present numerous challenges in theory and in numerical approximation, due to the fact that the solutions to such equations may exhibit finite time blow-up [2, 3, 18, 97]. To illustrate, let $\boldsymbol{w} = (w_1, \ldots, w_m)^\intercal \in \mathbb{R}^m$ be a population vector of m species in space and time. Consider the system,

$$\partial_t w_p \quad = \quad d_p \Delta w_p + s_p \Delta w_p^2 + f_p(\boldsymbol{w}), \quad p = 1, \ldots, m, \tag{6.11}$$

defined on $\mathbb{R}^+ \times \Omega$, where $\Omega \subset \mathbb{R}^2$ and Δ is the two-dimensional Laplacian operator. The nonlinear reaction function $\boldsymbol{f} = (f_1, \ldots, f_m)^\intercal \in \mathbb{R}^m$ is a smooth locally Lipshitz mapping from $\mathbb{R}$ into $\mathbb{R}^m$. The diffusion and self-diffusion coefficients d_p and s_p, respectively, are nonnegative. The self-diffusion term represents a severe penalty to overcrowding in a species, usually the top predator. We define $\boldsymbol{x} \in \Omega$ to be the spatial

coordinate vector. The initial conditions are smooth, bounded, and nonnegative functions. Further, we assume Dirichlet or Periodic boundary conditions.

By employing an appropriate spatial discretization, we can derive the following semi-discretized system of equations

$$\partial_t v_p = \left(c_p(P+R) + s_p(PD(v_p) + RD(v_p))\right) v_p + g_p, \quad p = 1, \ldots, m \tag{6.12}$$

where P, R, and $D(v_p)$ are matrices resulting from the discretization of the diffusion and self-diffusion terms, with $D(v_p)$ having entries depending on the vector v_p.

For each specie, a second-order Crank-Nicolson method with a variable time-step may be used to advance the solution in time, namely,

$$\begin{aligned}\left(I - \frac{\tau_k}{2}(P+R)\left(d_p + s_p D_{p_{k+1}}\right)\right) v_{p_{k+1}} &= \left(I + \frac{\tau_k}{2}(P+R)\left(d_p + s_p D_{p_k}\right)\right) v_{p_k} \\ &\quad + \frac{\tau_k}{2}\left(g_{p_{k+1}} + g_{p_k}\right)\end{aligned} \tag{6.13}$$

where $\{\tau_k\}_{k\geq 0}$ is a set of adaptive variable temporal steps, $D_{p_k} \equiv D(v_{p_k})$, g_{p_k} is the vector g_p evaluated at time t_k, v_{p_k} is the approximation to the solution of (6.12) at time $t_k = \sum_{i=0}^{k-1} \tau_i$.

A generalization of the results in [18] gives that for each p, (6.13) can be factored in an advantageous way. This factoring is given by the following theorem.

Theorem 6.5 [18]. *For each p,* (6.13) *may be factored as*

$$\begin{aligned}&\left(I - \frac{\tau_k}{2}d_p P\right)\left(I - \frac{\tau_k}{2}d_p R\right)\left(I - \frac{\tau_k}{2}s_p P D_{p_{k+1}}\right)\left(I - \frac{\tau_k}{2}s_p R D_{p_{k+1}}\right) v_{p_{k+1}} \\ &\quad = \left(I + \frac{\tau_k}{2}d_p P\right)\left(I + \frac{\tau_k}{2}d_p R\right)\left(I + \frac{\tau_k}{2}s_p P D_{p_k}\right)\left(I + \frac{\tau_k}{2}s_p R D_{p_k}\right) v_{p_k} \\ &\qquad + \frac{\tau_k}{2}(g_{p_k} + g_{p_{k+1}}) + \mathcal{O}\left(\tau_k^3\right), \quad \tau_k \to 0^+.\end{aligned} \tag{6.14}$$

The factorization (6.14) allows for a modified Douglass-Gunn splitting method to be employed for each p [18, 44], namely,

$$\left(I - \frac{\tau_k}{2}d_p P\right)\tilde{v}_p^{(1)} = \left(I + \frac{\tau_k}{2}\left(d_p P + 2d_p R + 2s_p(P+R)D_{p_k}\right)\right) v_{p_k} + \tau_k g_{p_k},$$

$$
\begin{aligned}
\left(I - \frac{\tau_k}{2} d_p R\right) \tilde{v}_p^{(2)} &= \tilde{v}_p^{(1)} - \frac{\tau_k}{2} d_p R v_{p_k}, \\
\left(I - \frac{\tau_k}{2} s_p P D_{p_{k+1}}\right) \tilde{v}_p^{(3)} &= \tilde{v}_p^{(2)} - \frac{\tau_k}{2} s_p P D_{p_k} v_{p_k}, \\
\left(I - \frac{\tau_k}{2} s_p R D_{p_{k+1}}\right) v_{p_{k+1}} &= \tilde{v}_p^{(3)} - \frac{\tau_k}{2} s_p R D_{p_k} v_{p_k} + \frac{\tau_k}{2} \left(g_{p_k} - g_{p_{k+1}}\right).
\end{aligned}
$$

Many aspects of a simplified model problem involving self-diffusion were explored in [18]. The simplified model problem employed the modified Douglass-Gunn splitting method outlined above to solve (6.14) efficiently. Further, the positivity and stability of the scheme were studied and guaranteed under appropriate restrictions [18]. However, there is still much work to be completed with the generalized factored scheme (6.14).

While any spatial discretization method may be implemented in (6.14), there is still a need for rigorous analysis of numerical schemes defined on arbitrary grids. Moreover, there is still a need to explore and develop a more complete stability analysis of (6.14) that is less restrictive. The scheme is (6.14) is complicated by the fact that the amplification matrices are nonlinear, not just the reaction term. In order to compensate for these complications, current efforts have required restrictions on the growth rate of the solution [18]. Further, there is a need to consider the convergence of these nonlinear problems. The nonlinear nature of the self-diffusion term give rise to novel issues that are not present in the quenching-combustion problems considered in this dissertation. However, the novel splitting approach (6.14) and development of rigorous numerical analysis will be a useful tool when considering nonlinear problems other than (6.11).

BIBLIOGRAPHY

[1] A. Abdennadher, M. Joelson, and M. C. Néel. Fractional Fick's law: The direct way. *J. Phys. A: Math. Theor.*, 40:8299–8314, 2007.

[2] H. A. Abderrahmane, A. R. Kasimov, N. Kumari, and R. D. Parshad. Turing patterns and long time behavior in a three-species model. *Nonlin. Anal. RWA*, 6:509–530, 2005.

[3] H. Abderrahmanne, N. Kumari, R. D. Parshad, and R. K. Upadhyay. Finite time blow-up in a realistic food chain model. *ISRN Biomathematics*, 2013:1–12, 2013.

[4] A. Acker and B. Kawohl. Remarks on quenching. *Nonlin. Anal.*, (13):53–61, 1989.

[5] A. Acker and W. Walter. The quenching problem for nonlinear parabolic differential equations. *Ordinary and Partial Differential Equations (Lecture Notes in Math., 564)*, pages 1–12, 1976.

[6] R. P. Agarwal and Q. Sheng. A note on asymptotic splitting. *Math. Comput. Modelling*, 20(12):45–58, 1994.

[7] O. P. Agrawal. Formulation of Euler-Lagrange equations for fractional variational problems. *J. Math. Anal. Appls*, 272(1):368–379, 2002.

[8] O. P. Agrawal and M Klimek. Fractional Sturm-Liouville problems. *Comput. Math. Appl.*, 66(5):798–812, 2013.

[9] O. P. Agrawal, J. A. Machado, and J. Sabatier. *Advances in Fractional Calculus*. Springer, Berlin, 2007.

[10] G. Akagi, G. Schimperna, and A. Segatti. Fractional Cahn-Hilliard, Allen-Cahn and porous medium equations. *J. Diff. Eq.*, 261:2935–2985, 2016.

[11] H. Amann. Fixed point equations and nonlinear eigenvalue problems in ordered banach spaces. *SIAM Rev*, (18):620–709, 1976.

[12] K. Atkinson and W. Han. *Elementary Numerical Analysis*. John Wiley & Sons, Inc., Somerset, NJ, 3rd edition, 2004.

[13] M. A. Aziz-Alaoui. Study of a Leslie-Gower type tri-trophic population model. *Chaos Solitons Fractals*, 14(8):1275–1293, 2002.

[14] M. A. Aziz-Alaoui and M. Daher-Okiye. Boundedness and global stability for predatory-prey models with modified Leslie-Gower and Holling-type II schemes. *Appl. Math. Lett.*, 16:1069–1075, 2003.

[15] G. A. Baker, Jr. and P. Graves-Morris. *Padé Approximants*, volume 59 of *Encyclopedia of Mathematics and its Applications*. Cambridge University Press, 2nd edition, 1996.

[16] M. A. Beauregard, K. Black, R. D. Parshad, and E. Quansah. Biological control via "ecological" damping: An approach that attenuates non-target effects. *Math. Biocsci.*, 273:23–44, 2016.

[17] M. A. Beauregard and J. Geiser. An extrapolated splitting method for solving semi-discretized parabolic differential equtaions. *Intern. J. Comput. Math.*, 2015.

[18] M. A. Beauregard, J. L. Padgett, and R. D. Parshad. A nonlinear splitting algorithm for systems of partial differential equations with self-diffusion. *J. Comput. Appl. Math.*, 321:8–25, 2017.

[19] M. A. Beauregard and Q. Sheng. A semi-adaptive compact splitting method for the numerical solution of 2-dimensional quenching problems. *Appl. Math. Comput.*, 218:1240–1254, 2012.

[20] M. A. Beauregard and Q. Sheng. An adaptive splitting approach for the quenching solution of reaction-diffusion equations over nonuniform grids. *J. Comp. App. Math.*, 241:30–44, 2013.

[21] M. A. Beauregard and Q. Sheng. Explorations and expectations of equidistribution adaptations for nonlinear quenching problems. *Advances in Applied Mathematics and Mechanics*, 5(4):407–422, 2013.

[22] J. Bebernes and D. Eberly. *Mathematical Problems from Combustion Theory*. Springer, New York, 1989.

[23] M. Bertsch, T. Nanbu, , and L. Peletier. Decay of solutions of a degenerate nonlinear diffusion equation. *Nonlin. Anal.*, 6:539–554, 1982.

[24] H. P. Bhatt and A. Q. M. Khaliq. A compact fourth-order L-stable scheme for reaction diffusion systems with nonsmooth data. *J. Comp. Appl. Math.*, pages 176–193, 2016.

[25] S. Blanes and F. Casas. On the necessity of negative coefficients for operator splitting schemes of order higher than two. *Appl. Numer. Math.*, 54:23–37, 2005.

[26] T. K. Boni and T. K. Kouakou. Continuity of the quenching time in a semilinear heat equation with a potential. *Revista Colombiana de Matemáticas*, 43:55–70, 2009.

[27] J. D. Buckmaster, G. Joulin, and P. D. Ronney. The structure and stability of non-adiabatic flame balls. *Combust. Flame*, 79:381–392, 1990.

[28] J. D. Buckmaster, G. Joulin, and P. D. Ronney. The structure and stability of non-adiabatic flame balls: II: Effects of far field losses. *Combust. Flame*, 84:411–422, 1991.

[29] S. Z. Burstein and A. A. Mirin. Third order difference methods for hyperbolic equations. *J. Comp. Phys.*, 5:547–571, 1970.

[30] W. Cao, W. Huang, and R. D. Russell. A study of monitor functions for two-dimensional adaptive mesh generation. *SIAM J. Sci. Comput.*, (20):1978–1994, 1999.

[31] F. Castella, P. Chartier, S. Descombes, and G. Vilmart. Splitting methods with complex time for parabolic equations. *BIT Numer. Math.*, 2009.

[32] R. Cesari, F. Mainardi, P. Paradisi, and F. Tampieri. The fractional Fick's law for non-local transport processes. *Phys. A*, 293:130–142, 2001.

[33] C. Y. Chan. Computation of the critical domain for quenching in an elliptic plate. *Neural Parallel Sci. Comput.*, 1:153–162, 1993.

[34] C. Y. Chan. A quenching criterion for a multi-dimensional parabolic problem due to a concentrated nonlinear source term. *J. Comput. Appl. Math.*, 2011.

[35] C. Y. Chan and C. S. Chen. A numerical method for semilinear singular parabolic quenching problems. *Quart. Appl. Math.*, 47:45–57, 1989.

[36] C. Y. Chan and Lan Ke. Parabolic quenching for nonsmooth convex domains. *J. Math. Anal. App.*, 186(1):52–65, 1994.

[37] C. Y. Chan and P. C. Kong. Channel flow of a viscous fluid in the boundary layer. *Quart. Appl. Math.*, 55:51–56, 1997.

[38] W. Cheney and D. Kincaid. *Numerical Analysis: Mathematics of Scientific Computing*. Brooks/Cole, Providence, RI, 3rd edition, 2002.

[39] H. Cheng, P. Lin, Q. Sheng, and R. Tan. Solving degenerate reaction-diffusion equations via variable step Peaceman-Rachford splitting. *SIAM J. Sci. Comput.*, 25(4):1273–1292, 2003.

[40] D. S. Cohen and H. B. Keller. Some positone problems suggested by nonlinear heat generation. *J. Math. Mech.*, 16(12):1361–1376, 1967.

[41] K. Deng and H. A. Levine. On the blowup of u_t at quenching. *Proceeding of the American Mathematical Society*, 106(4):1049–1056, Aug 1989.

[42] C. A. Desoer and M. Vidyasagar. *Feedback Systems: Input-Output Properties*. Elsevier, New York, 1975.

[43] E. A. Dorfi and L. O'c Drury. Simple adaptive grids for 1-d initial value problems. *J. Comput. Phys.*, 69:175–195, 1987.

[44] J. Douglas, Jr. and J. E. Gunn. A general formulation of alternating direction methods, part I: Parabolic and hyperbolic problems. *Numer. Math.*, 6:428–453, 1964.

[45] F. Dubois and S. Mengué. Mixed collocation for fractional differential equations. *Numer. Alg.*, 34:303–311, 2003.

[46] L. Evans. *Partial Differential Equations (Graduate Studies in Mathematics 19 American Mathematical Society)*. Springer, 1998.

[47] W. Fair and Y. Luke. Padé approximations to the operator exponential. *Numer. Math.*, (14), 1970.

[48] J. M. Coyleand J. E. Flaherty and R. Ludwig. On the stability of mesh equidistribution strategies for time-dependent partial differential equations. *J. Comput. Phys.*, (62):26–39, 1986.

[49] G. Folland. *Real Analysis: Modern Techniquesand Their Applications*. John Wiley & Sons, Inc., 1999.

[50] R. M. Furzeland, J. G. Verwer, and P. A. Zegeling. A numerical study of three moving-grid methods for one-dimensional partial differential equations which are based on the method of lines. *J. Comput. Phys.*, 89:349–388, 1990.

[51] S. Gakkhar and B. Singh. Complex dynamic behavior in a food web consisting of two preys and a predator. *Chaos Solitons Fractals*, 24:789–801, 2005.

[52] J. Geiser. Fourth-order spltting methods for time-dependent differential equations. *Numer. Math.*, 1:321–339, 2008.

[53] D. Goldman and T. J. Kaper. N-th-order operator splitting schemes and nonreversible systems. *SIAM J. Numer. Anal.*, (33):349–367, 1996.

[54] G. H. Golub and C. F. Van Loan. *Matrix Computations*. Johns Hopkins University Press, Baltimore, 3rd edition, 1996.

[55] V. Guyonne and P. Noble. On a model of flame ball with radiative transfer. *SIAM J. Appl. Math*, 67:854–868, 2007.

[56] E. Hansen and A. Ostermann. High order spltting methods for analytic semigroups exist. *BIT Numerical Math.*, 49(3):527–542, 2009.

[57] E. Hansen and A. Ostermann. High-order splitting schemes for semilinear evolution equations. *BIT Numer. Math.*, 56(4):1303–1316, 2016.

[58] P. Henrici. *Discrete Variable Methods in Ordinary Differential Equations.* John Wiley & Sons, Inc., New York, 1962.

[59] N. J. Higham. The scaling and squaring method for the matrix exponential revisited. *SIAM J. Matrix Anal. Applic.*, 26:1179–1193, 2005.

[60] R. Hilfer. *Applications of Fractional Calculus in Physics.* World Scientific Publishing, Singapore, 2000.

[61] R. A. Horn and C. R. Johnson. *Matrix Analysis.* Cambridge University Press, 2010.

[62] W. Huang, Y. Ren, and R. D. Russell. Moving mesh partial differential equations (mmpdes) based upon the equidistribution principle. *SIAM J. Numer. Anal.*, 31:101–116, 1994.

[63] W. Huang and R. D. Russell. *Adaptive Moving Mesh Methods.* Springer, 2010.

[64] A. Iserles. *A First Course in the Numerical Analysis of Differential Equations.* Cambridge University Press, 2nd edition, 2008.

[65] A. Iserles and Q. Sheng. Implementation of splitting methods. *DAMTP, Cambridge University Research Report*, 1987.

[66] G. Joulin. Point-source initiation of lean spherical fflame of light reactants: An asymptotic theory. *Combust. Sci. Tech.*, 185:99–113, 1985.

[67] R. Kannan and C. K. Krueger. *Advanced Analysis on the Real Line*, chapter Dini Derivatives, pages 55–80. Springer-Verlag, 1996.

[68] G. E. Karniadakis, F. Song, and C. Xu. A fractional phase-field model for two-phase flow with tunable sharpness: Algorithmsand simulations. *Comput. Meth. Appl. Mech. Engrg.*, 305:376–404, 2016.

[69] H. Kawarada. On solutions of initial-boundary value problems for $u_t = u_{xx} + 1/(1-u)$,. *Publ. Res. Inst. Math. Sci.*, 10:729–736, 1975.

[70] W. Kelley and A. C. Peterson. *Difference Equations: An Introduction with Applications.* Academic Press, New York, 1991.

[71] R. Kershner. Degenerate parabolic equations with general nonlinearities. *Nonlin. Anal.*, 4(6):1043–1062, 1980.

[72] A. Q. M. Khaliq, J. Martín-Vaquero, B. A. Wade, and M. Yousuf. Smoothing schemes for reaction-diffusion systems with nonsmooth data. *J. Comp. Appl. Math.*, (223):374–386, 2009.

[73] A. Q. M. Khaliq and Q. Sheng. A compound adaptive approach to degenerate nonlinear quenching problems. *Num. Meth. Part. Diff. Eq.*, 15(1):29–47, Jan 1999.

[74] A. Q. M. Khaliq and Q. Sheng. *Adaptive Method of Lines*, chapter Linearly implicit adaptive schemes for singular reaction-diffusion equations. 2001.

[75] A. Q. M. Khaliq and Q. Sheng. A revisit of the semi-adaptive method for singular degenerate reaction-diffusion equations. *East Asia J. Appl. Math.*, 2:185–203, 2012.

[76] A. A. Kilbas, H. M. Srivastava, and J. J. Trujillo. *Theory and Applications of Fractional Differential Equations*. Elsevier, 2006.

[77] C. Kirk and W. Olmstead. Blow-up in a reactive-diffusive medium with a moving heat source. *J. Math. Phys.*, 53:147–159, 2002.

[78] E. Kreyszig. *Introductory Functional Analysis with Applications*. John Wiley & Sons, Inc., 1978.

[79] J. Lang and A. Walter. An adaptive Rothe method for nonlinear reaction-diffusion systems. *Appl. Numer. Math.*, 13:135–146, 1993.

[80] P. Leslie. Some further notes on the use of matrices in population mathematics. *Biometrika*, 35:213–245, 1948.

[81] F. Lessman and H. Levy. *Finite Difference Equations*. Dover Publications, New York, 1992.

[82] R. J. LeVeque. *Time-split methods for partial differential equations*. PhD thesis, Stanford University, 1982.

[83] R. J. LeVeque and J. Oliger. Numerical methods based on additive splitings for hyperbolic partial differential equations. *Math. Comp.*, 40:469–497, 1983.

[84] H. A. Levine. Quenching, nonquenching, and beyond quenching for solution of some parabolic equations. *Annali di Matematica pura ed applicata*, 155:243–260, 1989.

[85] H. A. Levine and J. T. Montgomery. The quenching of solutions of some nonlinear parabolic equations. *SIAM J. Math. Anal.*, 11(5):842–847, Sep 1980.

[86] H. A. Levine and P. E. Sacks. Some existence and nonexistence theorems for solutions of degenerate parabolic equations. *J. Diff. Eq.*, 52(2):135–161, Apr 1984.

[87] S. H. Lui. On linear monotone and Schwarz methods for nonlinear elliptic pdes. *Numer. Math.*, (93):109–129, 1967.

[88] R. I. McLachlan and G. R. W. Quispel. Splitting methods. *Acta Numer.*, 11:341–434, 2002.

[89] C. D. Meyer. *Matrix Analysis and Applied Linear Algebra*. SIAM, 2000.

[90] C. Moler and C. Van Loan. Nineteen dubious ways to compute the exponential of a matrix, twenty-five years later. *SIAM Rev.*, 45(1):3–49, 2003.

[91] D. A. Murio. Implicit finite difference approximation for time fractional diffusion equations. *Comput. Math. Appl.*, 56:1138–1145, 2008.

[92] H. Ockendon. Channel flow with temperature-dependent viscosity and internal viscous dissipation. *J. Fluid Mech.*, 93:737–746, 1979.

[93] J. L. Padgett and Q. Sheng. *Modern Mathematical Methods and High Performance Computing in Science and Technology*, chapter On the Stability of a Variable Step Exponential Splitting Method for Solving Multidimensional Quenching-Combustion Equations, pages 155–167. Springer, Ghaziabad, India, 2016.

[94] J. L. Padgett and Q. Sheng. On the positivity, monotonicity, and stability of a semi-adaptive LOD method for solving three-dimensional degenerate Kawarada equations. *J. Math. Anal. Appls*, 439:465–480, 2016.

[95] J. L. Padgett and Q. Sheng. Nonuniform Crank-Nicolson scheme for solving the stochastic Kawarada equation via arbitrary grids. *Num. Meth. Part. Diff. Eq.*, 2017.

[96] G. Pagnini. Nonlinear time-fractional differential equations in combustion science. *Frac. Calc. Appl. Anal*, 14:80–93, 2011.

[97] R. D. Parshad and R. K. Upadhyay. Investigation of long time dynamics of a diffusive three species aquatic model. *Dyn. Part. Diff. Eq.*, 7(3):217–244, 2010.

[98] I. Podlubny. *Fractional differential equations*. Academic Press, San Diego, 1999.

[99] T. Poinset and D. Veynante. *Theoretical and Numerical Combustion*. Edwards Publisher, Philadelphia, 2nd edition, 2005.

[100] W. G. Price, E. H. Twizell, and Y. Wang. Chaos-free numerical solutions of reaction-diffusion equations. *Proc. Roy. Soc. London Sect. A*, 430:541–576, 1991.

[101] S. S. Rao. *Applied Numerical Methods for Engineers and Scientists*. Prentics-Hall, Upper Saddle River, NJ, 2002.

[102] W. Rudin. *Functional Analysis*. McGraw-Hill, Inc., New York, 2nd edition, 1991.

[103] M. Schatzman. Higher order alternate direction methods. *Comput. Meth. Appl. Mech. Engrg*, 116:219–225, 1996.

[104] M. Schatzman. Stability of the Peaceman-Rachford approximation. *J. Funct. Anal.*, (162):219–255, 1999.

[105] Q. Sheng. *Exponential Splitting Methods for Partial Differential Equations*. PhD thesis, DAMTP, Cambridge University, 1990.

[106] Q. Sheng. Global error estimates for exponential splitting. *IMA Journal of Numerical Analysis*, 14:27–56, 1993.

[107] Q. Sheng. *Integral Methods in Science and Engineering (Research Notes in Math)*, chapter A monotonically convergent adaptive method for nonlinear combustion problems, pages 310–315. Chapman and Hall/CRC, 2000.

[108] Q. Sheng. Adaptive decomposition finite difference methods for solving singular problems. *Frontiers Math. China*, (4):599–626, 2009.

[109] Q. Sheng. ADI, LOD and modern decomposition methods for certain multiphysics applications. *J. Algorithms & Computat Tech*, (9):105–120, 2015.

[110] Q. Sheng. *Encyclopedia of Applied and Computational Mathematics*, chapter ADI Methods. Springer Verlag GmbH, Heidelburg, 2015.

[111] E. Sousa and C. Li. A weighted finite difference method for the fractional diffusion equation based on the Riemann-Liouville derivative. *Appl. Num. Math.*, 90:22–37, 2015.

[112] G. Strang. On the construction and comparison of difference schemes. *SIAM J. Numer. Anal.*, 5:507–517, 1968.

[113] J. C. Strikwerda. *Finite Difference Schemes and Partial Differential Equations*. SIAM, Philadelphia, 2004.

[114] M. Suzuki. General thoery of fractal path iintegral with applications to many-body theories and statistical physics. *J. Math. Phys*, 32:400–407, 1991.

[115] J. Szarski. *Differential Inequalities*. Instytut Matematyczny Polskiej Akademi Nauk, Warsaw, 1965.

[116] V. Tarasov. *Fractional Dynamcis: Applications of Fractional Calculus to Dynamics of Particles, Fields, and Media*. Springer, Berlin, 2010.

[117] H. Y. Tian. Computations of critical domains for quenching problems by delta-shaped basis functions. *Neural Parallel Sci. Comput.*, 15:501–514, 2007.

[118] H. F. Trotter. Approximation of semi-groups of operators. *Pacific J. Math.*, 8:887–919, 1958.

[119] H. F. Trotter. On the product of semi-groups of opertors. *Proc. Amer. Math. Soc.*, 10:545–551, 1959.

[120] R. K. Upadhyay and V. Rai. Why chaos is rarely observed in natural populations. *Chaos Solitons Fractals*, 8(12):1933–1939, 1997.

[121] W. Walter. Parabolic differential equations with a singular nonlinear term. *Funkcial. Ekvac.*, 19:271–277, 1976.

[122] Y. Xu. Quenching phenomenon in a fractional diffusion equationand its numerical simulation. to appear in *Intern. J. Comput. Math.*, 2017.

[123] Y. Xu and Z. Zheng. Quenching phenomenon of a time-fractional diffusion equation with singular source term. *Math. Meth. Appl. Sci.*, 2017. doi:10.1002/mma.4424.

[124] K. Yosida. *Functional Analysis*. Springer-Verlag, Berlin, 6th edition, 1980.

[125] L. Zhao and W. Deng. High order finite difference methods on non-uniform meshes for space fractional operators. *Adv. Comput. Math.*, 42:425–468, 2016.